UNIVERSITÀ DEGLI STUDI DI PADOVA

Dipartimento di Fisica e Astronomia "Galileo Galilei"

Master Degree in Physics

Final Dissertation

Out-of-equilibrium thermodynamics in multi-component exact models

Thesis supervisors

Prof. Alessandro Sfondrini

Thesis co-supervisor

Prof. Pasquale Calabrese

Candidate

Alberto Brollo

Academic Year 2021/2022

Contents

Abstract

Many body integrable systems allow the exact calculation of the equilibrium spectrum through the thermodynamic Bethe ansatz (TBA). In particular, the macroscopic quantity encoding the information about the spectrum is the so-called root density. A recent theoretical development is Generalized Hydrodynamics (GHD) which provides exact equations for the time evolution of the root density. The prototypical setup in which these equations are tested is the quantum quench, i.e. a sudden change of some parameter of the Hamiltonian (typically related to the external potential). The goal of the thesis is to develop numerical simulation for the time evolution of single-component and multi-component gases. In particular, the first system studied in the thesis is the simplest many-body integrable model, the Lieb-Liniger gas, for which the harmonic trap release both at zero and finite temperature is presented. Next, the Yang-Gaudin model and the two-component spinor Bose gas are studied, two multi-component models that differs only for the statistics of the particles they described. Also in this case, the harmonic trap release is simulated, and both a qualitative and quantitative comparison is carried out in order to understand the role of the statistics in such a quench protocol.

Chapter 1

Introduction

> However, my personal reason for working on one-dimensional problems is merely that they are fun. A man grows stale if he works all the time on the insoluble and a trip to the beatiful work of one dimension will refresh his imagination better than a dose of LSD.
>
> *Freeman Dyson, 1967*

The experimental realisation of a Bose-Einstein condensate in 1995 [1–3] opened a world in the field of ultracold atoms physics both from a theoretical and an experimental point of view. In particular, in the last twenty years, the realisation of one-dimensional systems has been one of the main focuses in this field [4]. In these setups, ultracold atoms are tightly confined in two transverse directions, suppressing all the excitations, and weekly confined in the other direction. In this way, experimentalists manage to realise systems that can be effectively described by one-dimensional models. These novel techniques put it back in the spotlight a field that has been concealed for decades. The one-dimensional quantum world is interesting not only for practical reasons, like future outlooks in electronics, or in condensed matter physics, for instance, the description of the physics at the edge, but it also has a remarkable mathematical physical relevance. In one spatial dimension, physics is extremely different. In higher dimensions, many-body systems are described starting from the free theory and adding the interaction next, allowing for perturbative or mean field techniques, such as Fermi liquid theory. In one dimension, particles are not able to avoid themselves during their motion, hence they result to be always strongly correlated, regardless of the strength of the coupling. Hence, there is the loss of individual excitations in favour of the collectivisation of the excitations. Furthermore, the Coleman-Mermin-Wagner [5] theorem forbids the formation of long-range order, since fluctuations have a predominant role in one-dimensional systems. Hence, statistical approximations, such as mean-field theory, are out of their regime of applicability.

Some one-dimensional quantum systems are solvable via Bethe ansatz, i.e. they can be exactly solved thanks to a procedure that turns the Schrödinger partial differential equation into a set of algebraic relations between some quantities that effectively described the wavefunction of the eigenstates, the rapidities. This technique was born in 1931 [6] when Hans Bethe provides the solution for the Heisenberg XXX chain. During the sixties, this technique found a generalisation to a plethora of one-dimensional models [7–11] and also a technique for the exact solution in the thermodynamic limit was developed [12–14], the renowned Thermodynamic Bethe ansatz (TBA) which has recently found application also for extracting the spectrum of some particular models in string theory [15–18]. The study of these models has received renewed interest in the last decades since they have started to be experimentally realisable [19–24]. Since the Bethe ansatz allows us to exactly solve the model, physical hypothesis and intuition can be compared with experiments in detail creating a wonderful interplay between theory and experiment. Sometimes these models are referred to as *integrable*, even though in

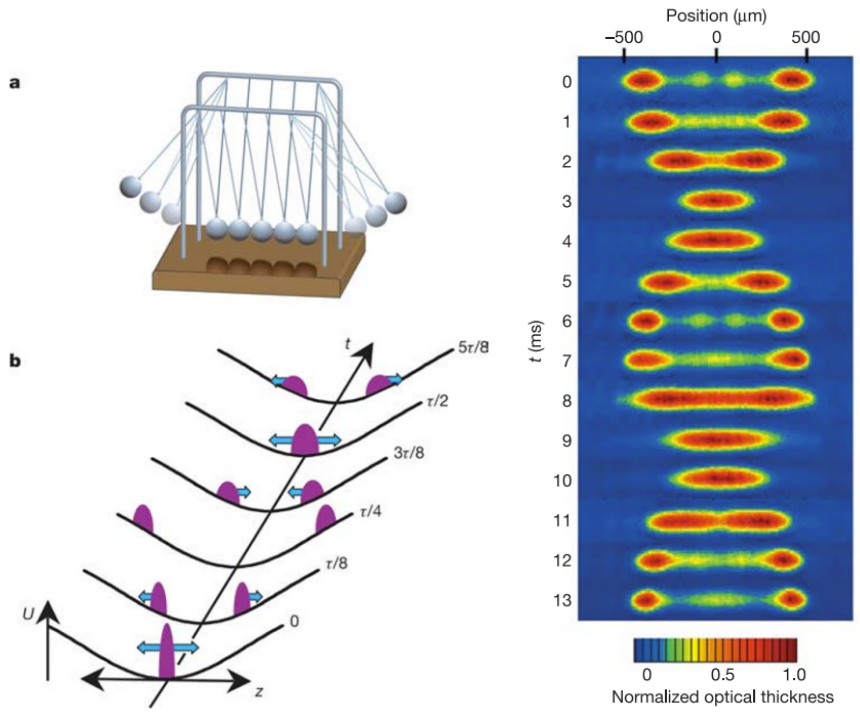

Figure 1.1: A quantum Newton cradle. From [29].

the quantum world there is not yet a complete and satisfactory definition of what quantum integrability is [25, 26], contrary to the classic world where there are solid and well-established definitions. For this reason, sometimes is preferable to refer to them as *exactly solvable models*.

Between the realm of the exactly solvable systems, there are the multi-component systems, i.e. systems whose solution via the Bethe ansatz requires the introduction of multiple sets of rapidities. The first one to be solved has been the Yang-Gaudin model in 1967 [8,9], which is about fermions with contact interactions. It is said to be *multi-component* because for its solution both a set of rapidities for the quasi-momenta and the spin excitations are introduced. These models provide a much richer phenomenology compared to the single-component ones. An example can be the fractalisation of the fundamental excitations, for instance in the Yang-Gaudin model one observe the phenomenon of the spin-charge separation [27, 28], where the excitation of charge and spin propagate separately, notwithstanding the gas is spinful.

After that in the sixties and the seventies, the exact solutions of these models has been investigated, in the last fifteen years, the interest of the community moved to the description of their out-of-equilibrium behaviour. The description of many-body systems, and especially of their non-equilibrium dynamics, is one of the most compelling problems in physics. Besides this, only the recent experimental novelties mentioned above allowed the realisation of closed and controlled systems to test the theoretical models. A noteworthy experiment that triggered the interest of the statistical physics community is the work of Kinoshita et al [29] in 2006. In this experiment, a gas of ^{87}Rb atoms is split into two clouds of opposite momentum and the system is left free to evolve. A naive way to imagine this dynamics is to think the initial system is confined in a double well which is suddenly changed into a harmonic potential. These kinds of protocols are called *quantum quenches*. In this experiment emerged that, for a large time window, the two clouds collide but the system does not thermalize and it pursues an oscillatory behaviour. Indeed, this experiment has been dubbed the quantum Newton cradle (see **Figure 1.1**). Quantum integrability is the key in order to explaining this lack of thermalization [30]. Actually, a low-density gas of Rubidium atoms is well described by the Lieb-Liniger integrable model of delta-interacting bosons [7,31]. Nevertheless, in those years numerical simulations were not able to explain such a phenomenon due to the exponential wall of quantum many-body physics.

A revolutionary contribution for the description of the out-of-equilibrium behaviour of integrable

systems has been published in 2016 [32, 33]. This theory, called Generalised Hydrodynamics (GHD), extend the principles of the standard hydrodynamics to the peculiar characteristic of integrable models of having an infinite set of conserved charges, providing a set of exact equations for the non-equilibrium dynamics of these systems whose numerical solution is much less expensive compared to the previous techniques. Since the theory turned out to be extremely versatile, after the two pioneering works of 2016, a lot has been done about this theory, adding diffusive contribution [34, 35], extending it to the presence of an external forcing field [36], and the requantisation of the theory to investigate equal-time correlation and entanglement [37–44]. The quantum Newton cradle experiment has been satisfactory explained [30], and other experimental test gave nice confirmation of the theory [45, 46].

So far, GHD has been mostly applied to single-component models, with some rare exceptions [27, 28, 47–50]. In these thesis we want to beat this path starting from a recently published paper on the GHD for the Yang-Gaudin model [28], and compare part of those results with the corresponding bosonic model, i.e. the so called two-component spinor Bose gas which describes two species of delta-interacting bosons. In particular, we will focus on a particular quench protocol which is the harmonic trap release, i.e. the sudden turning off of a harmonic trap that was initially confining the gas that is hence left free to expand. Since the two models are equivalent and the only difference lays in the statistics of the particles involved, with this study we want to probe both qualitatively and quantitatively the different behaviour of the two gases at different values of the temperature.

Organisation of the thesis In Chapter 2 we will study in detail the Bethe ansatz and the thermodynamic Bethe ansatz solution for the Lieb-Liniger model, with also **Section 2.9** dedicated to the description of the numerical algorithm for the solution of the TBA equations. In Chapter 3 we will essentially derived the theory for the Generalised Hydrodynamics, bases only on standard arguments from statistical mechanics. Also in this Chapter, we will narrowly describe the iterative numerical procedure to pursue an out-of-equilibrium evolution via the GHD equations. At the end of the Chapter we will present the results for a harmonic trap release of the Lieb-Liniger gas. In Chapter 4 it is review the Bethe ansatz solution for the two multi-component models protagonists of this thesis: the Yang-Gaudin models, for fermions, and the two-component spinor Bose gas, for bosons. Finally, in Chapter 5 we will compare the results of a harmonic trap release for this two.

Chapter 2

Bethe ansatz solvable models

> I got really fascinated by these (1 + 1)-dimensional models that are solved by the Bethe ansatz and how mysteriously they jump out at you and work and you don't know why. I am trying to understand all this better.
>
> *Richard Feynman, 1988*

The origin of this technique lays in 1931, when Hans Bethe found the exact solution of the XXX Chain[1] (or Heisenberg model) through a particular ansatz on the wavefunction. Historically, this has been the first interacting model exactly solved [6]. For this reason, in the following I'll give a brief sketch of the idea of Bethe for this model, next we'll move to the Lieb-Liniger model which is the first studied in this thesis. The analysis of the Heisenberg model follows mainly the notes by Fabio Faranchini, written-up for the lectures he gave for a class in SISSA on "*Introduction to Bethe Ansatz*" [31].

The Hamiltonian of this model is

$$\mathcal{H} = -J\sum_{n=1}^{N} \mathbf{S}_n \cdot \mathbf{S}_{n+1} = -J\sum_{n=1}^{N}\left[\frac{1}{2}\left(S_n^+ S_{n+1}^- + S_n^- S_{n+1}^+\right) + S_n^z S_{n+1}^z\right], \tag{2.1}$$

where $\mathbf{S}$ is the spin operator, $S^\pm$ the spin flip ones and S^z its projection on the z-axis. These operators satisfy the $SU(2)$ commutation rules. This model provides a simple description of a ferromagnet [51]. In particular, $J > 0$ favors a ferromagnetic alignment, while $J < 0$ an antiferromagnetic one. The Hilbert space for this Hamiltonian is a 2^N dimensional space spanned by the orthogonal basis vector $|\sigma_1 \dots \sigma_N\rangle$, where $\sigma_i = \uparrow$ means the spin is up in position i, while $\sigma_i = \downarrow$ means the spin is down.

If we apply a magnetic field, the system displays a manifest $U(1)$ symmetry, as well as discrete translational invariance. This means $[\mathcal{H}, S^z] = 0$, thus, the number of up and down spin is conserved. Therefore, we can factorize the Hilbert space in superselection sectors with fixed number of down spins R (or equivalently up spins, $U(1)$ includes parity). The $R = 0$ consists of a single vector, i.e. $|0\rangle = |\uparrow \dots \uparrow\rangle$. We can obtain a basis for the $R = 1$ sector applying the lowering operators

$$|n\rangle = S_n^- |0\rangle \qquad n = 1, \dots, N. \tag{2.2}$$

To construct the $R = 1$ eigenstates we must require also translational invariance, thus,

$$|\psi\rangle = \frac{1}{\sqrt{N}}\sum_{n=1}^{N} e^{ikn} |n\rangle\,, \tag{2.3}$$

[1] It's quite interesting googling "xxx model".

for wave numbers $k = 2\pi m/N, m = 0, \dots, N-1$, with unitary lattice spacing. These wavefunctions represent the famed *magnons* excitations. For a comprehension of magnons as excitations of spin waves take a look at [52].

Complications arise considering the $R > 1$ sectors. Actually, due to the interacting nature of the model, the eigenstates of these sectors are not simply given by *multi-magnons* superposition (as it is in free models). Let's consider for instance the $R = 2$ sector and take into account a generic wavefunction

$$|\psi\rangle = \sum_{1 \le n_1 \le n_2 \le N} f(n_1, n_2) \, |n_1, n_2\rangle \, , \tag{2.4}$$

where of course $|n_1, n_2\rangle = |n_2, n_1\rangle$, hence, there is such a constraint on n_1 and n_2 in the summation. The Bethe ansatz for the eigenstates' coefficients is [6]

$$f(n_1, n_2) = A_{12} e^{i(k_1 n_1 + k_2 n_2)} + A_{21} e^{i(k_2 n_1 + k_1 n_2)}, \tag{2.5}$$

i.e. a superposition of plane-waves. This ansatz solves the Schrödinger equation if

$$\frac{A_{12}}{A_{21}} = \frac{e^{i(k_1+k_2)} + 1 - 2e^{ik_1}}{e^{i(k_1+k_2)} + 1 - 2e^{ik_2}} \equiv e^{i\theta}. \tag{2.6}$$

The second key step of this procedure is imposing periodic boundary conditions (pbc) $f(n_1, n_2) = f(n_2, n_1 + N)$. Combining this with the previous conditions on the coefficients of the superposition, we obtain

$$e^{ik_1 N} = e^{i\theta}, \qquad e^{ik_2 N} = e^{-i\theta}. \tag{2.7}$$

As a result, we have obtained a set of two algebraic equations for the two unknown momenta called *Bethe equations*. To see that are algebraic, you have just to take the log of both sides (see (2.1)). I will not enter in the solution of this set of equations because we are going to see this in full detail for the Lieb-Liniger model. This ansatz is easily generalized to any sector of the system, so, any number of down spins. Again, we will see this generalisation in Lieb-Liniger.

Before doing this, I want to emphasise some considerations. This technique nowadays is called *coordinate* Bethe ansatz, to be distinguished with the *algebraic* Bethe ansatz, which I am not going to use in this thesis. For deepen this topic see again [31]. The beauty of this approach is that a simple superposition of plane-waves is surprisingly able to turn the Schrödinger PDE into a set of algebraic relations, thus, exactly solvable (at least numerically).

To catch the physical meaning of this mathematical relations, we firstly have to notice that in a 1+1 dimensional model with translational invariance like this, both energy and momentum are conserved. Thus, it's straightforward to realize that in a $2 \to 2$ scattering initial and final momenta must be equal. So, the only possible effect of interaction is a phase shift in the wavefunction. For this reason, the condition we get on the coefficients of the superposition in (2.6) can be seen as a *phase-shift* obtained exchanging the two magnons. In fact, notice that in (2.5) the two terms differ only for the exchange of the wavenumber of the spin waves. So, considering n_1 and n_2 the coordinates of the two magnons, we have substantially exchanged them and in 1 spatial dimension this means we have scattered them. Hence, from a particle physics point of view we can think of the function θ as a phase arising after scattering the two magnons excitations. Therefore, the Bethe ansatz consists in a *consistency condition* obtained imposing the equality between the pbc and the scattering of N-1 particle. In fact, the pbc imposes the equality of the first and last particle of the system, which can also be obtained scattering all the other N-1 particles and bringing the first particle to the last side. In this way the Schrödinger equation, a PDE, is transformed into a set of algebraic relations easier to solve.

Final remark, the two momenta k_1, k_2 are not the real momenta of the two magnons, that's because they are not physically accessible. In fact, the energy and the momentum of the system are

$$E = E_0 + J \sum_{j=1,2} (1 - \cos k_j) \qquad K = k_1 + k_2. \tag{2.8}$$

They are just bookkeeping artifacts of the Bethe ansatz, for this reason they are called *quasi-momenta*.

2.1 Lieb-Liniger

The previous model was a spin chain, hence, it is realized on a lattice. Now we move to a model in the continuum, probably the simplest interacting model one can think of. The model consists of N spinless bosons with contact interaction. The Hamiltonian reads

$$\mathcal{H} = -\sum_{j=1}^{N} \frac{\partial^2}{\partial x_j^2} + 2c \sum_{j<l} \delta(x_j - x_l), \tag{2.9}$$

where c parametrize the interaction strength. The name origins from Lieb and Liniger who solved it in 1963 [7]. Physically, this Hamiltonian modelize a 1D dimensional system with contact interactions. Experimental realization of this kind of system has received a great improvement in the last years using ultracold atoms [19–23]. The main limitation of this model is due to the fact that in real experimental setup the gas is confined by a trapping potential that breaks translational invariance and thus, integrability. For the moment, we neglect this complication that we will solve later in thermodynamic limit using the local density approximation, under the assumption of smooth enough confining potential (see **Section 3.5**). Now I am going to make some general considerations on the model, next I will solve it using the Bethe ansatz. Finally, I will consider the thermodynamic limit and discuss the so called *thermodynamic Bethe ansatz* and its numerical solutions.

Considering the system in a finite volume L, the Lieb-Liniger Hamiltonian can be rewritten in second quantised form as

$$\hat{H} = \int_0^L dx \Big[\partial_x \Psi^\dagger(x) \partial_x \Psi(x) + c \Psi^\dagger(x) \Psi^\dagger(x) \Psi(x) \Psi(x) \Big], \tag{2.10}$$

with the field operator normalized to the total number of particles $\int dx \Psi(x) = N$. To qualitatively understand a model, it is always convenient to extract dimensionless parameters, so the interaction strength can be captured by

$$\gamma \equiv \frac{2m}{\hbar^2} \frac{c}{n} \qquad n \equiv \frac{N}{L}. \tag{2.11}$$

We can distinctly recognize two extreme regimes. Firstly, the strong interacting one where $c, \gamma \to \infty$ and bosons behaves like fermions. This is called *Tonks-Girardeu regime* (TG) [53]. The other regime is the weak interacting one where c/n is small. Complete condensation is forbidden in one-dimensional systems due to the generalization of Mermin-Wagner theorem made by Coleman [5], that forbids long-range order due to the effect of fluctuations. That notwithstanding, a large fraction of particles occupy the lowest eingestate forming a "quasi-condensate" [54]. So, with a semiclassical treatment we obtain the 1D Gross-Pitaevski equation and the Lieb-Liniger model behaves as a 1D Non-Linear Schrödinger Hamiltonian [55].

Now we move to the exact solution of the model through Bethe ansatz. Also in this section I mainly follow the notes by Franchini [31].

2.2 The two particles problem

We start writing the generic symmetric wavefunction

$$\Psi(x_1, x_2) = f(x_1, x_2)\theta_H(x_2 - x_1) + f(x_2, x_1)\theta_H(x_1 - x_2), \tag{2.12}$$

where θ_H is the Heaviside step function, vanishing for negative argument and equal to one otherwise. Similarly to what Behte did for the XXX Chain, the ansatz Lieb and Liniger took for the wavefucntion is a superposition of plane-waves [7]

$$f(x_1, x_2) = A_{12} e^{i(k_1 x_1 + k_2 x_2)} + A_{21} e^{i(k_2 x_1 + k_1 x_2)}. \tag{2.13}$$

Inserting this ansatz in the Schrödinger equation, one find it is solved if

$$\frac{A_{12}}{A_{21}} = \frac{i(k_1 - k_2) - c}{i(k_1 - k_2) + c} \equiv e^{i\tilde{\theta}(k_1 - k_2)}, \tag{2.14}$$

with $\tilde{\theta}(k) \equiv -2\arctan\frac{k}{c} + \pi$ the phase shift due to the contact interaction. The phase shift is a unique signature of the model and it is strictly related to the S-matrix [56], as highlighted for the XXX chain (here that we have real particles exchange in the continuum, it could be clearer). As a consistency remark, note that for $c \to \infty$ we get a free fermionic wavefunction, according to what said previously. Another interesting remark is that the wavefunction vanishes if $k_1 = k_2$, displaying a fermionic behaviour for the quasi-momenta. It is usual to factor out this fermionic behaviour, rewriting (2.14) with $\theta \equiv -2\arctan\frac{k}{c}$ as

$$\frac{A_{12}}{A_{21}} = -e^{i\theta(k_1-k_2)}. \tag{2.15}$$

As we will see later, the scattering kernel $\theta(k)$ is the key quantity in an integrable system and quite everything could be calculated starting from that.

2.3 Generalisation to N particles

Now let's consider a system on N particles. We make an ansatz about the wavefunction, again as a linear superposition of plane-waves

$$\psi(x_1, ..., x_N) = \sum_{\sigma \in P_N} A_\sigma e^{i\sum_j k_{\sigma_j} x_j}, \tag{2.16}$$

where we set $x_1 < .... < x_N$ and P_N is the N-dimensional permutations group. Notice that thanks to the symmetrisation of the wavefunction, this is unambiguously extended to all $\mathbb{R}^N$. Any element of the permutations group can be factorize as a product of transpositions, physically equivalent to the two-particle scattering. Thus, if σ and σ' differ for a transposition, we have

$$\frac{A_\sigma}{A_{\sigma'}} = -e^{i\theta(k-k')} \tag{2.17}$$

where k and k' are the quasi-momenta interchanged in the transposition. Exploiting this consideration, or inserting (2.16) in the eigenstates equation, one find that it is solved if

$$A_\sigma = \Omega_N(-1)^\sigma \prod_{i<j} \big(k_{\sigma_i} - k_{\sigma_j} + ic\big), \tag{2.18}$$

where Ω_N is a normalization constant. Notice again that it vanishes if two quasi-momenta coincide. Anew, the quasi-momenta are just a mathematical artifact, and they have not a physical correspondence. In fact, easily the energy and the momentum are

$$E = \sum k_j^2 \qquad K = 2\sum k_j, \tag{2.19}$$

with the momentum operator defined as $\hat{K} = -2i\sum \frac{\partial}{\partial x_j}$. In general, the set of quasi-momenta allows us to construct infinite conserved charges $\sum_j (k_j)^n$ for $n \in \mathbb{N}$ (see **Section 3.3**).

2.4 The Bethe Equation

In order to renormalize the wavefunction of the Bethe ansatz, we put the system in finite volume and take pbc. Physically, this is like considering a system of N particle on a finite ring. As for XXX chain, imposing pbc gives a set of consistency equations. The interpretation is the same as before, to impose pbc we need to move a particle along all the circle, i.e. to scatter against all other N-1 particles. Through all these scattering events, it acquires a phase equal to the sum of all the scattering phases, plus the dynamical phase accumulated through the motion (namely, its quasi-momentum times L, length of the ring). So, given a certain permutation σ, the one obtained through the movement of the first particle to the last position, namely σ', we get

$$A_\sigma = A_{\sigma'} e^{ik_{\sigma_1} L}. \tag{2.20}$$

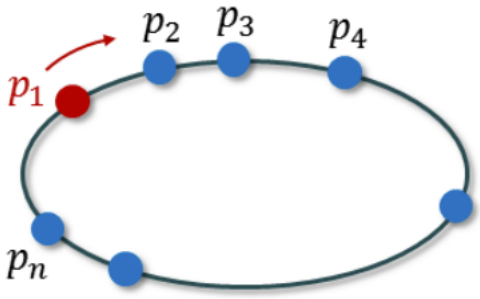

Figure 2.1: Pictorial representation of the physics underlying the Bethe ansatz. The system is a ring of N particle and we impose consistency between pbc and the scattering of the all the particles. Figure taken from [57].

Matching this with (2.18) we obtain

$$e^{ik_jL} = \prod_{i\neq j}\left(\frac{k_j - k_i + ic}{k_j - k_i - ic}\right) = (-1)^{N-1}\prod_{i=1}^{N} e^{i\theta(k_j - k_l)}, \qquad j = 1, ..., N, \tag{2.21}$$

which actually show how the dynamical phase (LHS) has to match the scattering phase (RHS). For a pictorial representation take a look at **Figure 2.1**. This is the *Bethe Ansatz equation for Lieb-Liniger*, which is non-linear, not analytically solvable, but being algebraic not hard as a PDE. In order to solve this equation, we start taking the log both sides

$$\begin{aligned} k_jL &= 2\pi\tilde{I}_j + (N-1)\pi - 2\sum_{i=1}^{N}\arctan\frac{k_j - k_i}{c} \\ &= 2\pi I_j + \sum_{i=1}^{N}\theta(k_j - k_i), \end{aligned} \tag{2.22}$$

where the $\tilde{I}_j$ are a set of integers which define the state. Consequently, the second set I_j can be both integers or half-integers. The latters are called *Bethe Integers* and they characterize uniquely the state. Since if two quasi-momenta coincide the wavefunction vanishes, it is clear that only a set of distinct Bethe integers correspond to physical solutions. Again, for $c \to \infty$ we have hard-core bosons with $k_j = 2\pi I_j/L$. The requirement of being distinct brings a formal analogy with the Fermi sea, in fact it's easy to see that the ground state in the Tonks-Girardeu regime is given by

$$I_j = -\frac{N+1}{2} + j \qquad j = 1, ..., N. \tag{2.23}$$

That's because this minimize energy and annul the momentum. In fact, since $\theta(-k) = -\theta(k)$, the momentum of the system is $K = \frac{2\pi}{L}\sum_j I_j$. If we now decrease the coupling from infinity we turn on a scattering phase so that, for fixed I_j, the k_j will move from the original regular distribution. However, there cannot be level crossing because there is no symmetry to protect a degeneracy and accidental ones (degeneracies) cannot happen in an integrable model.[2] Henceforth, the ground state is labeled by the previous set of Bethe integers for any value of the strength c.

2.5 Repulsive case: thermodynamic instability

Before moving to the thermodynamic limit, we want to show that this could be taken only for repulsive interaction. Starting from (2.15), a limiting solution for the two body scattering is the case in which

[2]In quantum mechanics, degeneracy is strictly related to symmetries. Of course if a system has a symmetry, the Hilbert space is a unitary representation of the universal covering group. If the latter presents some higher dimensional irreps, we are in presence of degeneracy. On the other hand, it is possible that a system displays more degeneracy than aspected. This is called *accidental degeneracy* and generally is related to some hidden symmetries (e.g. harmonic oscillator, hydrogen atoms).

either A_{12} or A_{21} vanishes, that is respectively

$$k_1 - k_2 = \pm ic. \tag{2.24}$$

To better understand the physics behind this solution, we introduce the center of mass reference frame

$$\begin{aligned} X &\equiv \frac{x_1 + x_2}{2}, \qquad x \equiv \frac{x_1 - x_2}{2}, \\ K &\equiv k_1 + k_2, \qquad k \equiv k_1 - k_2. \end{aligned} \tag{2.25}$$

Hence, the wavefunction can be rewritten as

$$\psi(X, x) = e^{iKX} \begin{cases} A_{12}e^{ikx} + A_{21}e^{-ikx}, & x > 0 \\ A_{21}e^{ikx} + A_{12}e^{-ikx}, & x < 0 \end{cases} . \tag{2.26}$$

Looking at the latter, we see that a condition for a meaningful wavefunction is $\mathrm{Im}\{K\} = 0$. For the same reason, if $\mathrm{Im}\{k\} > 0$ then $A_{21} = 0$ and viceversa $A_{12} = 0$. Thus, we see that the only solutions with complex quasi-momenta are (2.24) and they are consistent only if $c < 0$. This solution represent a bound state of two particles with quasi-momenta

$$k_{1,2} = \frac{K \pm ic}{2}, \qquad \mathrm{Im}\{K\} = 0 \tag{2.27}$$

with energy $E = K^2/2 - c^2/2$ and total momentum K. We can see that is a bound state writing explicitly the wavefunction

$$f(x_1, x_2) = e^{iK(x_1+x_2)/2} e^{c|x_1 - x_2|/2}, \tag{2.28}$$

where we recognize the boundedness in the exponential decay.

The same reasoning can be generalized to more particles. For $N = 3$ and $c < 0$, there are two type of solutions with complex quasi-momenta

$$k_1 = \alpha - i\frac{c}{2}, \qquad k_2 = \alpha + i\frac{c}{2}, \qquad k_3 = \beta \tag{2.29}$$

$$k_1 = k_3 - ic, \qquad k_2 = k_3 + ic, \qquad \mathrm{Im}\{k_3\} = 0. \tag{2.30}$$

The former is still a two-particle bound state, scattering with a third independent particle. The second is a proper three-particle bound state. In general, n-particle bound states appear in *strings* of particles with the same real part of the momentum. This string has quasi-momenta equispaced symmetrically with respect to the real axis and this is set by the interaction strength

$$k_j = \frac{K}{n} - i\frac{n + 1 - 2j}{2}c \qquad j = 1, 2, \ldots, n, \tag{2.31}$$

corresponding to total momentum K and energy

$$E = \frac{K^2}{2n} - \frac{n(n^2 - 1)}{24}c^2. \tag{2.32}$$

Here we see the $-N^3$ divergence in the thermodynamic limit. Henceforth, for $c < 0$ this configuration with complex quasi-momenta, i.e. bound states, has lower energy compared to the unbounded one, thus is the one towards the system goes in the thermodynamic limit. However this limit is ill-defined and the system in unstable. That's why, in the thermodynamic limit we must consider only $c > 0$.

We will meet again this strings solutions in the Yang-Gaudin model and in the two-component spinor Bose gas we will discuss in Chapter 4.

Before finally moving to the thermodynamic limit, I want to highlight that the final aim of the thesis is the comparison between the behaviour of multi-component 1D fermions and 1D bosons after a trap release. We will see that also the two-component spinor-Bose gas is unstable for attractive interaction. Moreover, the TBA for the Yang-Gaudin model is simpler when fermions repel each other. Thus, for once, we are lucky.

2.6 The thermodynamic limit

We have just seen we should consider only the $c > 0$ case, so, repulsive bosons. If we order the Bethe integers I_j in increasing order, we can write the Bethe equations as

$$k_j - \frac{1}{L}\sum_{i=1}^{N}\theta(k_j - k_i) = y(k_j), \tag{2.33}$$

where we defined the *counting function* $y(k)$ as an arbitrary function constrained by being monotonically increasing and by $y(k_j) = \frac{2\pi I_j}{L}$. Now, if we take the thermodynamic limit $N, L \to \infty$, keeping N/L finite, we want to introduce a density of quasi momenta, i.e. the *root density*, that we require satisfy

$$y'(k_j) = 2\pi\rho(k_j). \tag{2.34}$$

It it easy to see that a correct choice is

$$\rho(k_j) = \lim_{N,L\to\infty} \frac{1}{L(k_{j+1} - k_j)} > 0. \tag{2.35}$$

This can be checked constructing the difference quotient in (2.34). Keeping on to the thermodynamic limit, we replace sums with integrals over k as

$$\sum_j \to L\int \rho(k)dk, \tag{2.36}$$

and therefore

$$\frac{1}{2\pi}y(k) = \int^{k} \rho(k')dk', \tag{2.37}$$

establishing a direct connection between the distribution of the integers and the density of quasi-momenta. With these new thermodynamic definitions, we have turned the set of algebraic equations given by the Bethe equation into an integral equation for the counting function and the quasi-momenta distribution

$$y(k) = k - \int_{k_{min}}^{k_{max}} \theta(k - k')\rho(k')dk', \tag{2.38}$$

and by taking both sides the derivative with respect to k we get

$$\begin{aligned}\rho(k) &= \frac{1}{2\pi} - \frac{1}{2\pi}\int_{k_{min}}^{k_{max}} \theta'(k - k')\rho(k')dk' \\ &= \frac{1}{2\pi} - \frac{1}{2\pi}\int_{k_{min}}^{k_{max}} \mathcal{K}(k - k')\rho(k')dk',\end{aligned} \tag{2.39}$$

where we introduced the integral kernel

$$\mathcal{K}(k) \equiv \frac{\mathrm{d}}{\mathrm{d}k}\theta(k) = -\frac{2c}{c^2 + k^2}, \tag{2.40}$$

as the derivative of the scattering phase. The latter integral equation is known as the *Lieb-Liniger equation*. These equation determines the distribution of the quasi-momenta, which depends on the *Fermi points* k_{min} and k_{max}. In the ground states the Fermi points must be symmetric with respect to zero in order to minimize the momentum

$$p = \frac{K}{L} = 2\int_{-q}^{q} k\rho(k)dk = 0, \tag{2.41}$$

where we used the fact that (2.39) implies $\rho(-k) = \rho(k)$. In taking the thermodynamic limit, we lost the exact knowledge of the Bethe equation solution and thus, of the eigenstates. Moreover, we are advancing toward the understanding of the macroscopic properties of the system. The Lieb-Liniger

equation is a *Fredholm linear integral equation* and can be easily solved numerically. Now, we firstly make some analytical consideration on the solution and in the last section we are going to see how to numerically solve this kind of equation.

The solution of (2.39) explicitly depends on q which is physically constrained imposing $\int_{-q}^{q}\rho(k)dk = N/L$. To better catch the physics of the system is convenient to perform the rescaling

$$k \equiv qx \qquad c \equiv qg, \tag{2.42}$$

and defining $\tilde{\rho}(x) = \rho(qx)$ we get

$$\tilde{\rho}(x) = \frac{1}{2\pi} + \frac{1}{\pi}\int_{-1}^{1}\frac{g}{g^2+(x-y)^2}\tilde{\rho}(y)dy. \tag{2.43}$$

So, the physical quantities of the system can be rewritten as

$$\begin{aligned} n &\equiv \frac{N}{L} = qG(g), \qquad G(g) \equiv \int_{-1}^{1}\tilde{\rho}_g(x)dx, \\ e &\equiv \frac{E}{L} = q^3F(g), \qquad F(g) \equiv \int_{-1}^{1}x^2\tilde{\rho}_g(x)dx. \end{aligned} \tag{2.44}$$

Now, it's straightforward to see $\frac{c}{n} = \frac{g}{G(g)} \equiv \tilde{G}(g)$ and so we can finally write the ground state energy density as

$$e = n^3u(\gamma) \qquad u(\gamma) \equiv \frac{F(\tilde{G}^{-1}(\gamma))}{G^3(\tilde{G}^{-1}(\gamma))} \tag{2.45}$$

So system with the same value of $\gamma = c/n$ have the same physics.

Now we can look for the asymptotic regimes.

Strong repulsion We already pointed out that in the $c \to \infty$ regime the finite system behaves as spinless free fermions. We see the same for the thermodynamic limit, the kernel $\mathcal{K} \to 0$ and so the quasi-momenta distribution is given by

$$\tilde{\rho}(x) = \begin{cases} \frac{1}{2\pi}, |x| \le 1 \\ 0, |x| > 1 \end{cases}. \tag{2.46}$$

Finite interaction correction can be computed by expanding the kernel and the density in powers of $1/g$: at each order, the kernel is convoluted with the solution obtained at the previous order and thus the problem is reduced to integrating a rational function. In the way one get the following series expansion which is convergent for $\gamma > 2$

$$u(\gamma) = \frac{\pi^2}{3}\left[1 - \frac{4}{\gamma} + \frac{12}{\gamma^2} + \mathcal{O}\left(\frac{1}{\gamma^3}\right)\right]. \tag{2.47}$$

Weak interaction The $g \to 0$ limit is trickier because $\mathcal{K} \to -2\pi\delta(x)$, and so (2.39) becomes $\tilde{\rho}(x) = \frac{1}{2\pi} + \tilde{\rho}(x)$ which indicates that $\tilde{\rho}(x)$ is diverging. The $\gamma \to 0$ limit of this equation was rigorously studied in the context of the disk condenser (Love equation) by Hutson. We look for the leading term through an another method. Take (2.22) and apply the "duality" identity $\arctan x + \arctan\frac{1}{x} = sgn(x)\frac{\pi}{2}$, we get the rewriting

$$k_jL = 2\pi\left(I_j - j + \frac{N+1}{2}\right) + 2\sum_{i\neq j}\arctan\frac{c}{k_j - k_i} \qquad j = 1, 2, \ldots, N. \tag{2.48}$$

The term in parenthesis is zero for the ground state and in vicinity of $c = 0$ we can make the redefinition $k_j = \sqrt{2c/L}\chi_j$ and the expansion. The leading order gives

$$\chi_j = \sum_{i\neq j}\frac{1}{\chi_j - \chi_i} \qquad j = 1, 2, \ldots, N. \tag{2.49}$$

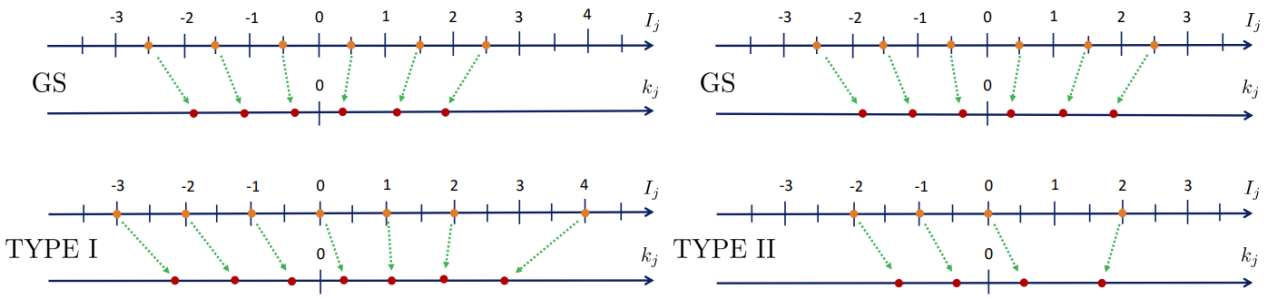

Figure 2.2: Pictorial representation of the two type of excitations. Firstly, we have a rearrangement of the quasi-momenta of all particles, due to the addition/removal of a particle. Then we either increase the Bethe integer of the greatest (or lowest) particle or remove a particle from the system. Figure taken from [31].

These $x_j's$ are the zeros of the Hermite polynomial of degree N. Their density in the asymptotic limit $N \to \infty$ is given by the Wigner semicircle law $\rho(x) = (1/\pi)\sqrt{2N - x^2}$. Making a change of variable from x to k and taking into account $q = 2\sqrt{cn}$ and $g = c/q$, we finally arrive at

$$\tilde{\rho}(x) \underset{g\to 0}{\sim} \frac{1}{2\pi g}\sqrt{1-x^2} \qquad u(\gamma) \underset{\gamma\to 0}{\sim} \gamma. \tag{2.50}$$

The full and correct expansion in g is

$$\tilde{\rho}(x) = \frac{1}{2\pi g}\sqrt{1-x^2} + \frac{1}{4\pi^2}\frac{1}{\sqrt{1-x^2}}\left[x \ln\frac{1-x}{1+x} + \ln\frac{16\pi e}{g}\right] + \mathcal{O}(1), \tag{2.51}$$

$$u(\gamma) = \gamma - \frac{4}{3\pi}\gamma^{3/2} + \mathcal{O}(\gamma^2). \tag{2.52}$$

2.7 Excitations

Before considering the finite temperature of the model, we should study the elementary excitations. There are two cases of these: we can add a *particle* with momentum $|k_p| > q$ or we can remove a particle with $|k_h| \leq q$ creating an *hole*. The excitation obtained taking a momenta inside the Fermi sea and move it above the threshold can be obtained as a combination of the latters. Let's start analyzing the first type of excitation, i.e. adding a particle. We know that the ground state is given by

$$\{I_j\} = \left\{-\frac{N-1}{2}, -\frac{N-3}{2}, \ldots, \frac{N-1}{2}\right\}, \tag{2.53}$$

adding a particle, say of positive momentum without loss of generality, the system rearrange itself

$$\{I'_j\} = \left\{-\frac{N}{2}, -\frac{N}{2}+1, \ldots, \frac{N}{2}-1, \frac{N}{2}+m\right\}. \tag{2.54}$$

A pictorial representation of what happens is shown in **Figure 2.2**. Such excitation has total momentum $K = \frac{2\pi}{L}m$[3] while the momentum of the added particle is $k_{N+1} = \frac{N\pi}{L} + \frac{2\pi}{L}m$. The latter is referred as *bare momentum* while the former *dressed momentum*, which is the one observed and obtained through a rearrangement of the whole system in reaction to the insertion of a new particle. This is a sign of the intrinsic non-local nature of one-dimensional system excitations and provides a concrete example of the concept that one-dimensional systems are intrinsically strongly interacting, regardless of the actual strength of the coupling constant. The same we get if we consider the insertion of a hole. We do not move on with the discussion of this point, which is fully treated in the lecture notes by Franchini [31]. We just emphasize that if one make the calculation for the changes of energy and momentum, these clearly display that this excitations has a collective nature and cannot be assigned simply at the single boson we added. This is the difference between the bare and dressed quantities. The final remark is that macroscopic observables are calculated by dressing their bare expressions, in contrast to what happens in higher dimensional systems. Later we will see how these dressing operation involves the integral kernel in (2.40), which encodes the effects of the interaction.

[3] Recall that the momentum is given by $K = \frac{2\pi}{L}\sum_j I_j$ regardless of c.

2.8 Thermodynamic Bethe ansatz and the Yang-Yang equation

Switching on the temperature, the particles undergo to excitations due to the thermal fluctuations. The procedure I'm going to show was firstly made by Yang and Yang [12] in 1969 and it is the first example of what is now called *Thermodynamic Bethe ansatz*(TBA). We will widely use this technique also for the Yang-Gaudin model and the two-component spinor-Bose gas.

As each eigenstate of the system is characterized by a set of Bethe numbers $\{I_j\}$, we can write the finite-temperature canonical partition function as

$$\mathcal{Z} = \frac{1}{N!}\sum_{\{I_j\}} \exp\frac{-E_N}{T} = \sum_{I_1<I_2<\ldots<I_N} \exp\frac{-E_N}{T}, \tag{2.55}$$

and for later convenience we introduce $n_j = I_{j+1} - I_j$

$$\mathcal{Z} = \sum_{n_1=1}^{\infty}\sum_{n_2=1}^{\infty}\cdots\sum_{n_{N-1}=1}^{\infty} e^{-E_N/T}, \tag{2.56}$$

where of course $E_N = \sum_{i=1}^{N} k_i^2$. In general, it is not easy to calculate the energy of the state directly from its quantum numbers ($\{I_j\}$). Thus, it is convenient to convert the sums into a functional integration over the rapidity density. In this way, we lose information on the microscopic of the state, setting the ground for the thermodynamic limit. We take the counting function $y(k)$ defined in (2.33), so $y(k_j) = \frac{2\pi}{L} I_j$. In general, due to excitations, the Bethe integers are not anymore ordered as in the ground state and there could be *holes* between two consecutive integers. This resembles the particle-hole formalism for the free fermions. Similarly, we are going to consider all the possible quasi-momenta for which the counting function takes a value $\frac{2\pi}{L}n$ for some n half-integer. We call these k_n^v *vacancies*

$$y(k_n^v) = \frac{2\pi}{L}n. \tag{2.57}$$

These vacancies are a sort of "placeholders" for the quantum numbers. The subset of $\{k_j\}$ that correspond to the Bethe numbers of the state are called *particles*, while the remaining solutions $\{k_j^h\} = \{k_n^v\}\backslash\{k_j\}$ are called *holes*. We can define the appropriate density of each of these, i.e. the density of quasi-momenta for the particles, holes and vacancies

$$\begin{aligned} \rho(k_j) &= \lim_{N,L\to\infty}\frac{1}{L(k_{j+1}-k_j)}, \qquad \rho_v(k_j^v) = \lim_{N,L\to\infty}\frac{1}{L(k_{j+1}^v - k_j^v)}, \\ \rho_h(k_j^h) &= \lim_{N,L\to\infty}\frac{1}{L(k_{j+1}^h - k_j^h)}. \end{aligned} \tag{2.58}$$

The physical meaning of that is given by the expression $L\rho(k)dk$ which states the number of particles in an interval dk and the same holds for particles and vacancies. So, holds the relation

$$y'(k_j^v) = \lim_{N,L\to\infty}\frac{y(k_j^v) - y(k_{j-1}^v)}{k_j^v - k_{j-1}^v} = \lim_{N,L\to\infty}\frac{2\pi}{L(k_j^v - k_{j-1}^v)} = 2\pi\rho_v(k_j^v), \tag{2.59}$$

and thus

$$y(k) = 2\pi\int^k \big[\rho(k') + \rho_h(k')\big]dk'. \tag{2.60}$$

We get another relation taking into account the thermodynamic limit of (2.33)

$$y(k) = k - \int_{-\infty}^{\infty}\theta(k-k')\rho(k')dk'. \tag{2.61}$$

Equating the RHS of the last two equations and taking the derivative with respect to k we get

$$\rho(k) + \rho_h(k) = \frac{1}{2\pi} - \frac{1}{2\pi}\int_{-\infty}^{\infty}\mathcal{K}(k-k')\rho(k')dk'. \tag{2.62}$$

The introduction of the density of holes removed the Fermi points, so now the integration is extended over the whole real axis. What's more, the most important difference compared to the zero temperature case is that the integral equation is not closed. Henceforth, differently from the case at zero temperature, the above thermodynamic limit of the Bethe ansatz equation will not be the master equation to solve the system, but we will use it as a constraint for further thermodynamic treatment.

We started this section with the task of calculate the canonical partition function of a N particle system. Now we want to take the thermodynamic limit

$$\begin{aligned} n_j &= I_{j+1} - I_j = \frac{L}{2\pi}[y(k_{j+1}) - y(k_j)] \\ &= \frac{L}{2\pi}\int_{k_j}^{k_{j+1}} \rho_v(k')dk' = \frac{L}{2\pi}\int_{k_j}^{k_j + \frac{1}{L\rho(k_j)}} \rho_v(k')dk' \simeq \frac{1}{2\pi}\frac{\rho_v(k_j)}{\rho(k_j)}. \end{aligned} \tag{2.63}$$

In taking the thermodynamic limit and switching to macroscopic quantities, we need to estimate the number of microstates which are not distinguishable in our macroscopic description, i.e. the entropy of each state. This can be calculated by counting in how many ways one can distribute a set of consecutive quantum numbers in an interval between particles and holes

$$\begin{aligned} d\mathcal{S} &= \ln \frac{[L(\rho(k) + \rho_h(k))dk]!}{[L(\rho(k)]![\rho_h(k))dk]!} \\ &\approx L[(\rho(k) + \rho_h(k)) \ln (\rho(k) + \rho_h(k)) - \rho(k) \ln \rho(k) - \rho_h(k) \ln \rho_h(k)]dk. \end{aligned} \tag{2.64}$$

This is also known as Yang-Yang entropy. Finally, taking the thermodynamic limit we send $N \to \infty$, so, the constraint in the number of particle given by the canonical ensamble is translated to the density of particle n. Thus, we obtain

$$\mathcal{Z} = const \int \mathcal{D}\left(\frac{\rho_v(k)}{\rho(k)}\right)\delta\left(\int \rho(k)dk - n\right)e^{\mathcal{S}-Le/T} \tag{2.65}$$

where e is of course the energy density per unit length of the state $e = E_N/L = \int k^2\rho(k)dk$. Now, we can move to the grancanonical ensamble, introducing the chemical potential μ, exploiting the equivalence between different ensambles in the thermodynamic limit. The reason for doing that is to easily compute the saddle point which is dominant for $L \to \infty$. In fact, this procedure is equivalent to minimize the canonical free energy with the number of particle constrained using the Lagrange multiplier method. This steps are taken from Takahashi [14]. The grancanonical free energy per unit length is

$$\begin{aligned} \mathcal{W} = e - Ts - \mu n = \int dk\big\{ &\big(k^2 - \mu\big)\rho(k) - \\ &T[(\rho(k) + \rho_h(k)) \ln (\rho(k) + \rho_h(k)) - \rho(k) \ln \rho(k) - \rho_h(k) \ln \rho_h(k)]\big\}. \end{aligned} \tag{2.66}$$

We have to minimize this both respect ρ and ρ_h and exploit the relation (2.62), that being linear is still valid for the differential of the root densities. Thus, imposing the saddle point for the free energy we have

$$0 = \int dk\left\{k^2 - \mu - T\ln\left(\frac{\rho(k) + \rho^h(k)}{\rho(k)}\right)\right\}\delta\rho(k) - T\ln\left(\frac{\rho(k) + \rho^h(k)}{\rho^h(k)}\right)\delta\rho^h(k). \tag{2.67}$$

Now from (2.62) we have the constraint

$$\delta\rho_h(k) = -\delta\rho(k) - \frac{1}{2\pi}\int_{-\infty}^{\infty} \mathcal{K}(k - k')\delta\rho(k')dk', \tag{2.68}$$

and substituting one gets

$$0 = \int dk\delta\rho(k)\left\{k^2 - \mu - T\ln\left(\frac{\rho^h(k)}{\rho(k)}\right) - \frac{T}{2\pi}\int dk'\mathcal{K}(k - k')\ln\left(1 + \frac{\rho(k')}{\rho^h(k')}\right)\right\}. \tag{2.69}$$

Introducing

$$\varepsilon(k) \equiv T \ln \frac{\rho_h(k)}{\rho(k)} \quad \text{equivalent to} \quad \frac{\rho_h(k)}{\rho(k)} = e^{\varepsilon(k)/T}, \tag{2.70}$$

we obtain the *Yang-Yang equation*

$$\varepsilon(k) = k^2 - \mu + \frac{T}{2\pi} \int_{-\infty}^{\infty} \mathcal{K}(k,k') \ln\left(1 + e^{-\varepsilon(k')/T}\right) dk'. \tag{2.71}$$

This is a non-linear Fredholm integral equation whose solution gives the dressed energy per particle excitation. The interpretation of the function $\varepsilon(k)$ is supported by noting that the number of particles over the number of available states is

$$n(k) \equiv \frac{\rho(k)}{\rho(k) + \rho_h(k)} = \frac{1}{1 + e^{\varepsilon(k)/T}}. \tag{2.72}$$

where we recognize the usual Fermi weight distribution. For a complete discussion about the interpretation of ε as dressed energy, take a look at [14]. We will often refer to $\varepsilon(k)$ as *dressed energy*. Finally, notice we have introduced the occupation function $n(k)$. The entropy evaluated at this saddle point gives

$$\mathcal{S} = L \int \left[\frac{1}{2\pi} \ln\left(1 + e^{-\varepsilon(k)/T}\right) + \frac{1}{T}(k^2 - h)\rho(k) \right] dk. \tag{2.73}$$

The free energy per unit length instead is

$$f = -\frac{T}{L} \ln \mathcal{Z} = \mu n - \frac{T}{2\pi} \int dk \ln\left(1 + e^{-\varepsilon(k)/T}\right). \tag{2.74}$$

We see now why the Bethe Ansatz construction is so powerful in addressing the thermodynamics of an integrable model: the free energy looks like the one of a non-interacting system with a non-trivial single particle spectrum $\varepsilon(k)$. So, once the Yang-Yang equation is numerically solved, the strongly interacting problem is reduced to the partition function of a free theory. Recall that the main difference with free theories is that here only dressed quantities are measurable, while the bare ones are not.

Final remark, the finite temperature description is quite independent from the original ansatz on the eigenstates. The only memory of the original model is encoded in the kernel. The density of quasi-momenta can be determined from the energy per particle as

$$2\pi\rho(k)\left[1 + e^{\varepsilon(k)/T}\right] = 1 - \int \mathcal{K}(k,k')\rho(k')dk'. \tag{2.75}$$

Zero temperature limit For the numerical treatment of the zero temperature case, it is useful to derive the limit of (2.71). We will see that it is useful both for getting the ground state and the time evolution. In order to take this limit, let's better understand the role that the dressed energy plays at $T = 0$. Because of there are no excitations, we have to reintroduce the Fermi points $\pm q$ and we require that

$$\begin{cases} n(k) = 1, & \text{for} \quad |k| \leq q \\ n(k) = 0, & \text{for} \quad |k| > q \end{cases}. \tag{2.76}$$

Thus, looking at the RHS of (2.72), we see that $\varepsilon(k) < 0$ for $|k| < q$ and $\varepsilon(k) > 0$ for $|k| > q$. Thus, $\varepsilon(\pm q) = 0$. Now, we take the limit separately for the two cases. For $\varepsilon > 0$, we have

$$\ln\left(1 + e^{-\varepsilon(k')/T}\right) \approx e^{-\frac{\varepsilon}{T}} \to 0. \tag{2.77}$$

Hence, there is no dressing. For $\varepsilon < 0$, we exploit

$$\ln(1+x) \underset{x\to\infty}{\approx} -\ln\left(\frac{1}{x}\right) + \frac{1}{x}. \tag{2.78}$$

Therefore $\ln\left(1+e^{-\varepsilon/T}\right) \approx -\frac{\varepsilon}{T}$. In the end, the $T=0$ version of the Yang-Yang equation is

$$\varepsilon(k) = k^2 - \mu - \int_{-q}^{q} \mathcal{K}(k,k')\varepsilon(k')dk', \tag{2.79}$$

with the boundary condition $\varepsilon(\pm q)=0$. Because of the occupation function is 1 for $k\in[-q,q]$ and 0 otherwise, the entropy of this system is zero. So we will refer to this case as the *zero entropy* case. It can be proved that the solutions of (2.79) satisfy the following properties:

$$\varepsilon'(k) > 0 \quad \text{for} \quad k>0, \tag{2.80}$$

$$\varepsilon(k) = \varepsilon(-k), \tag{2.81}$$

$$\varepsilon(k) < 0 \quad \text{for} \quad k<q, \tag{2.82}$$

$$\varepsilon(k) > 0 \quad \text{for} \quad k>q. \tag{2.83}$$

Finally, it can be shown that for $\mu<0$ the solution is $n=0$. Thus, we have to restrict to positive chemical potential, where dressed energy has two real zeros, i.e. the Fermi points.

2.9 Numerical solutions

Here I am going to present the algorithms for the numerical solutions of both the zero and finite temperature cases.

Zero entropy We saw that at zero temperature the master equation for the system is

$$\rho(k) = \frac{1}{2\pi} - \frac{1}{2\pi}\int_{-q}^{q} \mathcal{K}(k-k')\rho(k')dk', \tag{2.84}$$

which is a linear Fredholm integral equation (FIE). This kind of equations have a wide literature in mathematics, which we are not going to explore, but I will give a "practical" method for its solution. Generically, we can write a linear FIE as

$$h(x) = w(x) - \int_{x_-}^{x_+} dy\mathcal{K}(x-y)h(y). \tag{2.85}$$

For the numerical solution, we firstly discretize the space, thus, the continuous interval $[x_-,x_+]$ becomes the discrete set of M elements $x_j = x_- + \Delta j$ with $\Delta = \frac{x_+-x_-}{M-1}$ such that $x_0 = x_-$ and $x_{M-1}=x_+$. In this way, the functions $h(x)$ and $w(x)$ become M-dimensional vectors and the integral kernel $\mathcal{K}$ an $M\times M$ matrix. Thus, we obtained

$$h_j = w_j - \Delta\sum_{m=0}^{M-1}\mathcal{K}_{jm}h_m \quad \text{for} \quad j=0,\dots,M-1. \tag{2.86}$$

Absorbing Δ in $\mathcal{K}$ and using simple linear algebra, we get the result

$$\vec{\mathbf{h}} = (1+\mathcal{K})^{-1}\vec{\mathbf{w}}. \tag{2.87}$$

The flux diagram is reported in **Figure 2.3**, we gave to this "block" the name *LFIE_solver* because we are going to recall this later. The real problem we have to face is how to find the Fermi points. Before, we said that from a theoretical point of view, they can be set imposing $\int_{-q}^{q} dk\rho(k) = N/L$. Despite this is correct, such a condition is difficult to implement numerically. Thus, as promised, we are going to use (2.79). In fact, that is also a linear FIE, so, we can solve it as outlined above and next require to numerically find the value of q such that $\varepsilon(\pm q)=0$. An example of a root density at $T=0$ is provide in **Figure 2.4**.

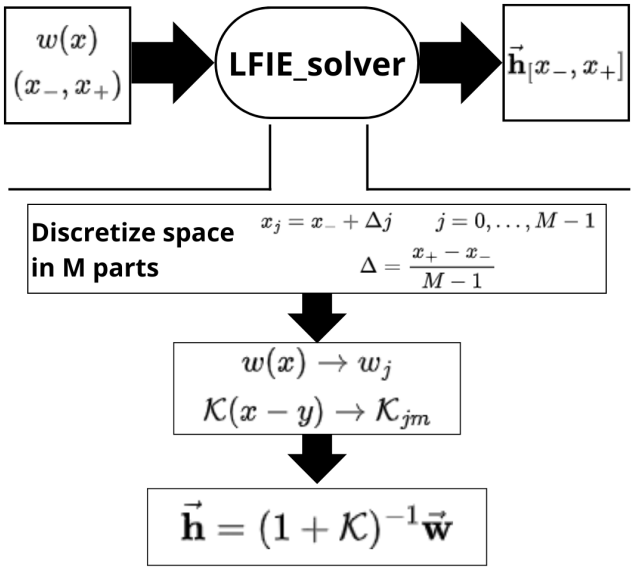

Figure 2.3: Flux diagram for the numerical solution of a linear Fredholm integral equation. We gave as input the bare function and the Fermi points, and the block returns the *dressed* function. We put the pedix on the output to stress that it depends on the input Fermi points.

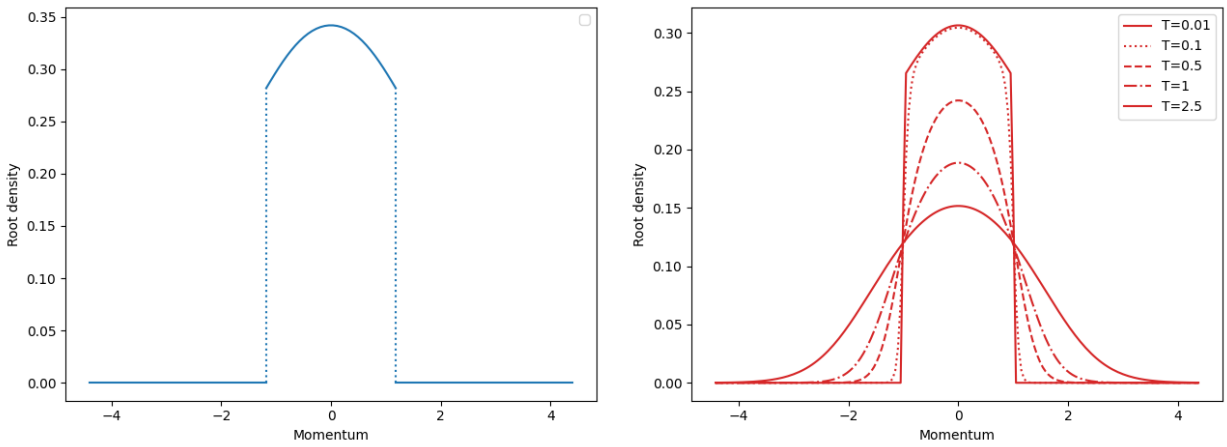

Figure 2.4: Root densities for a Lieb-Liniger gas with parameters are $c = 1$ and $\mu = 1$. On the left panel there is the T=0 case. We see that the density is not smooth and there is a rigid cutoff in the quasi-momenta. The Fermi points are ± 1.18. On the right panel there is the $T > 0$ case, with five different temperatures. We can distinctly see that for very low temperature the root density is similar to the $T = 0$ case. Increasing the temperature it starts smearing out.

Finite temperature In this case the Yang-Yang equation (2.71) is a non-linear Fredholm integral equation. Generically, we can write it as

$$h(x) = w(x) + \int_{-\infty}^{\infty} \mathcal{K}(x-y)F[h(y)]dy. \tag{2.88}$$

Because of in the RHS the function h appears inside a functional, the kernel inversion technique adopted for the zero entropy case is not still valid. Thus, we are going to use an iterative strategy that involves the fast Fourier transform (FFT). The idea of using the Fourier transform arises because the *dressing operation* is a convolution. Thus, a convolution transforms into a product in the Fourier dual space

$$\mathcal{K} * F[h] = \tilde{K} \cdot \tilde{F}. \tag{2.89}$$

The Fourier transform of the kernel can be analytically computed

$$\mathcal{F}[\mathcal{K}(x)](\omega) = \frac{1}{\sqrt{2\pi}} \int_{-\infty}^{\infty} e^{i\omega x}\mathcal{K}(x)dx = \sqrt{2\pi}e^{-c|\omega|}, \tag{2.90}$$

while, of course, we cannot compute analytically the Fourier transform of $F[h]$ because we do not know the function. Hence, the idea is again to discretize the set of momenta and exploit the FFT algorithm, which computes the Fourier dual of a discrete vector. For details on the FFT algorithm implemented in python, you can take a look to the scipy documentation. Even though the integration is in the entire real space, we can justify the discretization of the momenta by looking at **Figure 2.4**. We expect that at finite temperature some quasi-momenta above the Fermi points "activate". Therefore, we assume that for every T there is a sufficiently high cutoff in the quasi-momenta Λ, such that $\rho(k) = 0$ for $|k| > \Lambda$. In this way, the integral is turned into a summation. Although we could just compute this summation, the FFT algorithm is very fast and thus preferable. For the kernel we have just to compute the coefficient of the Fourier series, which can be done just inserting discrete frequencies in (2.90). In contrast the functional, which is become a vector after the discretization, is transformed via the FFT algorithm. A brief remark is that one has to match the Fourier transform make as in (2.90) and the definition of FFT of the algorithm in scipy. In particular, one can show that for the Yang-Yang equation (2.71)

$$\frac{2\Lambda}{M-1}\sum_{m=0}^{M-1}\mathcal{K}_{jm}F_j = -T\text{ifft}\Big[e^{-ij\pi}e^{-\frac{\pi c}{\Lambda}j}\tilde{F}_j\Big] \quad \text{for} \quad j = 0,\dots,M-1, \tag{2.91}$$

where $\tilde{F}_j$ is the FFT of the vector $\vec{\mathbf{F}}$ and "ifft" denotes the inverse FFT algorithm. Now we described the way to faster compute the convolution, we can easily compute the r.h.s. of equation (2.88)

$$(h)_j = (w)_j - T\text{ifft}\Big[e^{-ij\pi}e^{-\frac{\pi c}{\Lambda}j}\tilde{F}_j\Big] \quad \text{for} \quad j = 0,\dots,M-1. \tag{2.92}$$

We call this intermediate block *conv_solver* and the flux diagram is reported in **Figure 2.5**. At this point, we can solve the non-linear Fredholm in an iteratively way, inserting a mock value of the function h until convergence. In particular, the starting value will be the *bare*, i.e. non-dressed, function $w(x)$. Inserting this in the RHS of (2.88), we obtain h_{new}

I set that the algorithm converges when the greater between the absolute and relative error between h_{new} and h_{old} is under 10^{-12}. We call this block *NLFIE_solver* and we report the flux diagram in **Figure 2.5**. A plot of the root densities for different temperatures is reported in **Figure 2.4**.

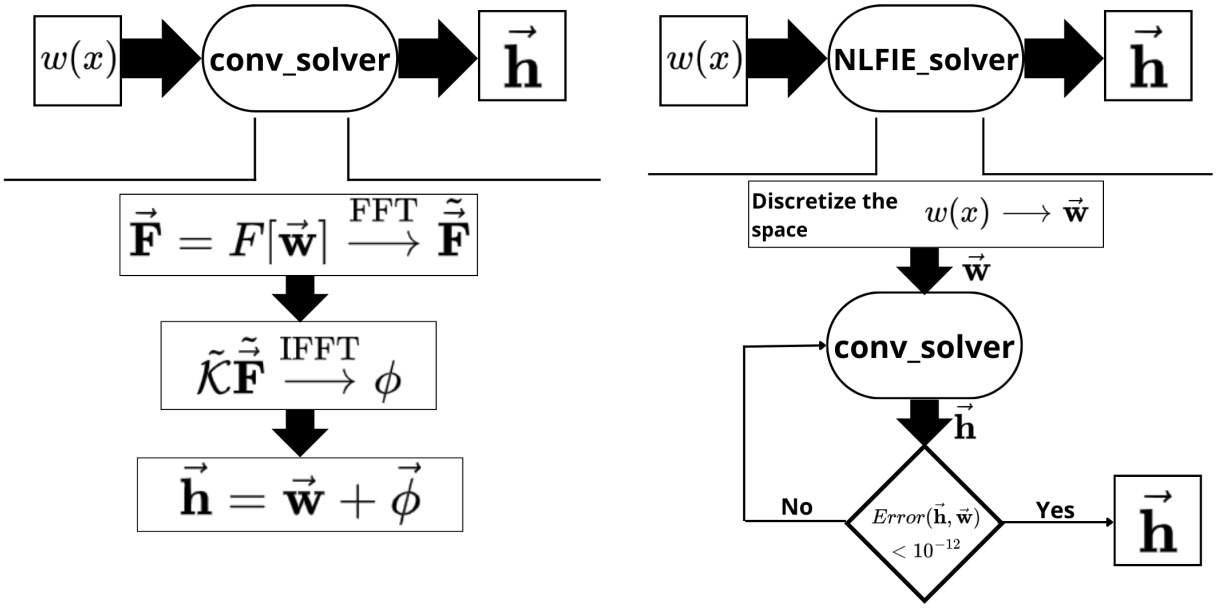

Figure 2.5: On the left panel the block *conv_solver* that recive as input a function $w(x)$ and gave as output the r.h.s. of (2.88). This the fundamental step for the iterative solution of the non-linear Fredholm equation. On the right panel the block that solves the non-linear Fredholm.

Chapter 3

Generalised Hydrodynamics

Beside the upsetting result of quantum Newton cradle experiment we mentioned in the Introduction, integrable systems has recently received a renewed interest, thanks to novel experimental techniques to trap cold atoms in one-dimensional setups, and because they are widely present in one-dimension. They present an extremely rich phenomenology and, since they allow us to find exact relations between physical quantities, they represent a nice way to test principles and paradigms of the physical theories. The study of the out-of-equilibrium behaviour of integrable systems received a revolutionary contribution in 2016 with the introduction of generalised hydrodynamics (GHD) [32, 33]. This theory has suddenly caught a lot of interest in the community. In the first papers were derived, both for continuum systems [32] and spin chains [33], the equations for the Euler hydrodynamics, i.e. without diffuse contribution. In the following years the theory has been proved to be extremely versatile, and several theoretical improvement has been added, like diffusive terms, external forcing potentials and it has also been applied for the computation of correlators. In this chapter we are going to review standard hydrodynamics and see how the introduction of the generalised Gibbs ensambles (GGEs) joint with the TBA machinery, leads to this theory for the the hydrodynamics of integrable systems. Next we are going to show how this theory can be used to predict the dynamics in quench protocols and we will study the explicit example of a harmonic trap release for a Lieb-Liniger gas. The numerical algorithm will be present both at finite and zero temperature. In particular, the latter case is special due to the fact of having zero entropy and substantial simplifications arise. In this Chapter I will mainly follow the lecture notes from Doyon [58].

3.1 Hydrodynamics as conservation laws

When we hear about hydrodynamics we are used to thinking to Euler and Navier-Stokes equations. Considering a one-dimensional Galileian fluid with $\rho(x,t)$ its local mass density, $v(x,t)$ its local velocity field, $P(\rho)$ the pressure as function of the local mass density and finally, ξ its viscosity, the two hydrodynamic equations take the form

$$\begin{aligned} &\partial_t \rho(x,t) + \partial_x[v(x,t)\rho(x,t)] = 0, \\ &\partial_t v(x,t) + v(x,t)\partial_x v(x,t) = \frac{1}{\rho(x,t)}[-\partial_x P(\rho(x,t)) + \xi\partial_x^2 v(x,t)]. \end{aligned} \tag{3.1}$$

The local mass density and the velocity are the fields that describe the dynamics of the system, while the pressure and the viscosity are model-dependent quantities. The first equation is manifestly the conservation of the mass of the fluid. The second equation tells us about the evolution of the velocity field in space and time in terms of the pressure and the viscosity. The second derivative term is usually referred to as the diffusive term. In full generalities these are the Navier-Stokes equation, while setting to zero the viscosity we get the Euler equations. Hydrodynamics is an old theory in physics and the validity of this equations is a well established experimental fact. From a theoretical point of view, the power of this approach is in the extreme reduction of the degrees of freedom from about the 10^{23} of the

individual particles to only the local density field $\rho(x,t)$ and the velocity field $v(x,t)$. This reduction of the degrees of freedom is at the hearth of every statistical approach to many-body systems. The second remarkable fact is that this two equations can be recast as conservation laws. Actually, defining $p = v\rho$ and $j_\rho = P + v^2\rho - \xi\partial_x v$ the equations take the form

$$\begin{aligned} &\partial_t \rho(x,t) + \partial_x p(x,t) = 0, \\ &\partial_t p(x,t) + \partial_x j_p(x,t) = 0. \end{aligned} \tag{3.2}$$

Thus, the core of hydrodynamics is in the conservation law of the macroscopic quantities we introduce for the coarse-grained description of the system. In the next section we will derive this equations exploiting the formalism of statistical mechanics. Next, we will specialize to integrable systems and see the peculiarities of these models.

3.2 Local entropy maximisation and Euler Hydrodynamics

Let's consider an homogeneous, isolated many-body one-dimensional system of infinite length with short-range interactions. Suppose that this system admits a set of locally conserved charges that satisfy conservation laws

$$Q_i = \int dx q_i(x,t), \qquad \partial_t q_i(x,t) + \partial_x j_i(x,t) = 0, \qquad \partial_t Q_i = 0, \tag{3.3}$$

for a certain current $j_i(x,t)$. The theory of statistical mechanics postulate that if any finite region of this system starts in an arbitrary homogeneous state, after a long enough time the system "relax" to a certain equilibrium state, with the rest of the infinite system acting as a bath. In particular, we know that the average of the local observables can be obtained through the density matrix ρ by

$$\langle o \rangle = Tr[\rho o]. \tag{3.4}$$

For all the chapter I am going to use the quantum mechanics formalism, that for instance involves the trace for the statistical average. Everything I am going to say is valid also for classical systems, with the prescription of substituting the trace with an integral with some appropriate measure in the phase space.

The equilibrium state is postulated to be the one which maximize the entropy of the system, defined as $S = -Tr[\rho \log \rho]$. Since we are at equilibrium, averages of conserved densities cannot change, and in the minimization procedure we have to introduce some Lagrange parameters for the constraints. In particular we will refer as β_i for the conserved quantities Q_i and α for the normalization of the density matrix. Hence, we get

$$\delta Tr\left[\rho\left(\log\rho + \sum_i \beta_i Q_i + \alpha\right)\right] = 0 \Longrightarrow Tr\left[\delta\rho\left(\log\rho + 1 + \sum_i \beta_i Q_i + \alpha\right)\right] = 0. \tag{3.5}$$

Hence, the *maximal entropy states* are of the Gibbs form [59]

$$\rho \propto e^{-\sum_i \beta_i Q_i}. \tag{3.6}$$

The Lagrange parameters β_i I introduced are often referred to as *generalised inverse temperatures* or *generalised chemical potentials*. These ensambles are called generalised Gibbs ensambles, for obvious reasons.

Now let's consider a many-body system in an inhomogeneous and non-stationary initial state. In such a configuration the local averages of the macroscopic observables depend on the position and change as the time passes. Hydrodynamics is the theory that describes how this averages evolve in time. The key concept of this theory is the *separation of scales*. We assume the existence of a mesoscopic scale intermediate between the microscopic and the macroscopic scale. The microscopic scale is the typical length, say a, for the elementary constitutes of the system, for instance the atoms or the molecules of

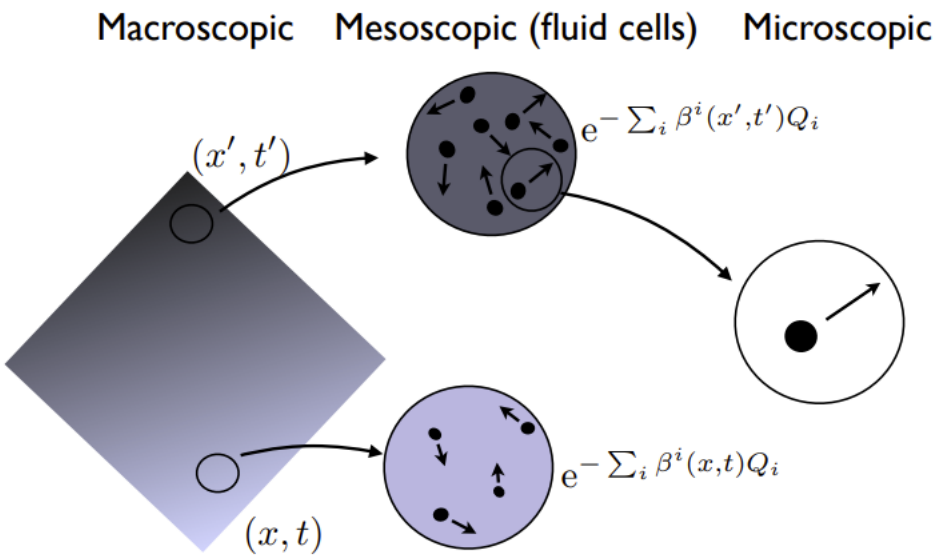

Figure 3.1: Pictorial representation of the separation of scales in the hydrodynamics theory. Figure taken from [58].

a gas. The dynamics is described by the equations of motion of the system. The macroscopic scale is instead the typical length for the thermodynamical treatment and cover the whole system, say of length L. In order to describe an inhomogeneous system, we assume the existence of an intermediate mesoscopic scale, still bigger than the microscopic scale a but smaller than the macroscopic length L. If we call this typical length l, the relation $a \ll l \ll L$ holds. For a pictorial representation see **Figure 3.1**. The idea at the core of hydrodynamics is to subdivide the inhomogeneous system at the mesoscopic scale into *fluid cells* that are approximately homogeneous. Thus, we introduce the basic assumption of hydrodynamics, i.e. the *local entropy maximisation*

$$\langle o(x,t)\rangle \approx \langle o(0,0)\rangle_{\beta(x,t)}\,, \tag{3.7}$$

where $\beta = \{\beta_1, \beta_2, \ldots, \beta_N\}$. The state $\langle\cdots\rangle_{\beta(x,t)}$ is the maximal entropy one, as defined above with the generalised inversed temperatures that depends on the fluid cell $\beta(x,t)$. Being this state homogeneous and stationary, we can position the observable at any point and for convention we chose the origin (0,0). The validity regime of this approximation is an involved question and it is discussed in Ref. [58]. In general, we could say that this assumption holds for homogeneous systems and it could be a good approximation also for slightly inhomogeneous ones. In particular, as we will see, the hydrodynamics equations we will derive in this regime are the Euler equations, thus neglecting the diffusive term. We will not deepen this topic because in this thesis I will use only the equations of the Generalised Hydrodynamics without the diffusion, as derived in the first papers [32,33]. The generalisation to the diffusive regime was done by De Nardis et al. in several works, for instance Refs. [34,35]. The main idea is to introduce a spatial derivative expansion for the Lagrange multipliers in the exponent of the density matrix of the Gibbs ensamble, in order to take account the spatial modulations. At first order one recover the Navier-Stokes equations. Now let's forget about this and let's move to the derivation of the Euler equations.

Once we assumed the local entropy maximisation inside the fluid cell, we can derive the Euler equations starting from the microscopic dynamics, in particular from the conservation laws (3.3). Let's rewritten these in integral form over a contour of dimension $[0,X]\times[0,T]$

$$\int_0^X dx(q_i(x,T) - q_i(x,0)) + \int_0^T dt(j_i(X,t) - j_i(0,t)) = 0. \tag{3.8}$$

Now let's introduce a notation for the local averages evaluated in the local entropy maximised state

$$\mathrm{q}_i(x,t) = \langle q_i(0,0)\rangle_{\beta(x,t)}\,, \qquad \mathrm{j}_i(x,t) = \langle j_i(0,0)\rangle_{\beta(x,t)}\,. \tag{3.9}$$

Evaluating equation (3.8) within the state $\langle\cdots\rangle_{\beta(x,t)}$ we obtain

$$\int_0^X dx(\mathrm{q}_i(x,T)-\mathrm{q}_i(x,0))+\int_0^T dt(\mathrm{j}_i(X,t)-\mathrm{j}_i(0,t))=0. \tag{3.10}$$

Despite this last equation resembles equation (3.8), there is an important conceptual difference. One is a relation between microscopic quantities, the other relates the averages in local maximal entropy states. If these averages are differentiable, we obtain the standard derivative form of the Euler equations

$$\partial_t \mathrm{q}_i(x,t)+\partial_x \mathrm{j}_i(x,t)=0, \tag{3.11}$$

where again I stress that it is a relation for the local averages. Note that the number of conserved charged densities $q_i(x,t)$ and the number of generalised inversed temperatures β_i are the same. Hence, to characterize a state we can either use the set of local Lagrange multipliers $\beta(x,t)$ or the averages of the conserved densities in the maximal entropy states $\mathrm{q}=\{\mathrm{q}_1,\mathrm{q}_2,\ldots,\mathrm{q}_N\}$. Hence, all the averages in these states can be expressed in term of q. In particular, the relations between the average currents on the average density are called *equations of state*

$$\mathrm{j}_i=\mathrm{j}_i(\mathrm{q}), \tag{3.12}$$

and are model dependent functions.

3.3 Integrable systems and generalised Gibbs ensamble

Now we want to apply the principles of hydrodynamics to integrable systems. This could be done both for classical and quantum systems, however for continuity with the previous Chapter and for consistency with the work of the thesis, we will use the concrete example of the Lieb-Liniger model. Furthermore, despite Lieb-Liniger describes a system of particles, this procedure also applies to spin chains. The discussion in this section will follow mainly Ref. [60]. Let's start considering the Lieb-Liniger model of N δ-interacting bosons with Hamiltonian

$$\hat{H}_{LL}=-\frac{1}{2}\sum_{j=1}^{N}\frac{\partial^2}{\partial x_j^2}+2c\sum_{j<l}\delta(x_j-x_l), \tag{3.13}$$

with c a positive constant that parameterise the interaction strength. This model is integrable in the sense that have infintely many conserved charges in involution.[1] The form of this conserved charges is quite complicated [61, 62]. For sure, we have the three conserved charge of a general Galileian gas

$$\hat{Q}_0=N\mathbb{I},\qquad \hat{Q}_1=\hat{P}=\sum_{i=1}^{N}(-i)\frac{\partial}{\partial x_i},\qquad \hat{Q}_2=\hat{H}_{LL}, \tag{3.14}$$

and in general they are some deformations of the charges of a free model, where $\hat{Q}_n=\frac{1}{n!}\sum(-i\frac{\partial}{\partial x_i})^n$. The important property of this infinite set of conserved charges is that they are in involution, i.e. $\left[\hat{Q}_n,\hat{Q}_m\right]=0$. In addition, we assume the extensivity of the conserved charges $\hat{Q}_n$, i.e. that they are the integral of some local density

$$\hat{Q}_n=\int dx\hat{q}_n(x,t), \tag{3.15}$$

and this local densities satisfy appropriate conservation laws

$$\partial_t\hat{q}_n(x,t)+\partial_x\hat{j}_n(x,t)=0, \tag{3.16}$$

for some local currents $\hat{j}_n(x,t)$. Although the explicit form of this conserved charges is difficult to construct in general, their eigenvalues can be obtained by acting on a generic state labelled by the

[1] Quantum integrability is a fascinating and delicate topic and there is still not a unique definition of what a quantum integrable system is. A thorough discussion of this is in Ref. [26].

quasi-momenta. In fact, as we saw in Chapter 2, any state in the Hilbert space of the Lieb-Liniger model can be described by a set of quasi-momenta. One can prove that these states are eigenvalues for the conserved charges, in particular

$$\hat{Q}_n \left|\{p_i\}\right\rangle = Q_n \left|\{p_i\}\right\rangle = \sum_i h_n(p_i) \left|\{p_i\}\right\rangle, \tag{3.17}$$

where $h_n(p_i)$ is the amount of charge $\hat{Q}_n$ carried by the particle with quasi-momentum p_i. For instance, for the three charges we explicitly wrote before we have

$$h_0(p) = 1, \qquad h_1(p) = p, \qquad h_2(p) = \frac{p^2}{2}, \tag{3.18}$$

and in general they take the form $h_n(p) \propto \sum_i p_i^n$. For the uppermost role that momentum and energy will have in the following derivation, we rename its charges $P(p) = h_1(p)$ and $E(p) = h_2(p)$.

In the previous section we derived the Euler equations relying on the assumption of local entropy maximisation, i.e. that the state of each fluid cell can be described by a Gibbs-like density matrix as (3.6). Now that the model has infinitely conserved charges, we guess that the relaxation happens with respect to the generalised Gibbs ensamble (GGE) [59], i.e.

$$\hat{\rho} \propto e^{-\sum_n^\infty \beta_n \hat{Q}_n}, \tag{3.19}$$

where we associated a Lagrange multiplier to each of the infinite conserved charges of the model. The GGEs are a quite complicated topic we will not deepen, however it has been extensively studied, see for instance Refs. [63–66]. For our purposes, we will rely on the validity of this ansatz. Again, being this a local maximisation of the entropy, this is supposed to be valid if the changes in the local averages happen at large enough scale in time and space. We can express (3.19) in terms of the eigenvalues of the conserved charges as

$$\hat{\rho} \propto e^{-\sum_i w(p_i)}, \tag{3.20}$$

where $w(p) = \sum_n^\infty \beta_n h_n(p)$ is the spectral function and fully fixes the GGE.

The power of integrable models lays in the fact that we can describe the GGEs via the TBA. Let's consider the thermodynamic limit of the states (3.19), the averages of the local observables are

$$\langle \cdots \rangle = \lim_{L\to\infty} Tr(\hat{\rho} \cdots), \tag{3.21}$$

and this can be computed exploiting the thermodynamic Bethe ansatz technology we introduced in the previous Chapter. We said that in the thermodynamic limit, the Bethe equation for the Lieb-Liniger model becomes

$$2\pi\rho^{tot}(p) = P'(p) - \int dp' \phi(p,p')\rho_p(p'), \tag{3.22}$$

where with P' we mean its first derivative, $\phi(p,p') = \frac{2c}{c^2+(p-p')^2}$ is the scattering kernel and ρ_p the particles density. In this way, once we have the particles density, from (3.17) we read that we can compute the averages of the conserved charges as

$$\lim_{L\to\infty} \frac{Q_n}{L} = \int dp h_n(p)\rho_p(p). \tag{3.23}$$

As we already saw in the section on Yang-Yang thermodynamics, the Bethe equation (3.22) is not closed, hence it cannot be used alone to solve the system. In that section we followed the procedure of Yang and Yang, building the partition function with respect to a grancanonical ensamble, thus, relaxing the system both with respect to energy and the number of particles. In this way, minimizing the free energy and imposing on the differentials a constrain given by the Bethe equation, we got

$$\frac{\varepsilon(p)}{T} = \frac{E(p)-\mu}{T} - \int \frac{dp'}{2\pi} \phi(p,p') \ln\left(1 + e^{-\varepsilon(p')/T}\right), \tag{3.24}$$

where $E(p)$ is the bare energy and μ the chemical potential. For the hydrodynamical treatment, we want to relax the system with respect to the GGE. The naive idea is to consider the whole system as a reservoir for each fluid cell, thus exchanging all the conserved charges of the system. Consequently, the partition function is given by

$$\mathcal{Z} = \int \mathcal{D}[\rho_p, \rho_h] \exp\left(\mathcal{S}_{YY}[\rho_p, \rho_h] - w[\rho_p]\right), \tag{3.25}$$

where $\mathcal{S}_{YY}$ is the Yang-Yang entropy defined as in Chapter 2, and $w[\rho_p] = \int dp w(p)\rho_p(p)$. Defining the dressed energy $\varepsilon/T = \log(\rho_h/\rho_p)$, the saddle point condition in this case gives

$$\frac{\varepsilon(p)}{T} = w(p) - \int \frac{dp'}{2\pi}\phi(p,p')\ln\left(1 + e^{-\varepsilon(p')/T}\right). \tag{3.26}$$

Defining the occupation function

$$n(p) = \frac{1}{1 + e^{\varepsilon(p)/T}}, \tag{3.27}$$

we can obtain the particles density $\rho_p = \rho^{tot} n$. In particular, if we introduce the *dressing operation* for a generic function, defined as the solution of the integral equation

$$h^{dr}(p) = h(p) + \int dp' \phi(p,p') n(p') h^{dr}(p'), \tag{3.28}$$

we can write

$$2\pi\rho^{tot} = (P')^{dr}. \tag{3.29}$$

Until now, we have introduced the GGEs and showed how we can compute the local averages of the conserved charges using the TBA technology. One have firstly to solve equation (3.26) to find the dressed energy, with which compute the occupation function. With the latters, one can solve the dressing in equation (3.29), obtaining the particles density for computing the averages of the charges as in equation (3.23).

The last step we need for the construction of the hydrodynamics of the integrable systems are the equations of state, i.e. the relations between the current densities and the charge densities. This result has been the main technical achievement of the first two papers on GHD [32,33]. We will follow the derivation of the original paper on GHD [32], reported also on the lecture notes from Benjamin Doyon [58]. Let's consider a relativistic quantum field theory. In general, we require that this satisfy the crossing symmetry, i.e. symmetry under a particular exchange of space and time $(x,t) \to (-it, ix)$. From the point of view of energy and momentum, this translates in $(p,E) \to (iE, -ip)$. Thus, under crossing densities and current are exchanged. Hence, the idea is that since we already know how to compute charge densities, we can apply crossing and compute the current densities exchanging energy and momentum. Equation (3.23) tells us that

$$\langle \hat{q_n} \rangle = \mathrm{q}_n = \int dp h_n(p)\rho_p(p), \tag{3.30}$$

which can be rewritten as

$$\mathrm{q}_n = \int \frac{dp}{2\pi}(P')^{dr} n(p) h_n(p). \tag{3.31}$$

Hence, with the prescription of exchanging energy and momentum, we guess that the current density is

$$\mathrm{j}_n = \int \frac{dp}{2\pi}(E')^{dr}(p) n(p) h_n(p). \tag{3.32}$$

Defining the effective velocity

$$v^{\mathrm{eff}}(p) = \frac{(E')^{dr}(p)}{1^{dr}(p)} = \frac{(E')^{dr}(p)}{2\pi\rho^{tot}(p)}, \tag{3.33}$$

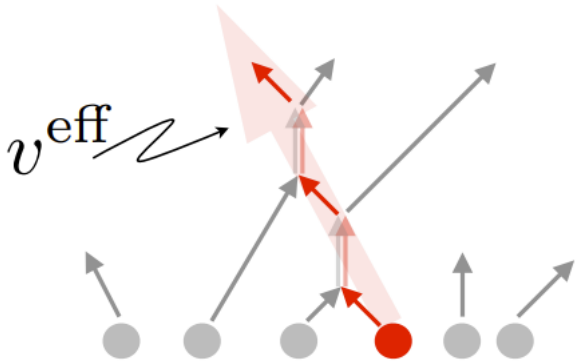

Figure 3.2: In this cartoon is shown how the effective velocity arise as large-scale velocity of a particle inside the gas due to the scattering with the other particles. Figure taken from [58].

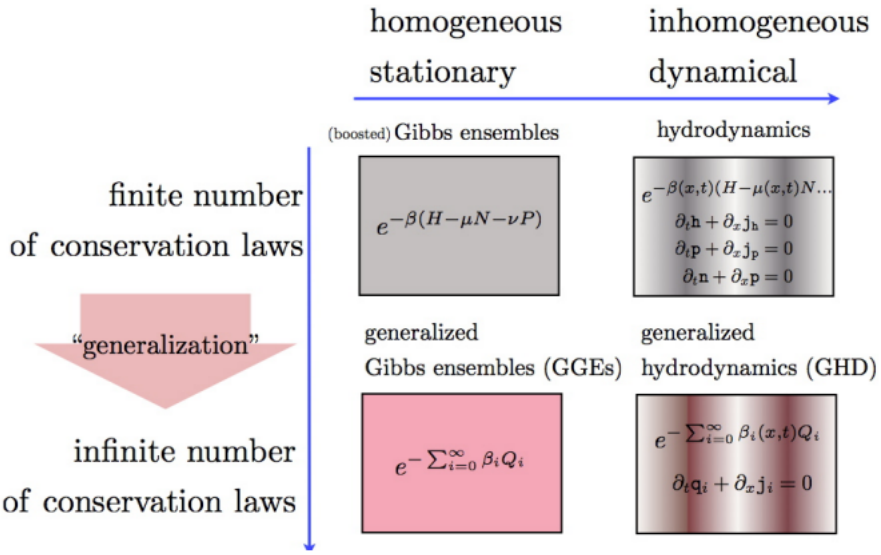

Figure 3.3: Schematics representation of the idea underlying the generalised hydrodynamics. Figure taken from [58].

we can rewrite the current density in a standard form where the group velocity is replaced by the effective velocity

$$\mathrm{j}_n = \int \frac{dp}{2\pi} v^{\text{eff}}(p)\rho_p(p)h_n(p). \tag{3.34}$$

In this form becomes natural to interpret the effective velocity as the large-scale velocity of the quasi-particle inside the gas, actually different from the group velocity $E'(p)$ due to the interaction with the other particles. A pictorial representation is in **Figure 3.2**.

All this derivation is based on the guess in equation (3.32). A formal proof for integrable spin chains has been recently derived by Pozsgay and Borsi [67], however it discussion is beyond the scope of this thesis. Furthermore, the equations of the generalised hydrodynamics that will arise from this are experimentally well tested [45, 46]. For a theoretical discussion on its validity check Ref. [58].

3.4 Fundamental equations of generalised hydrodynamics

Now we have all the ingredients to build the theory for the Euler hydrodynamics of integrable systems. Since this rely on the GGEs, it has been dubbed generalised hydrodynamics. See **Figure 3.3**.

Before explicitly derive the equations, I want to recall the two underlying assumption we made in this

derivation. The first one is that the variations in the system happens at large enough scales, so we are allowed to assume the local entropy maximization with respect to the GGE. The second assumption is that in each fluid cell the number of particles is high enough to allow using the TBA.

In the previous section, we saw how to compute the local averages in each fluid cell. Now, in order to write the equations for the hydrodynamics, we have to make this quantities dependent on space and time, i.e. different quantities for each fluid cell

$$\rho_p(p) \to \rho_p(p,x,t), \qquad n(p) \to n(p,x,t), \qquad v^{\text{eff}}(p) \to v^{\text{eff}}(p,x,t). \tag{3.35}$$

Now we have simply to insert the expression for the charges (3.30) and the currents (3.32) inside the Euler equations (3.11) we derived at the beginning of this Chapter. In this way, we get

$$\int dp h_i(p) \Big(\partial_t \rho_p(p,x,t) + \partial_x \Big[v^{\text{eff}}(p,x,t) \rho_p(p,x,t) \Big] \Big) = 0. \tag{3.36}$$

Since this has to be valid for every conserved charge, we obtain the Euler-scale GHD equations

$$\partial_t \rho_p(p,x,t) + \partial_x \Big[v^{\text{eff}}(p,x,t) \rho_p(p,x,t) \Big] = 0. \tag{3.37}$$

Due to the dependence of v^{eff} on ρ_p through interactions, this an integro-differential equation, which is first-order in derivatives and highly nonlinear. The analytical and numerical solution will be discussed in the next sections. In particular, we will see that important simplifications arise at $T = 0$. Finally, this continuity equation can be diagonalised using the occupation function [58]

$$\partial_t n(p,x,t) + v^{\text{eff}}(p,x,t) \partial_x n(p,x,t) = 0. \tag{3.38}$$

This version of the GHD equation tells us that the occupation function, which is the density of particles in an interval $[p, p+dp]$, is convectively transported. This is the most important version of the GHD equation and it will be our starting point for both the analytical and numerical solution.

Before moving to the quenches, I want to stress one final remark. Equations (3.37) and (3.38) are the simplest version of the GHD equations, as well as the ones who were derived in the originals papers [32,33] for a bipartitioning protocol where two different GGEs are joined together and let to unitarily evolve. We will extend this setting to generic inhomogeneuos profiles of the initial state, excluding more sophisticated effects, like diffusion or the presence of an external forcing [30,34,36,68,69]. Despite it is known how to take into account these effects, we will not consider these terms in this thesis.

3.5 Quench protocols

One of the most interesting setups in order to apply and test the generalised hydrodynamics are the quantum quenches. In these settings, the system is prepared in an initial equilibrium state, then suddenly this equilibrium is broken by changing a parameter in the Hamiltonian, and the system develops an out of equilibrium dynamics. In this thesis we will focus on the harmonic trap release, i.e. the quench protocol where the system is initially confined by a harmonic potential which is suddenly turned off and the system evolves freely. Despite the Euler hydrodynamics is valid in the limit in which the variations happen at large space and time, hence not suddenly, we observe that the dynamics is well described by the equations of GHD still at relatively small times. In this section we are going to see how to compute the initial state for the Lieb-Liniger model trapped by a harmonic potential, and in the next sections we will see how to numerically solve the GHD equations both at zero and finite temperature. In the next Chapter, we will apply this protocol to the two multi-component systems we will compare in this thesis, the Yang-Gaudin model and the two-component spinor Bose gas. Before moving further, I want to recall and stress that the GHD equations (3.37) apply only to a system that evolves freely, without an external potential. Despite one can add the acceleration with a minimal correction to those equations, since in this thesis we will focus on trap releases we will neglect this term. A complete discussion can be found in Ref. [69] and in the notes [58].

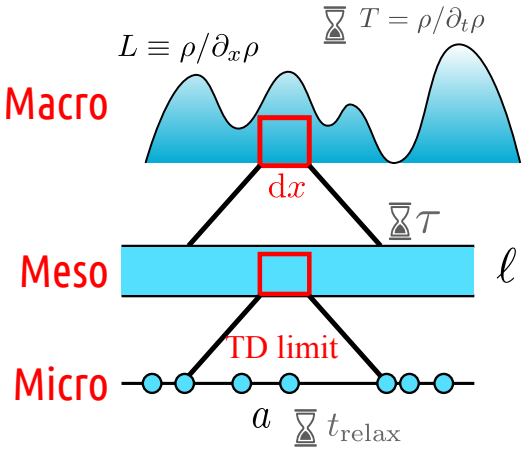

Figure 3.4: Illustration of the separation of scales assumption underlying the quench protocol.

Let's consider the Lieb-Liniger Hamiltonian with an external harmonic potential $V(x) = \omega^2 x^2$

$$\hat{H} = \int_0^L dx \Psi^\dagger(x)\big[-\partial_x^2 - \mu + V(x)\big]\Psi(x) + c\int_0^L dx \Psi^\dagger(x)\Psi^\dagger(x)\Psi(x)\Psi(x), \tag{3.39}$$

where $[0, L]$ is the region where the gas is confined due to the harmonic potential. The presence of the external field breaks the translational invariance of the system, and hence it spoils the integrability of the model. However, we can introduce an approximation that allows us to compute the initial state using the TBA. This approximation lays on the principle of the separation of scales we introduced in the previous sections. The length of the full system is L, and let's say that the microscopic scale of the system is a, typically of the order of the inverse of the particles density $\rho(x)^{-1}$. We assume the existence of an intermediate mesoscopic scale, say of length l, in which we can assume the potential is almost constant $V(x) \approx \text{const}$. This assumption is plausible if we are considering a sufficiently slow-varying potential, for instance a harmonic potential with a sufficiently low frequency. In this way, we can subdivide the system into fluid cells, each with an effective chemical potential $\mu(x) = \mu - V(x)$ and where the system can be well described by the Lieb-Liniger model without spoiling the integrability. This is called *local density approximation* (LDA). Furthermore, if we also assume that the fluid cells are sufficiently large in order to contain a thermodynamical number of particles, we can compute the state in each fluid cell using the TBA technology. The goodness of this ansatz relies on the assumption that the scale is mescoscopic, hence that $a \ll l \ll L$. A cartoon of this working hypothesis is reported in **Figure 3.4**.

Hence, the numerical procedure we will follow is to discretize the position space and for each position compute the root density of the equilibrium state $\rho_p(p, x)$ using the TBA equations with $\mu = \mu(x)$. We also add the x-dependence to the root density because now we have one for each fluid cell. If we integrate it in the momentum at every position, we get the spatial density of particles $\rho_p(x)$. We recall that the TBA equations in the zero temperature limit admit solution only if $\mu > 0$. Hence, we expect the system, at finite temperature, to be confined in a region whose boundaries are more and more above the solution of $\mu(x) = \mu - V(x) = 0$, increasing with the temperature. For an example, compare **Figure 3.8** and **Figure 3.9**.

3.6 Numerical solution of the GHD equations

When we derived the GHD equations, we claimed that their most important form is the one that involves the occupation function

$$\partial_t n(p, x, t) + v^{\text{eff}}(p, x, t)\partial_x n(p, x, t) = 0. \tag{3.40}$$

That's because this is a standard partial differential equation, who can be solved using the *method of characteristics*. The characteristic curve of a particle of quasi-momentum p, starting at position u, is

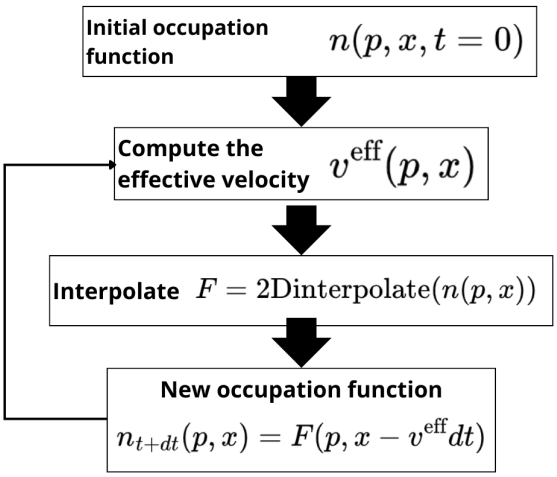

Figure 3.5: The flux diagram of the iterative algorithm for solving the GHD equations. The effectivisation of the group velocity can be done solving the dressing operation using the algorithm for the linear Fredholm integral equation, we already discussed.

defined as the curve $t \mapsto x(p, u, t)$ tangent to the effective velocity $v^{\text{eff}}(p, x, t)$ at every point

$$\frac{\partial x(p, u, t)}{\partial t} = v^{\text{eff}}(p, x(p, u, t), t) \qquad \forall t. \tag{3.41}$$

Actually, the occupation function along this curve solves the GHD equations

$$\left.\frac{\partial n(p, x(p, u, t), t)}{\partial t}\right|_{p,u} = \left[\partial_t n(p, x, t) + v^{\text{eff}}(p, x, t)\partial_x n(p, x, t)\right|_{x=x(p,u,t)} = 0. \tag{3.42}$$

In practise, if we consider a sufficiently small time increase dt, we can consider the quasi-particles moving along the characteristic curve evolving as

$$\begin{aligned} x(t + dt) &= x(t) + v^{\text{eff}}(p, x, t)dt, \\ p(x + dt) &= p(t). \end{aligned} \tag{3.43}$$

Since along the characteristic curve the occupation function is conserved, as showed in (3.42), we can construct an iterative numerical algorithm based on [70]

$$n(p, x, t + dt) \approx n(p, x - v^{\text{eff}} dt, t), \tag{3.44}$$

for dt sufficiently small. In practise, let's consider the case of a Lieb-Liniger gas confined by a harmonic potential which is suddenly turned off at t=0. The initial state, as said in the previous section, can be described discretizing the space and computing the occupation function for each position. That is, we have to solve equations (2.71) using the effective chemical potential $\mu(x) = \mu - V(x)$ and then compute the occupation function as in (2.72). Doing this for each fluid cell, we get the initial state $n(p, x, t = 0)$. Recall that for the numerical solution of the TBA equation, we discretize the momentum space. Hence, we have a grid in the phase space. Once we have the occupation function, we can compute the effective velocity as in equation (3.33)

$$v^{\text{eff}}(p) = \frac{(E')^{dr}(p)}{1^{dr}(p)} = \frac{(E')^{dr}(p)}{2\pi\rho^{tot}(p)}, \tag{3.45}$$

where the dressing of a function is defined as the solution of the integral equation

$$h^{dr}(p) = h(p) + \int dp' \phi(p, p') n(p') h^{dr}(p'). \tag{3.46}$$

Notice that this is a linear Fredholm integral equation as (2.85). The only difference is that here the integration is over all the real space, instead of having two Fermi points. However, since the quasi-momenta above the Fermi points are thermally activated, we set a cutoff Λ for which $n(p) \approx 0$ for $|p| > \Lambda$. In this way, we can apply the algorithm in **Figure 2.3** and solve the dressing equation both for $E'(p)$ and 1, obtaining the initial effective velocity $v^{\text{eff}}(p, x, t = 0)$. Now we can solve the GHD equations iteratively. Let's fix a sufficiently small time step dt. For the numerical computation of the initial state we have discretized both the position space and the momentum space. Since we have to compute the new occupation function as in (3.44), in order to have a greater precision, we interpolate the starting occupation function to recover a continuous coarse-grained function $F = \text{2Dinterpolate}(n(p, x, t))$. In python, this can be done with the method interpolate of the package scipy. Now we can define

$$n_{t+dt}(p, x) = F(p, x - v^{\text{eff}}). \tag{3.47}$$

In this way, we can compute the new effective velocity, dressing with respect to the new occupation function. At this point, we can proceed iteratively in this way until we reach the time we desire. The flux diagram of this algorithm and an example plot for the harmonic trap release of a Lieb-Liniger gas are represented in **Figure 3.5**. We will not discuss the numerical precision of this algorithm, however I just mentioned that for more complicated quenches, such as quartic-to-quadratic, higher precision could be required, and more sophisticated algorithms have been developed. Notwithstanding, these are technical refinements of this algorithm [36].

3.7 Zero entropy GHD

At zero temperature we can construct a more precise algorithm exploiting the peculiar structure of the occupation functions at $T = 0$ [37, 71]. In fact, if $\varepsilon(p)$ is the dressed energy that solves (2.79), the occupation function are defined as

$$n(p) = \frac{1}{1 + e^{\varepsilon(p)/T}}. \tag{3.48}$$

Hence, in the limit $T \to 0$ we have that the occupation function is 1 for the momenta with absolute value below the Fermi point, where the dressed energy is negative, and 0 otherwise. In particular, considering an occupation function that depend also on the position, and defining as $\pm Q(x)$ the Fermi points at position x, we have

$$\begin{cases} n(x, k) = 1, & \text{for} \quad |k| \leq Q(x) \\ n(x, k) = 0, & \text{for} \quad |k| > Q(x) \end{cases} . \tag{3.49}$$

In this way, all the information on the system is encoded in the contour of the occupation function, which is dubbed the *Fermi contour*. Such an occupation function correspond to zero Yang-Yang entropy. Since equation (3.42) tells us that this zero-entropy condition is preserved under the hydrodynamic flux, the idea is to develop an algorithm that cares only of the evolution of the Fermi points on the Fermi contour.

First of all, we have to compute the initial occupation function $n(p, x, t = 0)$. As before, we start by discretizing the position space and computing the Fermi points for each fluid cell $\pm Q(x)$. We recall that in the ground state the Fermi points have to be one the opposite of the other in order to minimize the total momentum. Numerically, the Fermi points are computed as explained in **Section 2.9**, where instead of the chemical potential we use the effective chemical potential $\mu(x) = \mu - V(x)$, with $V(x)$ the external confining potential. At this point, we have to compute the effective velocity by dressing the group velocity and dividing it for the root density (at T=0 we have $\rho^{tot} = \rho_p$ because there are no holes). Next, we can evolve the Fermi points and proceed iteratively. Notwithstanding, there is a problem in this procedure. We know that in the initial state $n(p, x, t = 0)$ we have just two opposite Fermi points for each position, hence the inhomogeneuos system is characterized by local Fermi seas. The same is not true out-of-equilibrium, where one typically observe a boost of the Fermi sea that makes the local two Fermi points not anymore equal in modulus. Henceforth, the most general configuration arising during the dynamics consists in the emergence of a *split Fermi sea*. In

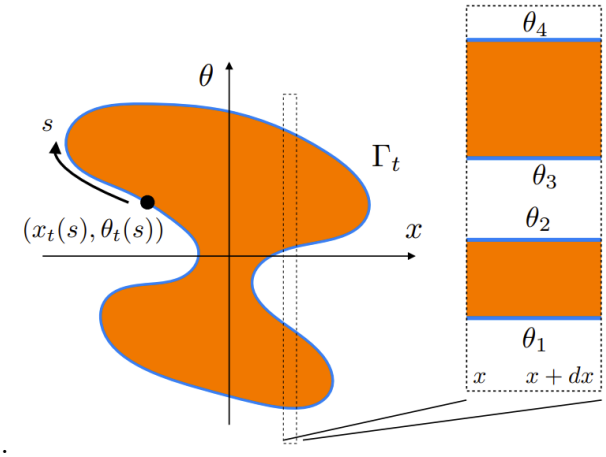

Figure 3.6: Example of a Fermi contour Γ_t where there are split Fermi seas. The orange region in the phase space (x, θ) is where the occupation function values 1. The blu curve is the Fermi contour that divides the two regions. Figure taken from Ref. [37].

particular, if we collect the Fermi points in pairs, for each position, and we introduce the notation $\{Q_{2\alpha-1}, Q_{2\alpha}\}_{\alpha=1,\dots,M}$, each pair defines a Fermi sea, see **Figure 3.6**. Thus, if we are in presence of M Fermi seas, the dressing operation (3.28) becomes

$$h^{dr}(p) = h(p) + \sum_{\alpha=1}^{M} \int_{Q_{2\alpha-1}}^{Q_{2\alpha}} dp' \phi(p, p') h^{dr}(p'). \tag{3.50}$$

This is still a linear Fredholm integral equation, and it can be solved with a technical generalisation of the *LFIE_solver* algorithm described in **Figure 2.3**. These split Fermi sea configurations arise when quasi-particles of large rapidity manage to overturn other quasi-particles with smaller rapidity during the propagation. For instance this happens in a quartic-to-quadratic quench, that implements a GHD realization of the quantum Newton cradle experiment.

As a result, in the iterative procedure we have to introduce a step that for every position detects the Fermi seas in order to compute the effective velocity. Hence, we define a block called *Roots_finder* that receives as input a point in the Fermi contour (x_0, p_0) and gives as output the set of Fermi points $\{Q_\alpha(x_0)\}$ at position x_0. Let's call the Fermi contour Γ, made of M points, and let's define as s the parameter that runs over the contour, i.e. $\Gamma(s) = (x_s, p_s)$ for $s = 0, \dots, M-1$. In this algorithm, we create a cycle along the Fermi contour that check if the spatial position of the initial point x_0 is between two consecutive Fermi points in the curve, i.e. if $x_{s-1} \leq x_0 \leq x_s$. In such a case, we store as Fermi point the linear interpolation between p_{s-1} and p_s evaluated at x_0. At the end of the cycle the block gives all the Fermi points at position x_0. The flux diagram of this block is in **Figure 3.7**.

Now we can correctly construct the iterative algorithm. So, if we discretize the position space in M points, we have a in initial Fermi contour which is a 2M-dimensional array $\Gamma_{t=0}$, because in the initial state we have two Fermi points for each position. At each position we compute the effective velocity via the dressing operation. Now we evolve the Fermi contour, if $\Gamma_t(s) = (x_s, p_s)$ according to (3.44) we define

$$\Gamma_{t+dt}(s) = (x_s + v_s^{\text{eff}} dt, p_s) \tag{3.51}$$

where $v_s^{\text{eff}} = v^{\text{eff}}(x_s, p_s)$. At this point, we gave each point of the new contour as input to the block *Roots_finder*, in order to find the split Fermi seas for each Fermi points $(x_s, \{Q_\alpha(x_s)\})$ and compute the new effective velocity $v^{\text{eff}}(x_s, p_s)$. We proceed iteratively in this way until we reach the desired time. The flux diagram is in **Figure 3.7**.

This algorithm provides a big simplification compared to the finite temperature case. In the latter we have to evolve all the points of the discretized phase space. In particular, if both position and momenta are discretized in M points, we have to evolve MxM points. In this case instead, we focus

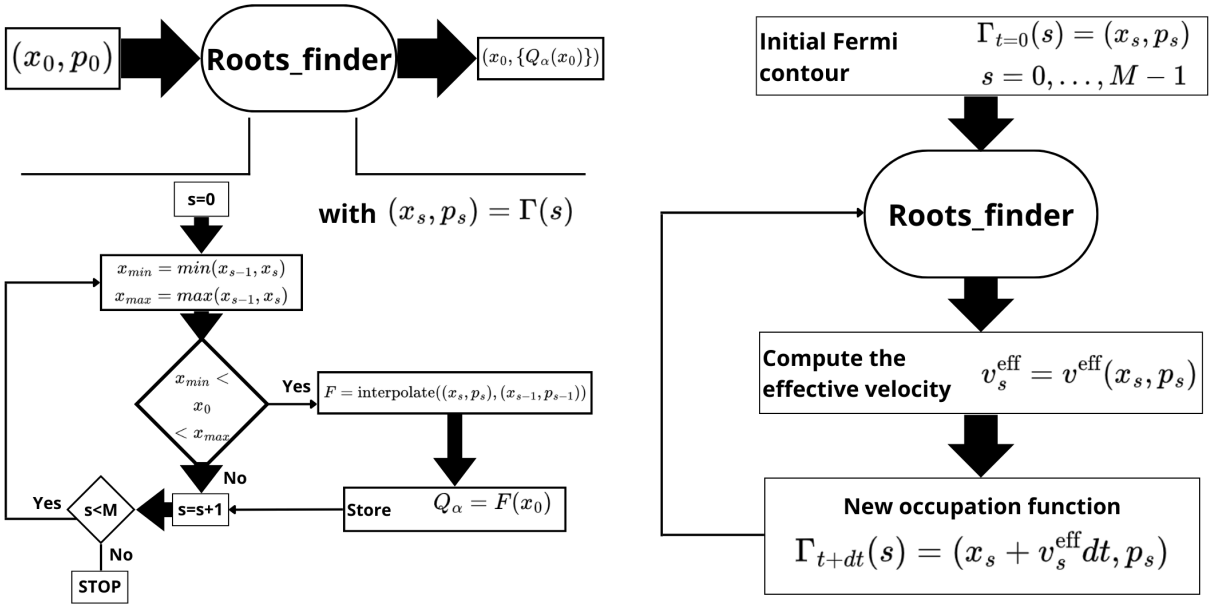

Figure 3.7: On the left panel the flux diagram of the block *Roots_finder* that compute the split Fermi seas for a point in the Fermi contour. On the right panel the complete algorithm for the zero entropy GHD.

only on the 2M points of the Fermi contour. Furthermore, the procedure is more neat because we do not have to interpolate the occupation function, introducing a further source of error. For these reasons, the zero entropy GHD algorithm is more stable and precise.

3.8 Non equilibrium dynamics of a single-component gas during a trap release

After having discussed the numerical algorithms for solving the GHD equations, let's discuss the physics of the harmonic trap release of a Lieb-Liniger gas. Let's start by the zero temperature case reported in **Figure 3.8**.. The initial state is exactly bounded in the spatial region where $\mu(x) = \mu - V(x) > 0$, and we observe an isotropic expansion towards an homogeneous system, since the Fermi points evolves with an horizontal shift. In particular, at $t > 0$ the local Fermi sea is boosted and the equilibrium configuration, where $Q_1(x) = -Q_2(x)$, is now broken. The area is shrinking and the boosted local Fermi sea becomes smaller and smaller at every point, in particular from the bulk to the tails. Furthermore, we observe that the evolution of the Fermi contour given by the zero entropy GHD leads to populate larger and larger regions. Hence, this bring to an expansion of the gas from the initial confinement, actually the density is given by

$$\rho(x) = \int_{Q_1(x)}^{Q_2(x)} \rho(x,k)dk. \tag{3.52}$$

In particular this is evident in the Tonks-Girardeu limit $c \to \infty$ where the root density is constant $\rho(k) = 1/2\pi$, hence the density at each point is directly proportional to the dimension of the local Fermi sea

$$\rho(x) = \int_{Q_1(x)}^{Q_2(x)} \frac{dk}{2\pi}. \tag{3.53}$$

Similarly, the dependence between the density and the dimension of the local Fermi sea is still true also at finite values of the interaction strength c. Thus, such an evolution of the Fermi contour tells us that we will have an increasingly populated region, with a lower and lower density.

At finite temperature, as we already outlined, the initial state presents thermal tails and it is not confined in the region where the effective chemical potential is positive, as we can see in **Figure 3.9**. However, the majority of the particles are in the bulk, thus, we observe an initial particles density

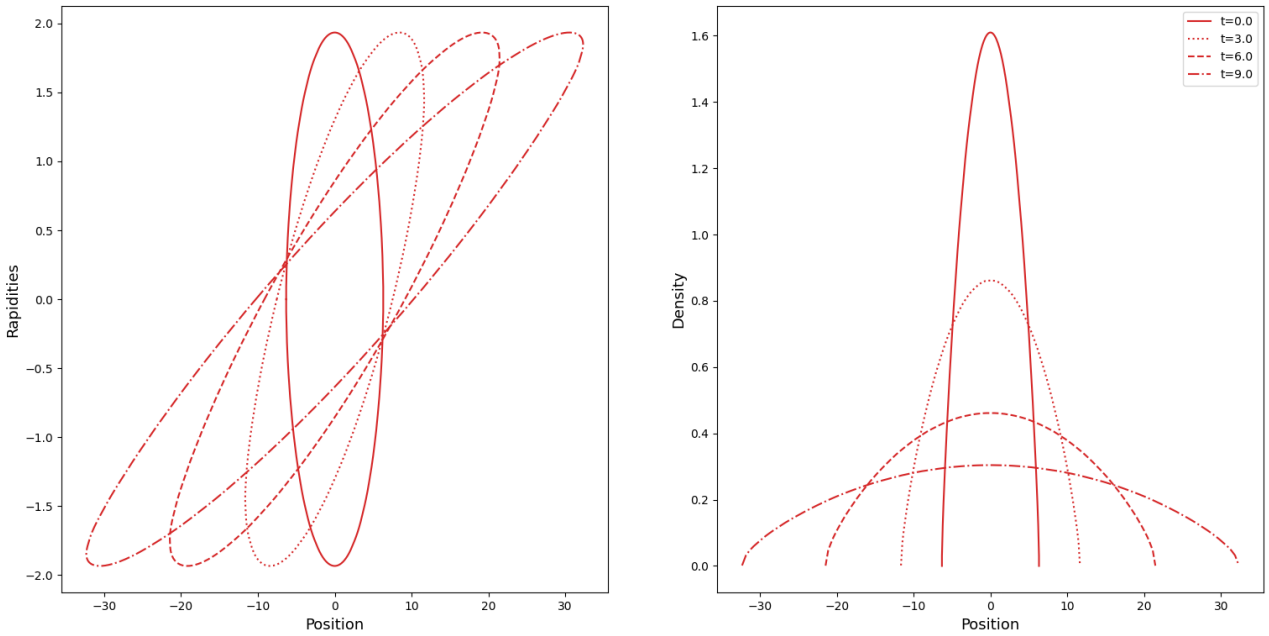

Figure 3.8: Zero entropy GHD evolution of the Lieb-Liniger gas. The quench protocol is a release of a harmonic potential $\omega = 0.25 \overset{t=0}{\to} 0$. On the left panel there is the evolution of the Fermi contour. We see that the Fermi points evolves with an horizontal shift. On the right panel are reported the corresponding particles density. The parameters are $c = 1$, $\mu = 2.5$.

tight and peaked in the origin. After the quench at $t = 0$, when the harmonic potential is turned off, the system is left free to evolve without any constrain. Thus, since the post-quench Hamiltonian is homogeneous (no external potential), and hence the initial configuration of the momenta is conserved, we expect an isotropic expansion of the gas with the particles density that starts to smear out, in order to reach a more and more homogeneous configuration with the increasing of time. This physical argument is also supported by equations (3.43) which tell us that under the GHD flow a quasi-particle evolves with an horizontal shift $dx \approx v^{\text{eff}} dt$. In addition, switching on the temperature the system gained energy with respect to the zero entropy case. Actually, we can see that the expansion of the gas proceed faster and with the same amount of time passed, the tails reach further regions. This is of course due to the thermal excitations that populated quasi-momenta above the Fermi points, that hence evolves faster.

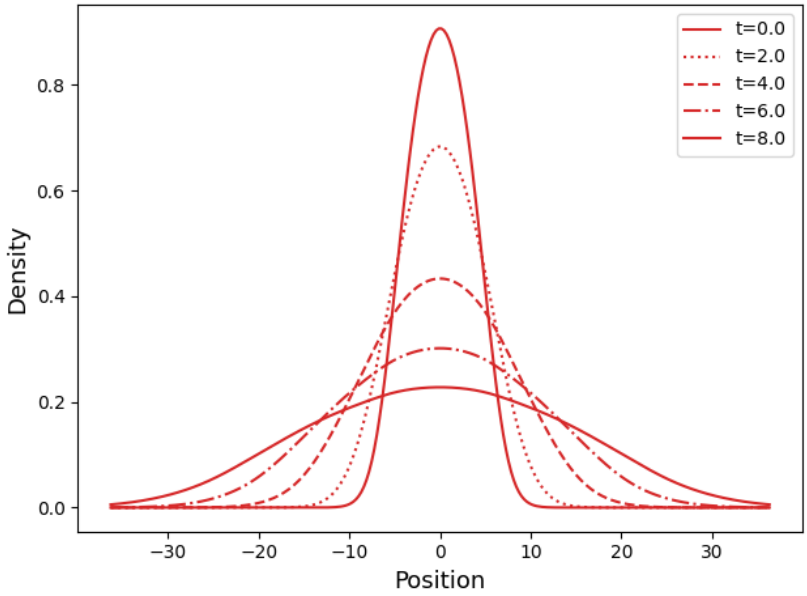

Figure 3.9: The GHD expansion of a Lieb-Liniger gas where the harmonic potential $V(x) = \omega^2 x^2$ has been instantaneously turned off at t=0. The parameters are setted to $T = 1$, $c = 1$, $\mu = 2.5$ and $\omega = 0.25$.

Chapter 4

Multi-component exactly solvable models

Now we move to the main topic of the thesis, i.e. *multi-component* exactly solvable models. As we will see, these models display a much more involved Bethe ansatz description characterized by the presence of multiple quasi-particles species. This feature gives rise to striking effects such as the fractalisation of elementary excitations. The scope of this thesis is to probe the non equilibrium dynamics of these models by means of GHD and to highlight the main difference with respect to single-component integrable models. Indeed, since its introduction in 2016 [32, 33], the GHD has been mostly applied to single-component systems, i.e. models that display a single set of rapidities, as the Lieb-Liniger gas. Exceptions are really rare, see [27, 28, 47–50]. In the first sections, we will discuss the problem of spin-1/2 fermions with contact interaction, i.e. the Yang-Gaudin model. This is the model that pioneered the study of multi-component integrable systems via Bethe ansatz. We will derive its TBA equations and discuss the harmonic trap release both at zero and finite temperature. In particular, Ref. [28] will be our main benchmark for this study. Next, we will discuss the two-component spinor Bose gas, which consists in two bosonic species with delta-interaction both intra and inter species. In particular, its GHD evolution has not yet been studied in literature and this represents part of the original work of the thesis. Moreover, since these two multi-component models have the same Hamiltonian and they differs only for the statistics of the particles they describe, the final aim of the thesis is to setup a qualitative comparison between the behaviour of these two models in the out-of-equilibrium dynamics. Because of we want compare the two models and due to the fact that the spinor Bose gas is thermodynamically unstable for attractive interaction (as Lieb-Liniger), we will discuss also the Yang-Gaudin model in the repulsive regime.

4.1 Yang-Gaudin Fermi gas

Yang-Gaudin model is about spin-1/2 fermions with contact interaction. The Hamiltonian for the system in a finite volume L is

$$\hat{H} = -\int_0^L dx \sum_{\sigma=\pm} \Psi_\sigma^\dagger(x)\big(\partial_x^2 + \mu + \sigma h\big)\Psi_\sigma(x) + c\int_0^L dx \Psi_+^\dagger(x)\Psi_-^\dagger(x)\Psi_-(x)\Psi_+(x), \tag{4.1}$$

where σ distinguishes the two spin species, μ is the chemical potential and h the external magnetisation, that in general we will consider uniform. As for Lieb-Liniger, c parametrise the interaction strenght. The system can be experimentally realised by trapping ^{6}Li atoms [24]. The two field operators satisfy CAR

$$\Big\{\Psi_\sigma^\dagger(x), \Psi_{\sigma'}(x')\Big\} = \delta_{\sigma,\sigma'}\delta(x-x'). \tag{4.2}$$

Similarly to the XXX chain, discussed in the Chapter 2, the system displays a $U(1)$ symmetry. Thus, the number of up spins N_+ and the number of down spins N_- are conserved. Henceforth, each field

operator is normalized to the number of particles with spin up and spin down $N_\pm$. Therefore, in order to solve the system we specialize in superselection sectors with fixed number of particles N and fixed number of down spins M. For each of these, the first quantised Hamiltonian is

$$\mathcal{H}_{N,M} = -\sum_{i=1}^{N}\left(\frac{\partial^2}{\partial x_i^2}+\mu\right) - h(N-2M) + 2c\sum_{i<j}\delta(x_i-x_j). \tag{4.3}$$

Due to its fermionic nature, the quantum numbers characterizing the wavefunction are both the coordinates $\{x_i\}_{i=1,\dots,N}$ and the spins $\{\lambda_\alpha\}_{\alpha=1,\dots,N}$. Actually, in the following sections we will see that the application of the Behte ansatz machinery will produce two sets of rapidities, the quasi-momenta and the spin rapidities.

The first attempt in solving this one-dimensional fermionic system is due to McGuire in 1965 and 1966. In this two papers, he found the Bethe equations for a system of N-1 spin up and 1 spin down, both for the repulsive [72] and the attractive [73] case. One year later, Flicker and Lieb [74] found the solution with two down spins. The same year, the general solution was found independently by Yang [8] and Gaudin [9]. That's why, the one-dimensional fermionic gas with contact interaction is usually refered to as Yang-Gaudin model. Finally, in 1971, Takahashi [13] and Lai [75] generalized the Yang-Yang's thermodynamical approach we saw in **Section 2.8**.

In the following, we are going to study the Bethe ansatz solution of the model and its TBA equations. Next, as for Lieb-Liniger, we will see the harmonic trap release both at zero and finite temperature. But, first of all, let's start by the two-particle problem. For a complete reference on the Bethe ansatz solution of the model see Takahashi's book [14].

4.2 The two-particle problem

Before considering the most general wavefunction, we must notice that if the two particles have the same spin, the interaction trivialize. In fact, if they have the same spin they could not also have the same position and so the system behave as free fermions. To avoid this trivialization, let's consider the case of one spin up and one spin down

$$\begin{aligned}\psi_{\uparrow\downarrow}(x_1,x_2) =&\theta_H(x_2-x_1)\Big(A_{12}^{\uparrow\downarrow}e^{i(k_1x_1+k_2x_2)}+A_{21}^{\uparrow\downarrow}e^{i(k_2x_1+k_1x_2)}\Big)\\ &+\theta_H(x_1-x_2)\Big(A_{12}^{\downarrow\uparrow}e^{i(k_2x_1+k_1x_2)}+A_{21}^{\downarrow\uparrow}e^{i(k_2x_2+k_1x_1)}\Big),\end{aligned} \tag{4.4}$$

where θ_H is the Heaviside step function. The notation for the coefficients is a bit tricky. The expression $A_{12}^{\uparrow\downarrow}$ means that, if we think the system on the real axis right-oriented, the up spin is on the left while the down spin on the right and the momentum k_1 is associated to the particle on the left while k_2 to the particle on the right. Same for the others coefficients. This wavefunction solves the eigenvalue problem if

$$\begin{pmatrix}A_{12}^{\uparrow\downarrow}\\ A_{12}^{\downarrow\uparrow}\end{pmatrix} = \begin{pmatrix}u_{21}-1 & u_{21}\\ u_{21} & u_{21}-1\end{pmatrix}\begin{pmatrix}A_{21}^{\uparrow\downarrow}\\ A_{21}^{\downarrow\uparrow}\end{pmatrix}, \qquad u_{jl}\equiv\frac{k_j-k_l}{k_j-k_l+ic}. \tag{4.5}$$

A solution for this equation is [14]

$$\begin{pmatrix}A_{12}^{\uparrow\downarrow}\\ A_{12}^{\downarrow\uparrow}\end{pmatrix} = \begin{pmatrix}k_1-\Lambda-ic/2\\ -(k_2-\Lambda+ic/2)\end{pmatrix}, \qquad \begin{pmatrix}A_{21}^{\uparrow\downarrow}\\ A_{21}^{\downarrow\uparrow}\end{pmatrix} = \begin{pmatrix}-(k_2-\Lambda-ic/2)\\ k_1-\Lambda+ic/2\end{pmatrix}, \tag{4.6}$$

where Λ is an arbitrary constant. Differently from Lieb-Liniger, here it appears a further rapidity over the two quasi-momenta k_1 and k_2. This will generalize to the case of N particles and M down spins, where we will have $\mathbf{k}=\{k_1,\dots,k_N\}$ the set of quasi-momenta and $\lambda=\{\lambda_1,\dots,\lambda_M\}$ the set of spin rapidities.

4.3 Nested Bethe ansatz

The complete derivation of the Bethe equation is very technical and not so interesting for our purposes, thus, I am not going to reproduce it and it can be checked in Ref. [14]. The main points of this procedure are two. Firstly, as narrowly underlined in Chapter 2, that the Bethe equation arises as consistency condition between the p.b.c. and the dynamical phase that arises when 1 particles scatters the other N-1 along the ring. Secondly, for a multi-component system, the Bethe ansatz wavefunction requires two sets of rapidities. This two sets appear coupled in the Bethe equations, thus, this are called *nested* Bethe equations. For the Yang-Gaudin model these are

$$e^{ik_jL} = \prod_{\alpha=1}^{M} \frac{k_j - \lambda_\alpha + ic/2}{k_j - \lambda_\alpha - ic/2} \qquad j = 1, \dots, N, \tag{4.7}$$

$$\prod_{j=N}^{M} \frac{\lambda_\alpha - k_j + ic/2}{\lambda_\alpha - k_j - ic/2} = -\prod_{\beta=1}^{M} \frac{\lambda_\alpha - \lambda_\beta + ic}{\lambda_\alpha - \lambda_\beta - ic} \qquad \alpha = 1, \dots, M, \tag{4.8}$$

where $\mathbf{k} = \{k_1, \dots, k_N\}$ is the set of quasi-momenta, $\lambda = \{\lambda_1, \dots, \lambda_M\}$ is the set of spin rapidities, N the number of fermions and M the number of down spins. A solution of this two equations characterize uniquely the wavefunction. As for the Lieb-Liniger case, the energy of the system is $\sum_j k_j^2$. Before moving further, I want to stress that the two sets of rapidities are not in some sense decoupled. I mean, the set of quasi-momenta is not an effective description for the density degree of freedom only, as instead it is for Lieb-Liniger, and idem for the spin rapidities, they are not about the magnetisation only. Since the equations are nested, each rapidity is about both spin and density. This reflects the fact that the particles composing the Yang-Gaudin gas are spinful and the carry both a mass and a spin. This should be clear by the expression of the energy written slightly above. Of course, it should depend also on the distribution of the spins, however only the k_j's appear.

Now, let's move to the solution of the equations. As we saw in **Section 2.5**, the k_j's can be complex. In order to simplify the expression of these equations, Takahashi made two conjectures.

Conjecture 1. *If a set that solves (4.7) and (4.8) contains a complex k or λ, then also its complex conjugate is in the set.*

Thus, the set rapidities is symmetric with respect to the real axis. A particular configuration arises in the repulsive case $c > 0$, for whom all the k_j's are real. Indeed, looking at (4.7) we can chack that if $\mathrm{Im}\{k_j\} > 0$ the absolute value of the l.h.s. is less than unity, while the absolute value of the r.h.s. is greater than unity. Viceversa for $\mathrm{Im}\{k_j\} < 0$. Thus, we must require $\mathrm{Im}\{k_j\} = 0$ for $c > 0$.

Conjecture 2. *The set of spin rapidities groups in spin-strings up to finite size effects that go exponentially with L*

$$\lambda_\alpha^{n,j} = \lambda_\alpha^n + (n + 1 - 2j)\frac{c}{2}i + \textit{deviations} \qquad j = 1, 2, \dots, n. \tag{4.9}$$

These spin-strings are centered on a real value λ_α^n. The index n refers to the length of the string, the index α labels the strings (there could be more than one string of length n) and the index j run over the string itself. Simirarly to what we saw in **Section 2.5**, the interpretation of these string is that of n-bound state of spin quasi-particles. This conjecture bring a semplification because the spin centers itselves solve the Bethe equations. Thus, we can work just with the real centers. This two conjectures togheter form the so-called *string hypothesis*. Applying this hypothesis and taking the log of the nested Bethe equations we get

$$k_jL = 2\pi I_j - \sum_{n=1}^{\infty}\sum_{\alpha=1}^{M_n} \theta\left(\frac{k_j - \lambda_\alpha^n}{nc/2}\right), \qquad j = 1, \dots, N, \tag{4.10}$$

$$\sum_{j=1}^{N} \theta\left(\frac{\lambda_\alpha^n - k_j}{nc/2}\right) = 2\pi J_\alpha^n + \sum_{m=1}^{\infty}\sum_{\beta=1}^{M_m} \Theta_{nm}\left(\frac{\lambda_\alpha^n - \lambda_\beta^m}{c/2}\right), \tag{4.11}$$
$$\alpha = 1, \dots, M_n, \quad n \geq 1,$$

where M_n is the number of string of length n, $\{I_j\}_{j=1,\dots,N}$ and $\{J^n_\alpha\}_{\alpha=1,\dots,M_n}$ are infinite distinct sets of Bethe integers, $\theta(x) \equiv 2\arctan x$ and $\Theta_{nm}(x)$ is a combination of θ's quite tedious to write and not interesting for us. You can find it, as everything, in Takahashi's book or paper [13, 14]. For sake of completness, we stress that this Bethe integers must satisfy some algebraic relations, differently from the Lieb-Liniger case where they could be any half-integer. I do not report this relations because they are not relevant for the further thermodynamical treatment. As said before, the application of the Bethe ansatz technique to Yang-Gaudin is highly non trivial.

For what we said until now, a set of half-integers $\{I_j, J^n_\alpha\}$, which satisfy certain constraints, uniquely determines the rapidities of the system and, thus, the wavefunction. The allowed half-integers that do not belong to the set are called *holes*, while the ones who belong are called *particles*. In order to move towards the thermodynamical limit, we introduce the counting functions for the Bethe integers of both particles and holes (compare with **Section 2.6**)

$$Lh(k) = 2\pi I, \qquad Lj_n(\lambda^n) = 2\pi J^n. \tag{4.12}$$

Thus, we can rewrite (4.10) and (4.11) as

$$h(k) = k + \frac{1}{L}\sum_{n=1}^{\infty}\sum_{\alpha=1}^{M_n}\theta\Big(\frac{k-\lambda^n_\alpha}{nc/2}\Big), \tag{4.13}$$

$$j_n(\lambda) = \frac{1}{L}\sum_{j=1}^{N}\theta\Big(\frac{\lambda-k_j}{nc/2}\Big) - \frac{1}{L}\sum_{m=1}^{\infty}\sum_{\beta=1}^{M_m}\Theta_{nm}\Big(\frac{\lambda-\lambda^m_\beta}{c/2}\Big). \tag{4.14}$$

Now we introduce the distribution functions of k's and λ's

$$\frac{\mathrm{d}}{\mathrm{d}k}h(k) = 2\pi\Big(\rho(k) + \rho^h(k)\Big) \equiv 2\pi\rho^{tot}(k), \tag{4.15}$$

$$\frac{\mathrm{d}}{\mathrm{d}k}j_n(k) = 2\pi\Big(\sigma_n(k) + \sigma^h_n(k)\Big) \equiv 2\pi\sigma^{tot}_n(k), \tag{4.16}$$

where the apex h state for holes' densities. Hence, we can substitute the summations with integrations over $\mathbb{R}$ weighted by the densities of particles

$$h(k) = k + \sum_{n=1}^{\infty}\int\theta\Big(\frac{k-k'}{nc/2}\Big)\sigma_n(k')dk', \tag{4.17}$$

$$j_n(k) = \int\theta\Big(\frac{k-k'}{nc/2}\Big)\rho(k')dk' - \sum_{m=1}^{\infty}\int\Theta_{nm}\Big(\frac{k-k'}{c/2}\Big)\sigma_m(k')dk'. \tag{4.18}$$

Now we can insert this two equations in (4.15) and (4.16). In this way, we get the *Bethe-Gaudin-Takahashi* (BGT) equations

$$\rho^{tot}(k) = \frac{1}{2\pi} + \sum_{n=1}^{\infty}\phi_n * \sigma_n(k), \tag{4.19}$$

$$\sigma^{tot}_n(k) = \phi_n * \rho(k) - \sum_{m=1}^{\infty}\Phi_{nm} * \sigma_m(k), \tag{4.20}$$

where

$$\phi_n(k) \equiv \frac{1}{\pi}\frac{2nc}{(nc)^2 + 4k^2}, \qquad \phi_0(k) \equiv \delta(k), \tag{4.21}$$

$$\Phi_{nm} \equiv (1-\delta_{n,m})\phi_{|n-m|}(k) + 2\phi_{|n-m|+2} + \ldots + 2\phi_{n+m-2}(k) + \phi_{n+m}(k), \tag{4.22}$$

and the convolution is defined as

$$f * g(k) = \int dk' f(k-k')g(k'). \tag{4.23}$$

As we saw for the Lieb-Liniger gas, at finite temperature excitations, hence holes, appears. Thus, the BGT equations are non closed and so, not sufficient to solve the system. In 1971, Takahashi [13] generalized Yang-Yang's idea of using the Bethe equations as constraints in the minimization of the thermodynamical free energy. We can write the Gibbs free energy as

$$G(T,\mu,h) = E[\rho] - \mu N[\rho] - h(N[\rho] - 2M[\sigma_n]) - TS[\rho,\rho^h,\sigma_n,\sigma_n^h], \tag{4.24}$$

where

$$\begin{aligned}
&\frac{E}{L} = \int k^2\rho(k)dk, \qquad \frac{N}{L} = \int \rho(k)dk,\\
&\frac{M}{L} = \sum_{n=1}^{\infty} n\int \sigma_n(k)dk,\\
&\frac{S}{L} = \int dk(\rho+\rho^h)\ln\rho + \rho^h - \rho\ln\rho - \rho^h\ln\rho^h\\
&+\sum_{n=1}^{\infty}\int dk(\sigma_n+\sigma_n^h)\ln\sigma_n + \sigma_n^h - \rho\ln\rho - \sigma_n^h\ln\sigma_n^h.
\end{aligned} \tag{4.25}$$

Notice that S is the Yang-Yang entropy of the system. Thus, the free energy is a functional of $\{\rho,\rho^h,\sigma_n,\sigma_n^h\}$ and it must be minimized under the constraint given by the BGT equations. Because equations (4.19) and (4.20) are linear, the following relation on the differentials holds

$$\delta\rho^h = -\delta\rho + \sum_{n=1}^{\infty}\phi_n * \delta\sigma_n, \tag{4.26}$$

$$\delta\sigma_n^h = \phi_n * \delta\rho - \delta\sigma_n - \sum_{m=1}^{\infty}\Phi_{nm} * \delta\sigma_m. \tag{4.27}$$

Inserting these two in the minimization of the free energy we get

$$\begin{aligned}
0 = \frac{\delta G}{TL} = &\int\left\{\frac{k^2-\mu-h}{T} - \ln\frac{\rho^h}{\rho} - \sum_{n=1}^{\infty}\phi_n * \ln\left(1+\frac{\sigma_n}{\sigma_n^h}\right)\right\}\delta\rho dk\\
&+\sum_{n=1}^{\infty}\int\left\{\frac{2nh}{T} - \ln\frac{\sigma_n^h}{\sigma_n} - \phi_n * \ln\left(1+\frac{\rho}{\rho^h}\right) + \sum_{m=1}^{\infty}\Phi_{nm} * \ln\left(1+\frac{\sigma_m}{\sigma_m^h}\right)\right\}\delta\sigma_n dk.
\end{aligned} \tag{4.28}$$

Now let's introduce the dressed energies

$$\frac{\rho^h(k)}{\rho(k)} \equiv \exp(\varepsilon_1(k)/T), \qquad \frac{\sigma_n^h(k)}{\sigma_n(k)} \equiv \exp(\varepsilon_{2,n}(k)/T). \tag{4.29}$$

We have finally obtained the coveted TBA equations for the Yang-Gaudin model

$$\varepsilon_1(k) = k^2 - \mu - h - T\sum_{n=1}^{\infty}\phi_n * \ln\Big(1+e^{-\varepsilon_{2,n}/T}\Big)(k) \tag{4.30}$$

$$\begin{aligned}
\varepsilon_{2,n}(k) = 2nh - T\phi_n * \ln\Big(1+e^{-\varepsilon_1/T}\Big)(k) + T\sum_{m=1}^{\infty}\Phi_{n,m} * \ln\Big(1+e^{-\varepsilon_{2,m}/T}\Big)(k)\\
n = 1,2,\dots
\end{aligned} \tag{4.31}$$

These functions give the dressed energy for each quasi-particle excitation. From these we can define the occupation functions

$$n_1(k) \equiv \frac{\rho_1(k)}{\rho^{tot}(k)} = \frac{1}{1+e^{\varepsilon_1/T}}, \qquad n_{2,n}(k) \equiv \frac{\sigma_n(k)}{\sigma_n^{tot}(k)} = \frac{1}{1+e^{\varepsilon_{2,n}/T}}. \tag{4.32}$$

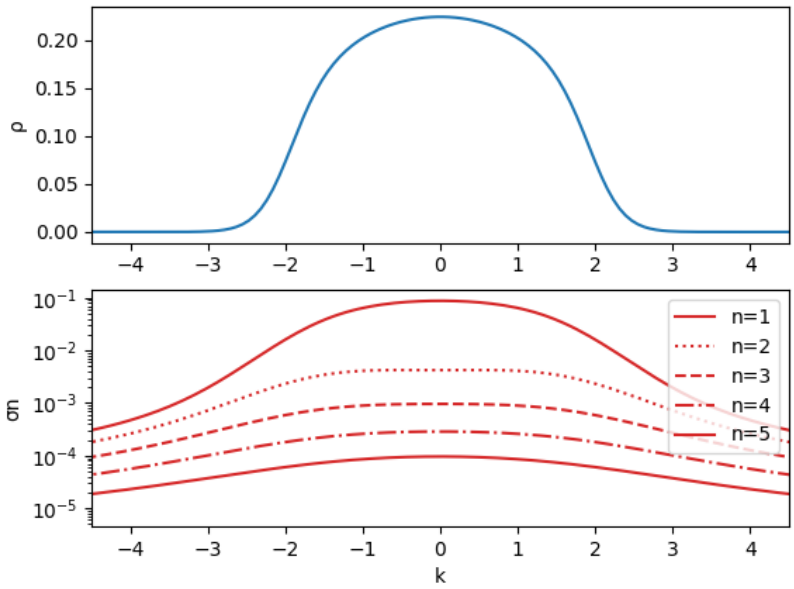

Figure 4.1: Root densities ρ and σ_n for a Yang-Gaudin gas at $T = 1$. The parameters are $c = 1$, $\mu = 2$ and $h = 0.5$.

The TBA equations are of Fredholm non-linear type and thus, them could be solved as the Yang-Yang equation (2.71). The algorithm is a non trivial, but technical, generalization of the one reported in **Section 2.9**. The only remarkable consideration is that because (4.30) and (4.31) are an infinite set of equations, we approximated the numerical solution truncating the number of strings. A posteriori, one has to check the numerical stability of the solution by increasing the cutoff value. Generically, higher strings are exponentially suppressed at low temperature or by the external magnetic field (see **Figure 4.1**). Hence, by retaining a few string, one can already observe a good convergence of the TBA algorithm.

In general, every bare quantity, say $\{\zeta_1, \zeta_{2,n}\}$, can be dressed via the equations

$$\zeta_1^{dr}(k) = \zeta_1 + \sum_{n=1}^{\infty} \phi_n * \zeta_{2,n}^{dr} n_{2,n}(k), \tag{4.33}$$

$$\zeta_{2,n}^{dr}(k) = \zeta_{2,n} + \phi_n * \zeta_1^{dr} n_1(k) - \sum_{m=1}^{\infty} \Phi_{n,m} * \zeta_{2,m}^{dr} n_{2,m}(k) \qquad n = 1, 2, \dots, \tag{4.34}$$

that can be solved iteratively starting from the bare quantities. In particular, from the BGT equations (4.19) and (4.20) we can read that the total root densities ρ_1^{tot} and $\rho_{2,n}^{tot}$ can be computed by dressing the bare quantities $\{1/2\pi, 0\}$. Once we get the total densities, we can compute the quasi-particles densities multiplying the total ones for the occupation functions $\rho = \rho^{tot} n$. An example of root densities is reported in **Figure 4.1**.

Zero temperature limit The core idea for the solution of the model at zero temperature is that strings are thermally activated. In order to understand why, let's state a remarkable fact. The TBA equations (4.30) and (4.31) allowed a *partially decoupled* rewrite

$$\varepsilon_1(k) = k^2 - \mu - h - Tr * \ln\left(1 + e^{-\varepsilon_1/T}\right)(k) - Ts * \ln\left(1 + e^{\varepsilon_{2,1}/T}\right)(k), \tag{4.35}$$

$$\varepsilon_{2,1}(k) = Ts * \ln\left((1 + e^{\varepsilon_{2,1}/T})/(1 + e^{-\varepsilon_1/T})\right), \tag{4.36}$$

$$\varepsilon_{2,n}(k) = Ts * \ln\left((1 + e^{\varepsilon_{2,n-1}/T})(1 + e^{\varepsilon_{2,n+1}/T})\right) \qquad n \geq 2, \tag{4.37}$$

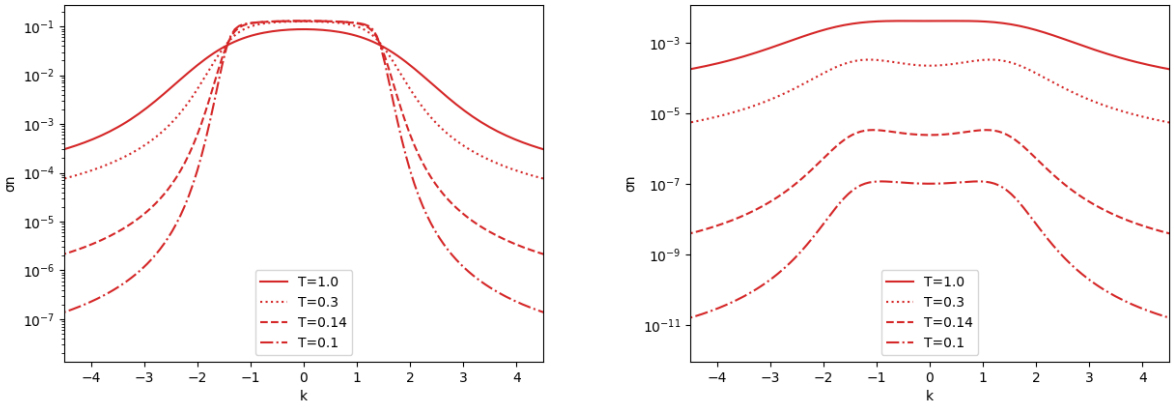

Figure 4.2: Comparison of Yang-Gaudin spin-strings at different temperature. On the left the n=1 string, i.e. the single spin quasi-particle, while on the right the n=2 string, i.e. a simple bound state. We can see directly the fact that for $n \geq 2$ the strings are thermally activated. The parameters are $c = 1$, $\mu = 2$ and $h = 0.5$.

with the boundary condition $\lim_{n\to\infty} \varepsilon_{2,n} = 2nh$ and

$$s(k) = \frac{\mathrm{sech}(\pi k/c)}{2c}, \qquad r(k) = \phi_1 * s(k). \tag{4.38}$$

The derivation of this decoupled form is reported in **Appendix A**. Now, let's take a look at (4.37). It is clear that $\varepsilon_{2,n} \geq 0$ for any $n \geq 2$. Thus, from equation (4.32) we can read that $n_{2,n} \to 0$ for $T \to 0$. Hence, bound states are exponentially suppressed at low temperatures. That's a remarkable fact. On the other hand, ε_1 and $\varepsilon_{2,1}$ can also be negative. In addition, it can be shown that both are monotonically increasing. Thus, the occupation functions becomes step functions at the Fermi points $Q_{1,2}$, determined by $\varepsilon_j(Q_j) = 0$. A numerical picture of this is shown in **Figure 4.2**. Due to the introduction of Fermi points, the convolutions become

$$[g * f]_Q(k) = \int_{-Q}^{Q} dk' g(k-k') f(k'). \tag{4.39}$$

Now, we can take the $T \to 0$ limit of (4.30) and (4.31) as we done for (2.79). We obtain

$$\varepsilon_1(k) = k^2 - \mu - h + [\phi_1 * \epsilon_2]_{Q_2}(k), \qquad k \in [-Q_1, Q_1] \tag{4.40}$$

$$\varepsilon_2(k) = 2h + [\phi_1 * \epsilon_1]_{Q_1}(k) - [\phi_2 * \varepsilon_2]_{Q_2}(k), \qquad k \in [-Q_2, Q_2]. \tag{4.41}$$

At this point, we can numerically solve the zero temperature case exactly as for Lieb-Liniger. The BGT equations (4.19) and (4.20) are now closed, i.e. two equations for two unknown functions

$$\rho(k) = \frac{1}{2\pi} + [\phi_1 * \sigma]_{Q_2}(k), \qquad k \in [-Q_1, Q_1] \tag{4.42}$$

$$\sigma(k) = [\phi_1 * \rho]_{Q_1}(k) - [\phi_2 * \sigma]_{Q_2}(k), \qquad k \in [-Q_2, Q_2]. \tag{4.43}$$

For the numerical solution we have to find the Fermi point solving $\varepsilon_j(Q_j) = 0$ for $j = 1, 2$. Apparently, there is a difference with respect to Lieb-Liniger, i.e. that both for densities and dressed energies we have two equations and not one. Thus, it seems that we cannot apply the algorithm reported in **Figure 2.3**.

A useful trick is to set a sufficiently high cutoff in the momenta $\Lambda > Q_1, Q_2$ and discretise the momentum space in M parts, hence, $k_j = -\Lambda + \Delta * j$ for $j = 0, \ldots, M-1$ and $\Delta = 2\Lambda/(M-1)$. Thus, equations (4.40) and (4.41) can be rewritten as

$$(\varepsilon_1)_j = k_j^2 - \mu - h + \Delta \sum_{m=0}^{M-1} (\phi_1)_{jm} (\varepsilon_2)_m \theta_H(Q_1 - |k_m|), \tag{4.44}$$

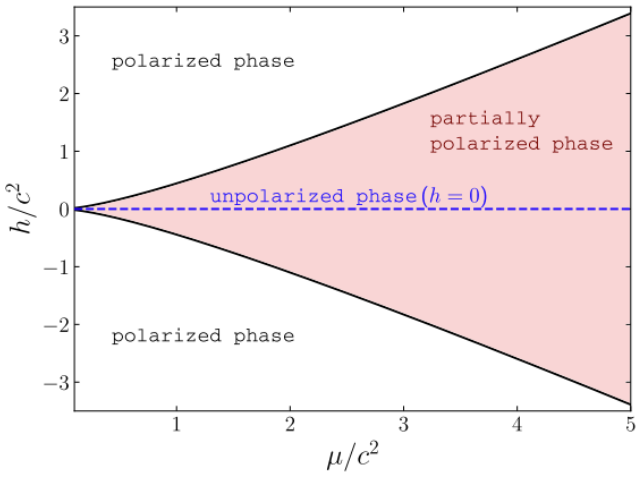

Figure 4.3: Phase diagram for the Yang-Gaudin model at T=0. Depending on the external magnetisation and the chemical potential, we could distinguish between an unpolarized phase, a partial polarized phase and a totally polarized phase. The black solid line represents the critical magnetisation $h_c(\mu)$ and is obtained numerically solving equation (4.47). The picture is taken from Ref. [28].

$$(\varepsilon_2)_j = 2h + \Delta \sum_{m=0}^{M-1} (\phi_1)_{jm}(\varepsilon_1)_m \theta_H(Q_1 - |k_m|) - \Delta \sum_{m=0}^{M-1} (\phi_2)_{jm}(\varepsilon_2)_m \theta_H(Q_2 - |k_m|), \tag{4.45}$$

where I add the Heaviside theta's in order to stop the summations at the borders of the Fermi points. Now we can group together these two equations in matrix form. With an abuse of notation, still rather clear, we can write

$$\begin{pmatrix} \varepsilon_1 \\ \varepsilon_2 \end{pmatrix} = \begin{pmatrix} k^2 - \mu - h \\ 2h \end{pmatrix} + \begin{pmatrix} 0 & \phi_1 \\ \phi_1 & \phi_2 \end{pmatrix} \begin{pmatrix} \varepsilon_1 \\ \varepsilon_2 \end{pmatrix}. \tag{4.46}$$

Now using simple linear algebra, we can explicit the dressed energies as in equation (2.87). Now using a numerical algorithm for the solution of this kind of equation, we can find the Fermi Points Q_1, Q_2 imposing $\varepsilon_j(Q_j) = 0$ and next apply the same technique also for the densities in equations (4.42) and (4.43).

An interesting feature of the Yang-Gaudin model is the phase diagram that arise at T=0 [11, 28]. This is represented in **Figure 4.3**. Through the TBA equations, one can find the equation for the critical magnetic field h_c, which separates the partially polarized phase by the fully polarized one. This equation reads

$$h_c + \frac{1}{\pi}\left[\frac{c}{2}\sqrt{\mu + h_c} - \left(\mu + h_c + \frac{c^2}{4}\right) \arctan\left(\frac{\sqrt{\mu + h_c}}{c/2}\right)\right] = 0. \tag{4.47}$$

More precisely, we can distinguish three distinct phases depending on h,μ and c, each of these has peculiar configuration for the Fermi points. I want to recall that the Fermi points are the higher and lower momenta of the particle excitation, which are symmetric in the ground state. These can be found imposing the equation $\varepsilon(k) = 0$. For a thorough discussion see Chapter 2. The three distinct phases are:

- the *polarized phase (PP)*, for $h \geq h_c$ all spins are up and spin's excitations are suppressed. This imply that the spin's Fermi points vanish, i.e. $Q_2 = 0$. Thus, the gas behaves as spinless non-interacting particles with Fermi point $Q_1 = \sqrt{\mu + h}$;
- the *unpolarized phase (UP)*, for $h = 0$ the gas is diamagnetic and the spin's excitations are unbounded, thus, $Q_2 \to \infty$. Q_1 is instead determined by equation (4.30);
- the *partially polarized phase (PPP)*, for $0 < h < h_c$ the system is paramagnetic and the Fermi points are regularly extracted from equations (4.30) and (4.31).

As we will see later, this phase transitions will be important in order to understand the initial state of the following quench protocol.

4.4 Two-component spinor Bose gas

This model, also known as Yang-Gaudin Bose gas, describes a one-dimensional bosonic system of two components with contact interaction. The second quantised Hamiltonian is

$$\hat{H} = -\int_0^L dx \left\{ \sum_{\sigma=\pm} \Psi_\sigma^\dagger(x)\big(\partial_x^2 + \mu + \sigma\Omega\big)\Psi_\sigma(x) + c : \left(\sum_{\sigma=\pm} \Psi_\sigma^\dagger(x)\Psi_\sigma(x)\right)^2 : \right\}. \tag{4.48}$$

As before, L is the length of the system, $\mu = (\mu_1 + \mu_2)/2$ is the average of the different chemical potentials of the species, $\Omega = (\mu_1 - \mu_2)/2 > 0$ half of their difference and c the interaction strength. The index σ labels the two different species. This internal degree of freedom is usually called *psuedospin* and it can be experimentally achieved through two different hyperfine states of ^{87}Rb [76]. With respect to the Yang-Gaudin case, we no longer have an external magnetisation, however, from the Hamiltonian is easy to notice that the imbalance between the chemical potentials of the two species do the same work. On top of that, the field operators satisfy CCR

$$\left[\Psi_\sigma^\dagger(x), \Psi_{\sigma'}(x')\right] = \delta_{\sigma,\sigma'}\delta(x - x'). \tag{4.49}$$

Two peculiarities of the model, which guarantee its integrability, are that the two species have the same mass and the interaction is the same intra-species and inter-species. Note that also the Yang-Gaudin Hamiltonian (4.1) can be written exactly in the form (4.48). However, due to CAR, just one interaction term survives. The only difference between this gas and a Lieb-Liniger one is that the wavefunction is symmetric only under the exchange of particles with the same pseudospin. This feature provides a significantly richer phenomenology [77–79]. As I will show later, the ground state of the system is ferromagnetic, in a pseudospin sense, and the excitations at strong coupling correspond to the ones of an XXX chain. Thus, the system disclose thermodynamical proprieties extremely different with respect to the single-component case [80].

This model is Bethe ansatz solvable. In 1968 Sutherland [10] generalized Yang and Gaudin solution to any symmetrisation of the wavefunction, while, as far as I concern, the Bethe equations for this very system was firstly found in 2002 [81] as well as its TBA equations [82].

Because of the system with attractive interaction $c < 0$ is thermodynamically unstable [79], we will restrict ourselves to $c > 0$. Specializing to the case of N particles, M of which with down pseudospin, the Bethe equations are [78]

$$e^{ik_j L} = \prod_{i\neq j} \frac{k_j - k_i + ic}{k_j - k_i - ic} \prod_{\alpha=1}^{M} \frac{k_j - \lambda_\alpha - ic/2}{k_j - \lambda_\alpha + ic/2} \qquad j = 1, \dots, N, \tag{4.50}$$

$$\prod_{j=N}^{M} \frac{\lambda_\alpha - k_j + ic/2}{\lambda_\alpha - k_j - ic/2} = -\prod_{\beta=1}^{M} \frac{\lambda_\alpha - \lambda_\beta + ic}{\lambda_\alpha - \lambda_\beta - ic} \qquad \alpha = 1, \dots, M, \tag{4.51}$$

where $\mathbf{k} = \{k_1, \dots, k_N\}$ are the quasi-momenta and $\lambda = \{\lambda_1, \dots, \lambda_M\}$ are the pseudospin rapidities. A set of rapidities that solves equations (4.50) and (4.51) fully characterizes the wavefunction. The structure of this equations is very interesting if compared to the ones of Yang-Gaudin and the one of Lieb-Liniger. The first equation has two products. The first is exactly the Lieb-Liniger piece, while the second is the Yang-Gaudin one with the numerator and the denominator reversed. By thinking at that product in term of scattering phase, that reversal can be heuristically justified as the removal of the minus sign due to the exchange of fermions. The second equation, instead, is equal to the one of the Yang-Gaudin model. As already seen for the Yang-Gaudin model, the solution of the nested Bethe equations is rather involved. Thus, we will once again exploit the string hypothesis [78].

Consequently, for $c > 0$ the k_j rapidities are real, while the λ's arrange themselves into strings which represent n-bound states

$$\lambda_\alpha^{n,j} = \lambda_\alpha^n + (n+1-2j)\frac{c}{2}i + \text{deviations} \qquad j = 1, 2, \ldots, n, \tag{4.52}$$

with deviations that vanish exponentially in the infinite size limit. As we are interested in the hydrodynamic evolution of the system, we want to move toward the TBA equations. As we are going to see, these are straightforwardly obtained combining the ones of the two model previously studied. Let's start by taking the log of (4.50) and (4.51)

$$k_j L = 2\pi I_j - \sum_{i=1}^{N} \theta\left(\frac{k_j - k_i}{c}\right) + \sum_{n=1}^{\infty}\sum_{\alpha=1}^{M_n} \theta\left(\frac{k_j - \lambda_\alpha^n}{nc/2}\right), \qquad j = 1, \ldots, N, \tag{4.53}$$

$$\begin{aligned} &\sum_{j=1}^{N} \theta\left(\frac{\lambda_\alpha^n - k_j}{nc/2}\right) = 2\pi J_\alpha^n + \sum_{m=1}^{\infty}\sum_{\beta=1}^{M_m} \Theta_{nm}\left(\frac{\lambda_\alpha^n - \lambda_\beta^m}{c/2}\right), \\ &\alpha = 1, \ldots, M_n, \quad n \geq 1, \end{aligned} \tag{4.54}$$

where M_n is the number of string of length n, $\{I_j\}_{j=1,\ldots,N}$ and $\{J_\alpha^n\}_{\alpha=1,\ldots,M_n}$ are two distinct sets of Bethe integers, $\theta(x) \equiv 2\arctan x$ and $\Theta_{nm}(x)$ is the same as for Yang-Gaudin (see equation (4.11)). With the equations written in this form, what we said previously is extremely clear. In equation (4.53) we have the same kernel of Lieb-Liniger and the one of Yang-Gaudin with reversed sign. Instead, equation (4.54) is equal to (4.11). At this point, the derivation of the Bethe-Gaudin-Takahashi equations follows the same steps as for the Yang-Gaudin model, and we are not going to repeat them. After having introduced the densities both of particles and holes for the quasi-momenta ρ, ρ^h and the spin-strings σ_n, σ_n^h, we get

$$\rho^{tot}(k) = \frac{1}{2\pi} + \phi_2 * \rho - \sum_{n=1}^{\infty} \phi_n * \sigma_n(k), \tag{4.55}$$

$$\sigma_n^{tot}(k) = \phi_n * \rho(k) - \sum_{m=1}^{\infty} \Phi_{nm} * \sigma_m(k), \tag{4.56}$$

where the kernels are the same defined in equations (4.21) and (4.22), and the convolution is again defined as

$$f * g(k) = \int dk' f(k-k')g(k'). \tag{4.57}$$

Because of these equations follow directly from the Bethe equations by taking the thermodynamic limit, we again see that the first equation has the Lieb-Liniger piece and the Yang-Gaudin one with the minus sign, while the second is equal to the Yang-Gaudin one.

The BGT equations are not sufficient to characterize the state in the finite temperature case. Thus, we have to apply the Yang-Yang derivation also to this model. As before, the Gibbs free energy is given by

$$G(T, \mu, \Omega) = E[\rho] - \mu N[\rho] - \Omega(N[\rho] - 2M[\sigma_n]) - TS[\rho, \rho^h, \sigma_n, \sigma_n^h], \tag{4.58}$$

with the quantities defined as in (4.25). Minimizing the Gibbs free energy and inserting the constraint given by the BGT equations, we get

$$\begin{aligned} 0 = \frac{\delta G}{TL} = &\int \left\{ \frac{k^2 - \mu - \Omega}{T} - \ln\frac{\rho^h}{\rho} - \phi_2 * \ln\left(1 + \frac{\rho}{\rho^h}\right) - \sum_{n=1}^{\infty} \phi_n * \ln\left(1 + \frac{\sigma_n}{\sigma_n^h}\right) \right\} \delta\rho dk \\ &+ \sum_{n=1}^{\infty} \int \left\{ \frac{2n\Omega}{T} - \ln\frac{\sigma_n^h}{\sigma_n} + \phi_n * \ln\left(1 + \frac{\rho}{\rho^h}\right) + \sum_{m=1}^{\infty} \Phi_{nm} * \ln\left(1 + \frac{\sigma_m}{\sigma_m^h}\right) \right\} \delta\sigma_n dk. \end{aligned} \tag{4.59}$$

Now let's introduce the dressed energies

$$\frac{\rho^h(k)}{\rho(k)} \equiv \exp(\varepsilon_1(k)/T), \qquad \frac{\sigma_n^h(k)}{\sigma_n(k)} \equiv \exp(\varepsilon_{2,n}(k)/T). \tag{4.60}$$

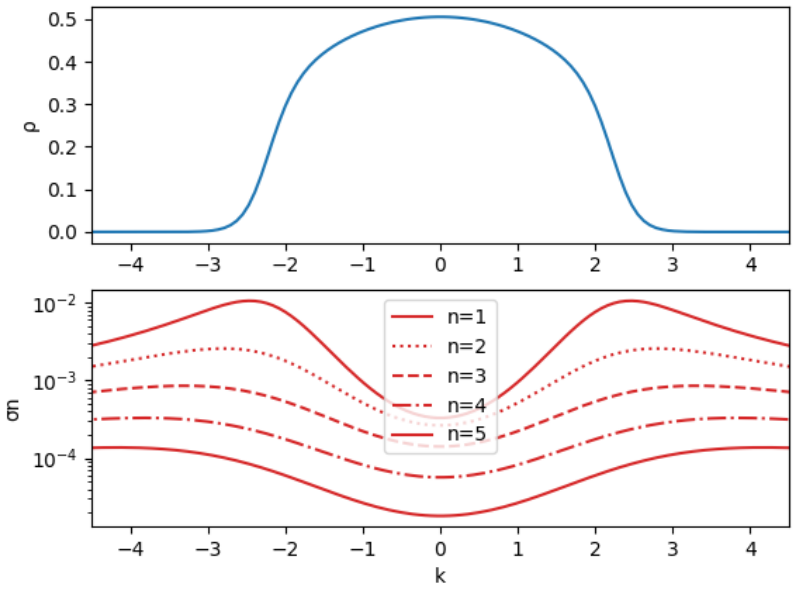

Figure 4.4: Root densities ρ and σ_n for two-component spinor Bose gas at $T = 1$. The parameters are $c = 1$, $\mu = 2$ and $\Omega = 0.5$.

We have finally obtained the TBA equations for this two-component spinor Bose gas

$$\varepsilon_1(k) = k^2 - \mu - \Omega - T\phi_2 * \ln\Big(1 + e^{-\varepsilon_1/T}\Big)(k) - T\sum_{n=1}^{\infty} \phi_n * \ln\Big(1 + e^{-\varepsilon_{2,n}/T}\Big)(k) \tag{4.61}$$

$$\varepsilon_{2,n}(k) = 2nh + T\phi_n * \ln\Big(1 + e^{-\varepsilon_1/T}\Big)(k) + T\sum_{m=1}^{\infty} \Phi_{n,m} * \ln\Big(1 + e^{-\varepsilon_{2,m}/T}\Big)(k) \qquad n = 1, 2, \dots \tag{4.62}$$

Comparing these with the dressed energies of the Yang-Gaudin model (4.30) and (4.31), we notice an extra dressing term for ε_1 which correspond to the one of Lieb-Liniger, as expected. Instead, the second equation in the r.h.s. has a crucial sign difference in the second term. Next we will see why it is crucial. The occupation functions are obviously defined

$$n_1(k) \equiv \frac{\rho_1(k)}{\rho^{tot}(k)} = \frac{1}{1 + e^{\varepsilon_1/T}}, \qquad n_{2,n}(k) \equiv \frac{\sigma_n(k)}{\sigma_n^{tot}(k)} = \frac{1}{1 + e^{\varepsilon_{2,n}/T}}. \tag{4.63}$$

In general, every bare quantity, say $\{\zeta_1, \zeta_{2,n}\}$, can be dressed via the equations

$$\zeta_1^{dr}(k) = \zeta_1 + \phi_2 * \zeta_1^{dr} n_1(k) + \sum_{n=1}^{\infty} \phi_n * \zeta_{2,n}^{dr} n_{2,n}(k), \tag{4.64}$$

$$\zeta_{2,n}^{dr}(k) = \zeta_{2,n} - \phi_n * \zeta_1^{dr} n_1(k) - \sum_{m=1}^{\infty} \Phi_{n,m} * \zeta_{2,m}^{dr} n_{2,m}(k) \qquad n = 1, 2, \dots. \tag{4.65}$$

The equations are solved as for Yang-Gaudin. An example of root densities is reported in **Figure 4.4**. We can see that, with respect to the fermionic case in **Figure 4.1**, the root density ρ is bolder. Since its integral is the density of particle, as stated in (4.25), we see that the bosonic system has a grater density, as expected.

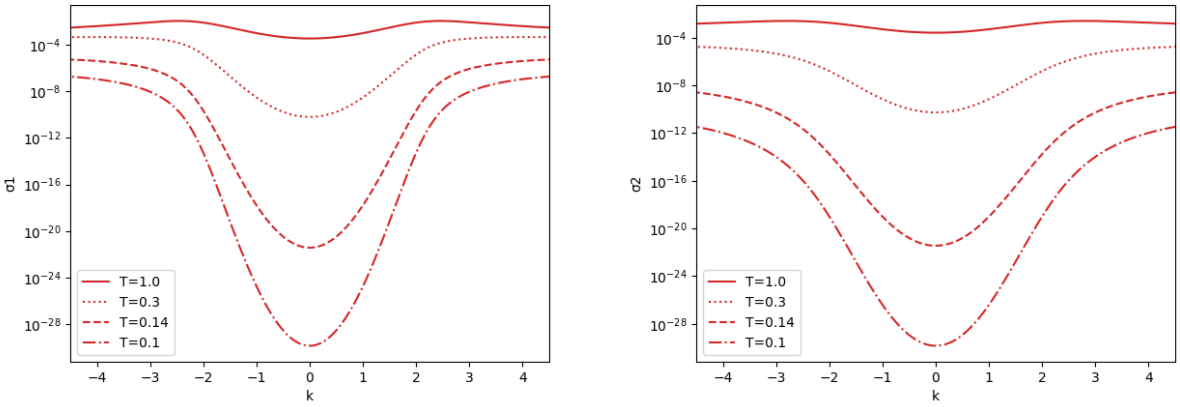

Figure 4.5: Comparison of the spin-strings at different temperature in the two-component spinor Bose gas. On the left the n=1 string, i.e. the single spin quasi-particle, while on the right the n=2 string, i.e. a simple bound state. We can see directly the fact that both are thermally activated. The parameters are $c = 1$, $\mu = 2$ and $\Omega = 0.5$.

Zero temperature limit In the limit of zero temperature, the two-component spinor Bose gas reduces to a Lieb-Liniger model. In fact, the decoupled version the the TBA equations (4.61) and (4.62) is [79]

$$\begin{aligned}\varepsilon_1(k) = k^2 - \mu - \Omega - T\phi_2 * \ln\left(1 + e^{-\varepsilon_1/T}\right)(k) + Tr * \ln\left(1 + e^{-\varepsilon_1/T}\right)(k) \\ - Ts * \ln\left(1 + e^{\varepsilon_{2,1}/T}\right)(k),\end{aligned} \tag{4.66}$$

$$\varepsilon_{2,1}(k) = Ts * \ln\left((1 + e^{\varepsilon_{2,1}/T})(1 + e^{-\varepsilon_1/T})\right), \tag{4.67}$$

$$\varepsilon_{2,n}(k) = Ts * \ln\left((1 + e^{\varepsilon_{2,n-1}/T})(1 + e^{\varepsilon_{2,n+1}/T})\right) \qquad n \geq 2, \tag{4.68}$$

with the boundary condition $\lim_{n\to\infty} \varepsilon_{2,n} = 2n\Omega$ and

$$s(k) = \frac{\operatorname{sech}(\pi k/c)}{2c}, \qquad r(k) = \phi_1 * s(k). \tag{4.69}$$

Notice that in the equation for $\varepsilon_1(k)$ there is an extra Lieb-Liniger piece and that the convolution with r changed sign. However, the most significant difference is in equation (4.67) where inside the log there is a product and no longer a quotient. Thus, also $\varepsilon_{2,1} > 0$ and so it is thermally activated. Physically, this means that all the pseudospin excitations are suppressed and the ground state is ferromagnetic. Hence, the system behave as Lieb-Liniger for T=0. So, its TBA equations for the dressed energy and the root density are

$$\varepsilon(k) = k^2 - \mu - \Omega + [\phi_2 * \varepsilon]_Q(k), \qquad k \in [-Q, Q], \tag{4.70}$$

$$\rho(k) = \frac{1}{2\pi} + [\phi_2 * \rho]_Q(k), \qquad k \in [-Q, Q], \tag{4.71}$$

where Q is the Fermi point. Notice that $\mu + \Omega = \mu_1$, accordingly to the fact that one species disappears. A numerical plot that show the thermal suppression of the pseudospin excitations is shown in **Figure 4.5**.

Chapter 5

Generalised Hydrodynamics of multi-component gases

Now we are going to study and compare the two multi-component models I introduced in the previous chapter, when they are subject to the same quench. The two models are both multi-component with contact interaction, the only difference lays in the statistics of the particles they describe. Hence, the intent of this section is to find and motivate qualitative difference between the behaviour of the the models due to the different statistics. From the theory of the previous Chapter, we already know of an important difference between the two models, i.e. the spin excitations. At zero temperature, the fermionic model still preserve one quasi-particle spin excitation, despite the bound state are suppressed. On the contrary, the bosonic gas is pseudospin ferromagnetic at zero temperature. This has physical consequences on the magnetisation that it is enhanced for the bosons. When we turn on the temperature, the spin strings excitations start to become relevant for both the models. However, if we take a look at the plots of the first two spin string in **Figure 4.2** and **Figure 4.5**, we can see that these are much more suppressed in the bosonic gas. Thus, this preserves a strong tendency to stay ferromagnetic. In this section we are going to study what effects this differences bring in the out of equilibrium dynamics of the two gases. We will analyze the zero temperature case, where the quantum effects due to the statistics are higher, and three finite temperature regime: low, intermediate and high.

5.1 Quench protocol: harmonic trap release

The quench protocol we will study is again a harmonic trap release, thus, we start with an initial state with external potential $V(x) = \omega^2 x^2$ and at $t = 0$ we turn it off, i.e. $\omega \overset{t=0}{\to} 0$ (see **Figure 5.1**). As for the Lieb-Liniger gas in Chapter 3, the presence of the external potential spoils the integrability of the two models. However, if we assume the existence of a mescoscopic scale where the potential is approximately constant, but such that it is populated by a thermodynamical number of particles, we can still apply the TBA equations. Actually, the external potential enters in the Hamiltonian with a term like $V(x)\sum_{\sigma=\pm}\Psi^\dagger_\sigma(x)\Psi_\sigma(x)$, thus it can be recollect with the chemical potential μ to give an effective chemical potential $\mu(x) = \mu - V(x)$. Thus, at each position we can solve the TBA equations using the effective chemical potential. Notice that the external magnetic field h (or Ω for the spinor Bose gas) does not enter in the effective chemical potential, since it distinguishes between the two spin species. The effective chemical potential takes the form $\mu(x) = \mu + h - V(x)$ only if one of the species is suppressed, hence in the fully polarized regime of Yang-Gaudin, or for the spinor Bose gas at T=0.

As for the Lieb-Liniger gas in Chapter 3, for the numerical solution of the initial state, I discretized the space and for each position I solved the TBA equations, with $\mu = \mu(x)$, obtaining the dressed energies and the root densities, as explained in the previous sections. Integrating the root densities in the momentum space and repeating the procedure for each position one gets the distribution of the particles in the harmonic trap.

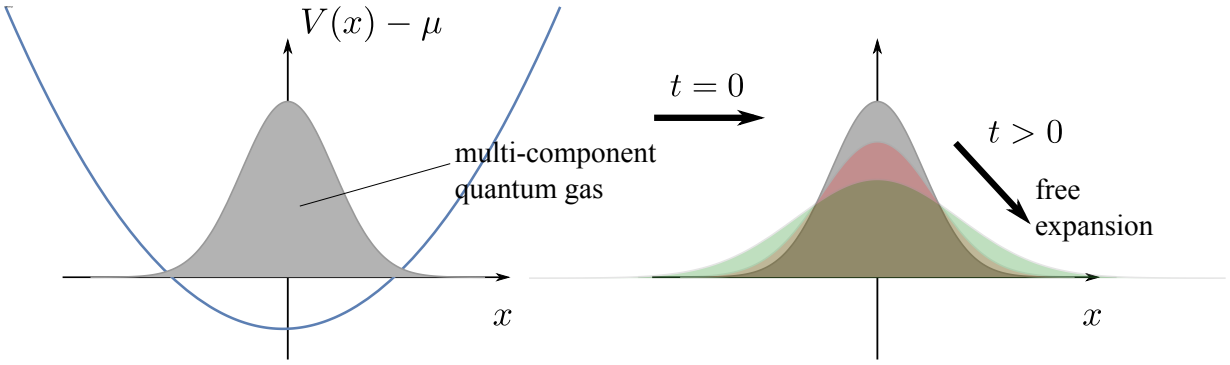

Figure 5.1: Cartoon of a harmonic trap release. On the left there is the system prepared in an initial state where is confined by a harmonic potential $V(x) = \omega^2 x^2$. At $t = 0$ we turn it off, i.e. $\omega \overset{t=0}{\to} 0$, and the system pursue a free expansion, represented on the right.

In the analysis of this chapter, we will compare the expansion of the two gases with the same interaction strength c, chemical potential μ and external magnetic field h (or Ω). As we will see, in such a setup the two systems occupy the same volume in the initial state.

The power of our simulations is that the out of equilibrium evolution is achieved through the equations of the Generalised Hydrodynamics, that provide a simple exact framework for the hydrodynamics of integrable systems. These equations for the occupation functions are

$$\begin{aligned}(\partial_t + v_1(t,x)\partial_x)n_1(t,x) &= 0,\\ (\partial_t + v_{2,n}(t,x)\partial_x)n_{2,n}(t,x) &= 0,\end{aligned} \tag{5.1}$$

where the effective velocities v_1 and $v_{2,n}$ are given by the standard formula

$$v_1 = \frac{\partial_k \varepsilon_1(k)}{2\pi\rho^{tot}(k)}, \qquad v_{2,n} = \frac{\partial_k \varepsilon_{2,n}(k)}{2\pi\sigma_n^{tot}(k)}. \tag{5.2}$$

The equations (5.1) give the time evolution for the occupation functions. From these we can compute all the macroscopic quantities of the system, such as the root densities, via the dressing procedure, as explained in Chapter 3 and Chapter 4.

The equations of the generalised hydrodynamics are numerically solved by a procedure which is a generalisation of the one described in Chapter 3, i.e. modified to account for multiple quasi-particle species. Differently from the Lieb-Liniger gas, in this case we have an infinite set of occupation functions n_1 and $n_{2,n}$ which evolves according to the equations of GHD. The algorithm is the same, and is based on the solution provided by the methods of characteristics. Since numerically we cannot solve an infinite set of equations, we exploit the fact that the strings are thermally activated to cutoff its number.

In the plots I am going to present in this section, I will not report the densities for the spin strings, but in its place the magnetisation density, which has a more physical meaning. If the system of volume L has N particles, M of which with spin down, the density of magnetisation of the system is $m = \frac{N-2M}{2L}$. Thus, in terms of the root densities

$$m = \frac{1}{2}\int dk \rho_1(k) - \sum_{n=1}^{\infty} n \int dk \rho_{2,n}(k). \tag{5.3}$$

For the spinor Bose gas, we will improperly use the term magnetisation as if the two pseudospin species were effectively spins, in analogy with the fermionic system. Another quantity I will report on the plots is the current both for the particles density and the magnetisation density. These are

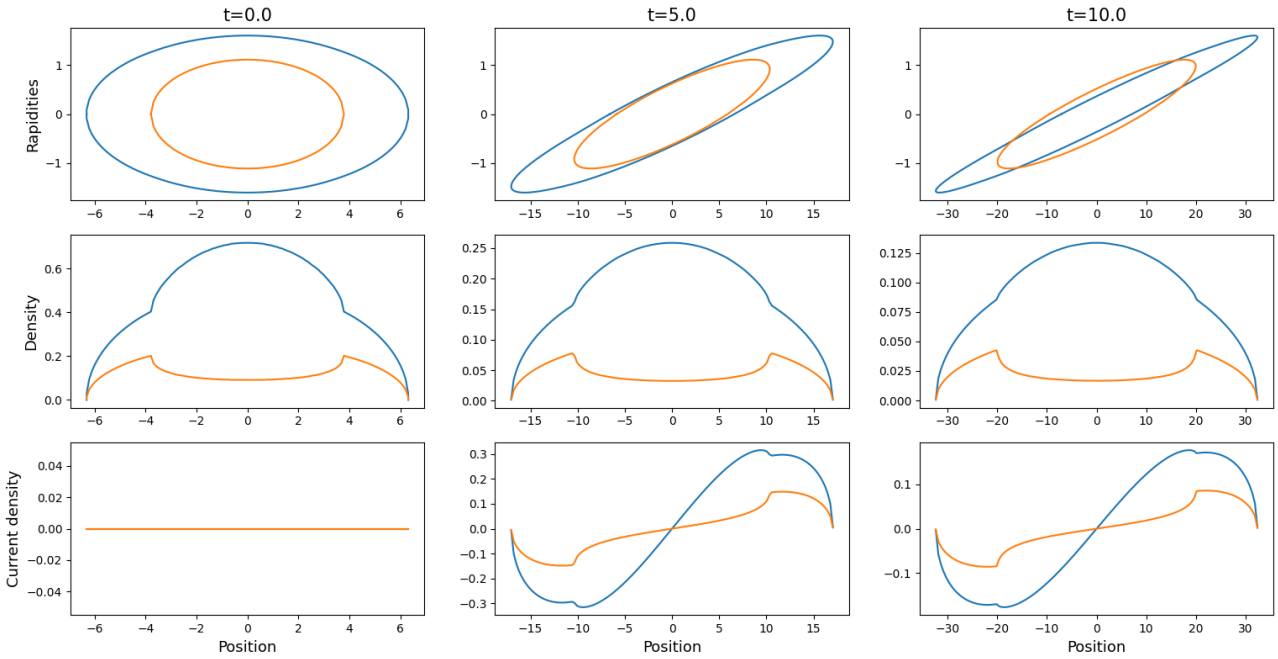

Figure 5.2: Zero entropy GHD evolution of the Yang-Gaudin gas. The parameters are $c = 1$, $\mu = 2$ and $h = 0.5$. The quench protocol is a release of a harmonic potential $\omega = 0.25 \overset{t=0}{\to} 0$. In the upper row is shown the evolution of the Fermi contours for the quasi-momenta (blue line) and the spin rapidities (orange line). In the middle and bottom rows are shown the evolutions for the particles density and current (blue line) and for the magnetisation density and current (orange line).

defined as accordingly to equation (3.34)

$$\begin{aligned} j_\rho(x) &= \int dk \rho_1(x,k) v_1(x,k), \\ j_m(x) &= \frac{1}{2} \int dk \rho_1(x,k) v_1(x,k) - \sum_{n=1}^{\infty} n \int dk \rho_{2,n}(x,k) v_{2,n}(x,k). \end{aligned} \tag{5.4}$$

In the rest of the chapter, I will present the results of the quenches both for the bosonic and the fermionic gases at different temperature. This part is the original one of the thesis. Parts of the results for the Yang-Gaudin model are presented in Ref. [28], while in literature is not present a GHD work on the two-component spinor Bose gas.

5.2 Non equilibrium dynamics at zero temperature

We begin by considering the two gases at zero temperature. As we already saw, the fermionic gas with non vanishing external magnetic field, could be either partially polarized or fully polarized. We chose the parameters $\{\mu, c, h\}$ in order to have a partially polarized system in the origin, where $\mu(x) = \mu$. Moving away from the origin, the effective chemical potential decreases until it reaches the critical value for the phase transition to the fully polarized system $\mu(x) = \mu_c(h; c)$, where $\mu_c(h; c)$ is obtained inverting the relation (4.47) (see **Figure 4.3**). Now the effective chemical potential becomes $\mu(x) = \mu + h - V(x)$ and the system is hence bounded by the positions that are solutions of $\mu(x) = 0$. For the spinor Bose gas, instead, the system is always fully polarized at zero temperature, hence the chemical potential is always $\mu(x) = \mu + \Omega - V(x)$ and bounded by $\mu(x) = 0$. For this reason, if the two systems have the same set of parameters $\{\mu, h, c\}$, they result to be confined in the same volume.

Let's start by studying the free expansion at temperature zero. As we said before, in the bosonic system we do not have spin excitations, hence the magnetisation is half of the particles density according to equation (5.4). For this reason, we expect a significantly different phenomenology between the two

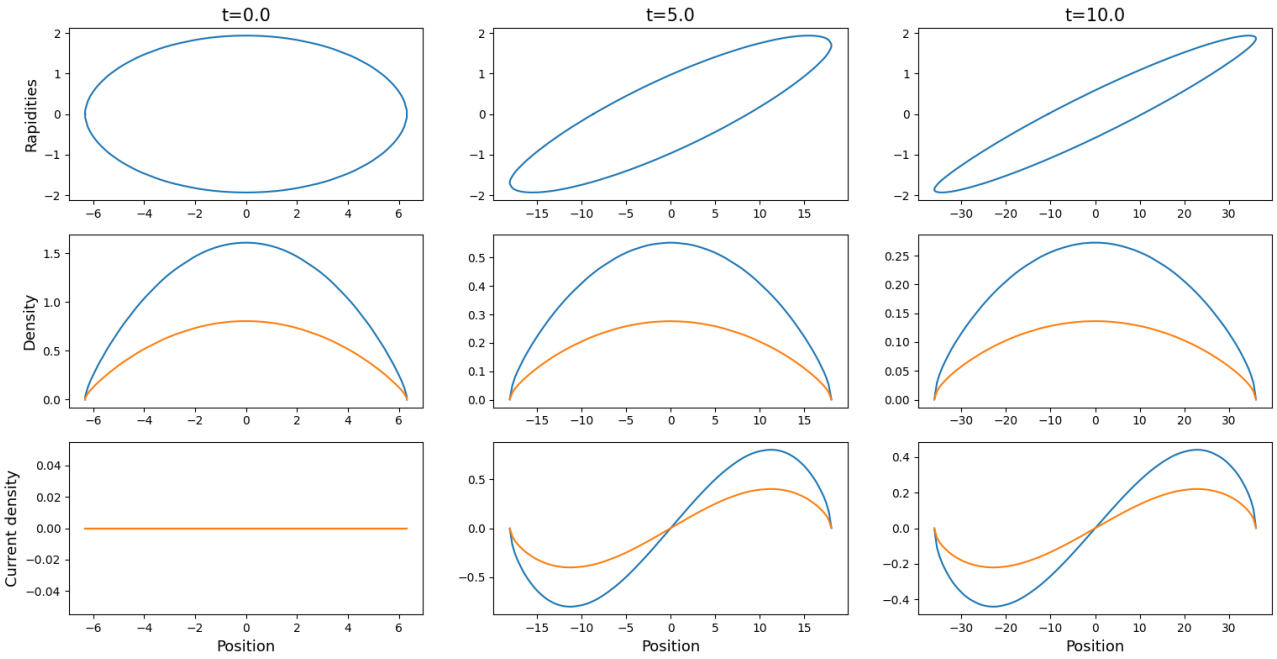

Figure 5.3: Zero entropy GHD evolution of the spinor Bose gas. In this setup the system reduce to Lieb-Liniger. The parameters are $c = 1$, $\mu = 2$ and $\Omega = 0.5$. The quench protocol is a release of a harmonic potential $\omega = 0.25 \overset{t=0}{\to} 0$. In the upper row is shown the evolution of the Fermi contours for the quasi-momenta. In the middle and bottom rows are shown the evolutions for the particle density and current (blue line) and for the magnetisation density and current (orange line).

gases. Starting from equation (5.2), we can recast the equations for the effective velocities in the form of a linear Fredholm equation, which can be numerically solved as explained in **Section 2.9**. For the Yang-Gaudin model these equations are

$$v_1(k)\rho_1(k) = \frac{k}{\pi} + [\phi_1, \rho_2 v_2]_{Q_2}(k) \qquad k \in [-Q_1, Q_1], \tag{5.5}$$

$$v_2(k)\rho_2(k) = [\phi_1, \rho_1 v_1]_{Q_1}(k) - [\phi_2, \rho_2 v_2]_{Q_2}(k) \qquad k \in [-Q_2, Q_2], \tag{5.6}$$

where I set $v_{2,1} \equiv v_2$ because for $n \geq 2$ they are all zero, and $\pm Q_{1,2}$ are the Fermi points for the two species. On the other hand, for the two-component spinor Bose gas we have just one quasi-particle excitation, whose effective velocity is given by

$$v_1(k)\rho_1(k) = \frac{k}{\pi} + [\phi_2, \rho_1 v_1]_{Q}(k) \qquad k \in [-Q, Q]. \tag{5.7}$$

Notice that the physics of the spinor Bose gas, at zero temperature, resembles the one of the Lieb-Liniger gas discussed in chapter 3. The plots for the expansion of the two gases are reported in **Figure 5.2** for the fermions and in **Figure 5.3** for the bosons. Since we are at zero temperature, we see the densities of the two gases to not have thermal tails, but to be strictly confined in the region where the effective chemical potential is positive. In addition, for both the gases we see that the expansion proceed as described in Chapter 3, i.e. with a small horizontal shift in the Fermi points at each time step. In this way, the free expansion of the gases result in a smearing out of the gases towards a more homogeneous configuration. However as expected, the two systems display significantly different behaviours. Firstly, we notice the presence of the cusps in the densities of the fermions, which state the presence of the phase transition from a partially polarized system in the bulk to a full polarization in the borders, while the bosons are everywhere fully polarized. A remarkable effect of the fermions is that since the velocity of the first quasi-particle is greater, the size of fully polarized regions increases with respect to the partially polarized one. This effect is called *dynamical polarization* [28]. Another source of difference we would expect is related to the instrinsic repulsion of the fermions, due to the Pauli principle. Actually, with the same repulsion strenght c, we would expect fermions to display

an higher repulsive behaviour inherent to its nature. This can be seen in the fact that the density is noticeably higher in the bosonic system, hence to confine the two systems in the same one-dimensional volume, we need an higher number of bosons. On the other hand, a remarkable fact is that non-trivially the two gases expand at the same velocity. This gives us a quantitative estimation of the effect of the statistics during the expansion of the gas. Namely, given a specific quench protocol, we are able to predict the ratio of particles N_B/N_F and the difference in the polarisation $P_B - P_F$ that are required to compensate Pauli repulsion and observe an expansion of the gases at the same velocity. In particular $N_{B,F}$ is the total number of particles for bosons or fermions, and if $M_{B,F}$ is the number of down spins, the polarisations are given by

$$P_{B,F} = \frac{N - 2M}{N} = 1 - \frac{2M}{N}, \tag{5.8}$$

where on the numerator there is the difference between the number of particles of the two species, and on the numerator the total number of particles. For our choice of parameters at temperature zero, this ratios are $N_B/N_F = 2.27$ and $P_B - P_F = 0.51$.

Before moving to the finite temperature case, we want to stress that observing the same expansion for the clouds is non trivial and requires the use of GHD.

5.3 Non equilibrium dynamics at finite temperature

Switching on the temperature, thermal tails appears and the system occupy a greater volume. However, we can see that at equal temperature the tails are similar for the two gases. Thus, the aim of this section is to compare the behaviour of the two gases if they are confined in a region of equal volume. We already know that an important effect emerges, i.e. at finite temperature the spinor Bose gas starts to have spin waves excitations. Thus, in both gases we expect an increasing suppression of the magnetisation with the temperature. In general, since the different statistical behaviour of fermions and bosons is a quantum effect, this is smoothed out by the temperature. Thus, with its increasing we expect a more and more similar behaviour of the two gases. In particular, since the spinor Bose gas has a stronger tendency to stay ferromagnetic compared to Yang-Gaudin, we expect three regimes: the low temperature one, where in both cases the suppression of the magnetisation is small and the phenomenology is similar to the zero temperature case, the medium temperature one, where the magnetisation is higly suppressed for the fermions and not for the bosons, and the high temperature one, where the suppression is high for both.

At finite temperature the effective velocities can be obtained as the solution of a set of non-linear Fredholm integral equations (see **Section 2.9**). For the Yang-Gaudin model these are

$$v_1(k)\rho_1^{tot}(k) = \frac{k}{\pi} + \sum_{n=1}^{\infty} \phi_n * v_{2,n}\rho_{2,n}(k), \tag{5.9}$$

$$v_{2,n}(k)\rho_{2,n}^{tot}(k) = \phi_n * v_1\rho_1(k) - \sum_{m=1}^{\infty} \Phi_{n,m} * v_{2,m}\rho_{2,m}(k) \qquad n = 1, 2, \ldots, \tag{5.10}$$

while for the spinor Bose gas

$$v_1(k)\rho_1^{tot}(k) = \frac{k}{\pi} + \phi_2 * v_1\rho_1(k) + \sum_{n=1}^{\infty} \phi_n * v_{2,n}\rho_{2,n}(k), \tag{5.11}$$

$$v_{2,n}(k)\rho_{2,n}^{tot}(k) = -\phi_n * v_1\rho_1(k) - \sum_{m=1}^{\infty} \Phi_{n,m} * v_{2,m}\rho_{2,m}(k) \qquad n = 1, 2, \ldots. \tag{5.12}$$

In order to numerically solve this, we have to cutoff the number of strings, paying attention to the fact that their contribution is more and more relevant with the increasing of the temperature. Thus, for the high temperature regime we will run the algorithm taking into account an higher number of spin strings with respect to the low temperature regime.

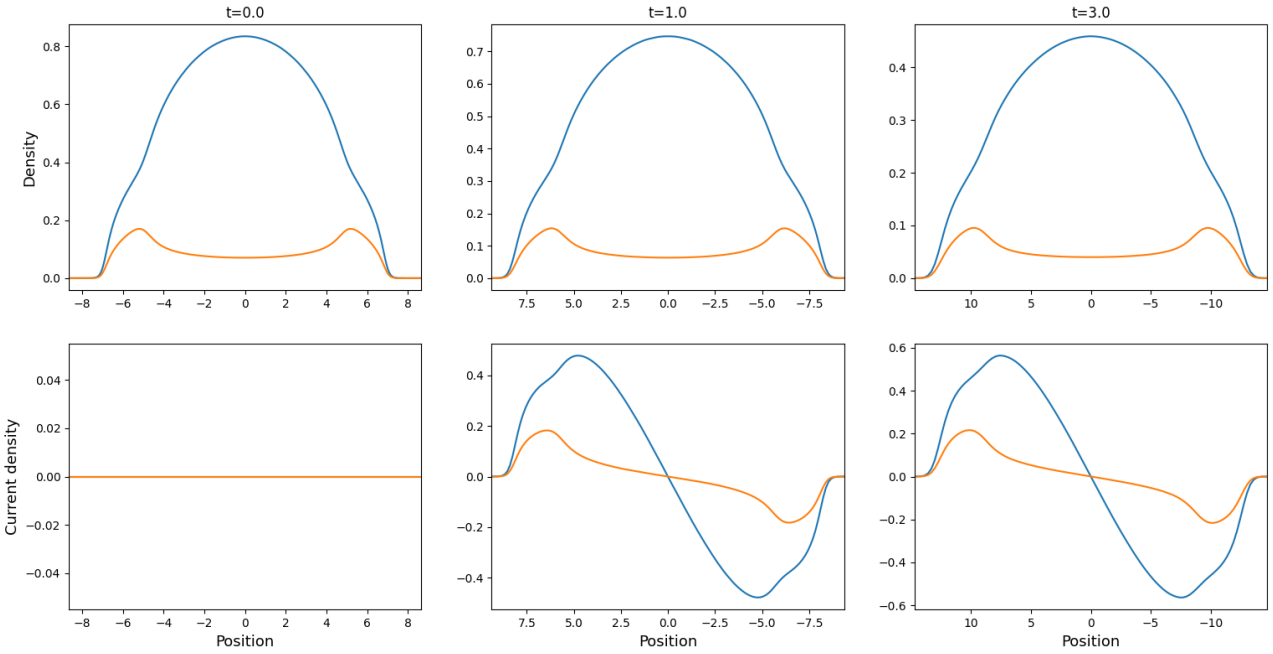

Figure 5.4: GHD evolution of the Yang-Gaudin gas at T=0.1. The parameters are $c = 1$, $\mu = 2$ and $h = 0.5$. The quench protocol is a release of a harmonic potential $\omega = 0.25 \overset{t=0}{\rightarrow} 0$. In first row is shown the evolution for the particle density (blue line) and the magnetisation density (orange line). In the lower row is the same for the current densities.

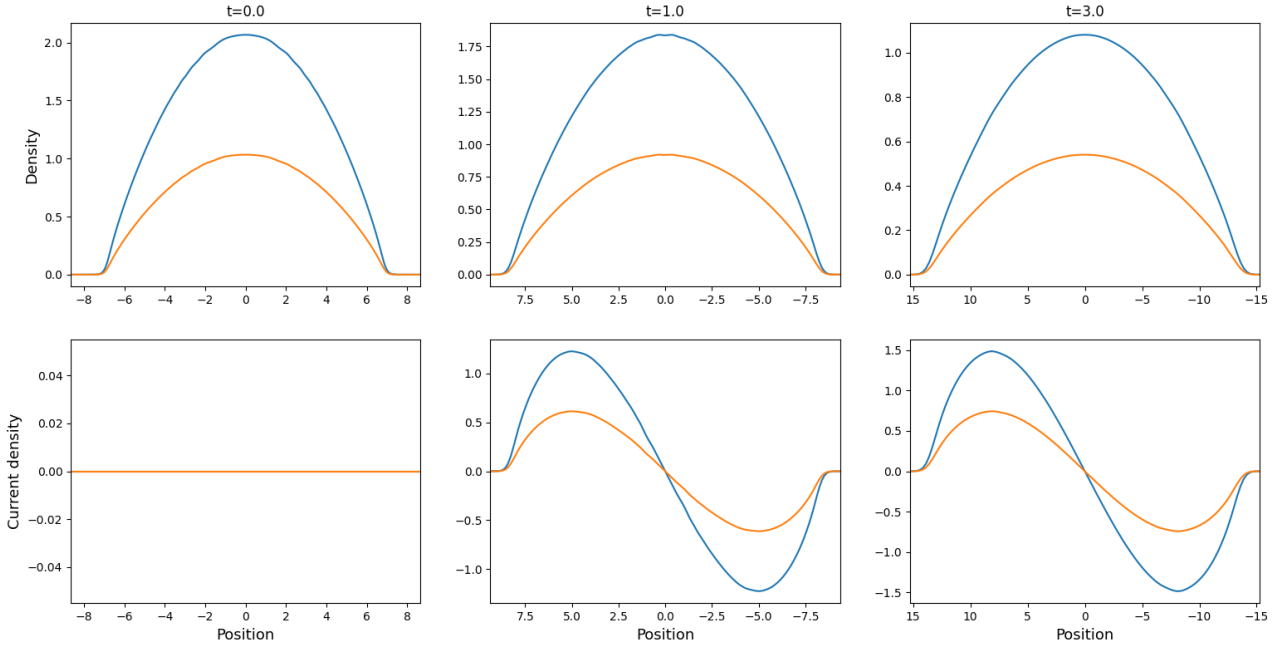

Figure 5.5: GHD evolution of the spinor Bose gas at T=0.1. The parameters are $c = 1$, $\mu = 2$ and $\Omega = 0.5$. The quench protocol is a release of a harmonic potential $\omega = 0.25 \overset{t=0}{\rightarrow} 0.$. In first row is shown the evolution for the particle density (blue line) and the magnetisation density (orange line). In the lower row is the same for the current densities.

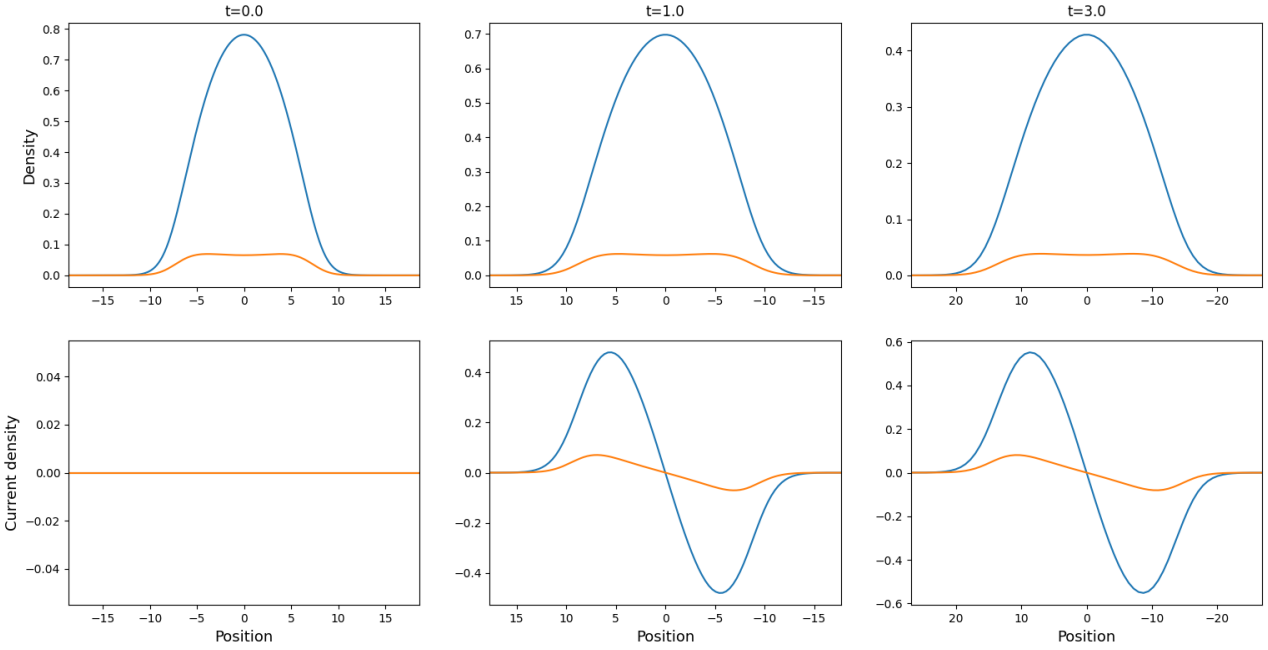

Figure 5.6: GHD evolution of the Yang-Gaudin gas at T=1. The parameters are $c = 1$, $\mu = 2$ and $h = 0.5$. The quench protocol is a release of a harmonic potential $\omega = 0.25 \overset{t=0}{\to} 0$. In first row is shown the evolution for the particle density (blue line) and the magnetisation density (orange line). In the lower row is the same for the current densities.

Low temperature At low temperatures the suppression of the magnetisation due the excitation of the strings is still low for both the two gases, hence they behave similarly to the zero entropy case. The expansion still proceed with the spreading of the density along the real axis. In the fermionic gas in **Figure 5.4** we still see some effects related to the phase transition that happens at T=0. In fact, the profiles of the densities and the currents are similar to the zero temperature case, but the spikes are smoothed out. In the bosonic gas in **Figure 5.5** we have the magnetisation that is substantially unchanged, so still high. In the same way of the zero temperature case, the expansion of the two gases proceed at the same velocity. In this case the ratios are $N_B/N_F = 2.42$ and $P_B - P_F = 0.65$.

Intermediate temperature Thermal tails appear in the densities profiles, but the two gases still occupy the same volume, as we guessed. In this intermediate regime, the effect of the temperature in the fermionic gas in **Figure 5.6** becomes evident. The magnetisation diminishes significantly with respect to the low temperature case. That's because the thermal fluctuations activate the spin-wave excitations and thus the polarization of the gas decreases. On the contrary, in the bosonic gas in **Figure 5.7** the effect of the temperature on the magnetisation is quite soft, since this is still high. From the point of view of the free expansion of the gases, this again proceed at the same velocity and the density of bosons is still quite high compared to the one of the fermions. The ratios at this regime are $N_B/N_F = 2.30$ and $P_B - P_F = 0.54$.

High temperature In the fermionic gas in **Figure 5.8** the magnetisation is almost all suppressed due to the thermal fluctuations. Thus, the two spin species are almost equally present. Also in the bosonic gas in **Figure 5.9** the magnetisation is strongly reduced compared to the previous regimes. Notwithstanding, the qualitative behaviour of the two gases is the same of the other two regimes. The bosons density is still significantly high and anew the expansion of the two gases occur at the same velocity. The quantifier we defined before now decrease substantially, acutally they are $N_B/N_F = 1.96$ and $P_B - P_F = 0.24$.

As a result, we found that if we confine the two systems in a region of equal volume via a harmonic trap and at a certain point we suddenly switch off the external potential and we let the systems to evolve freely, the expansion occurs at the same velocity for the two gases. This is possible because the

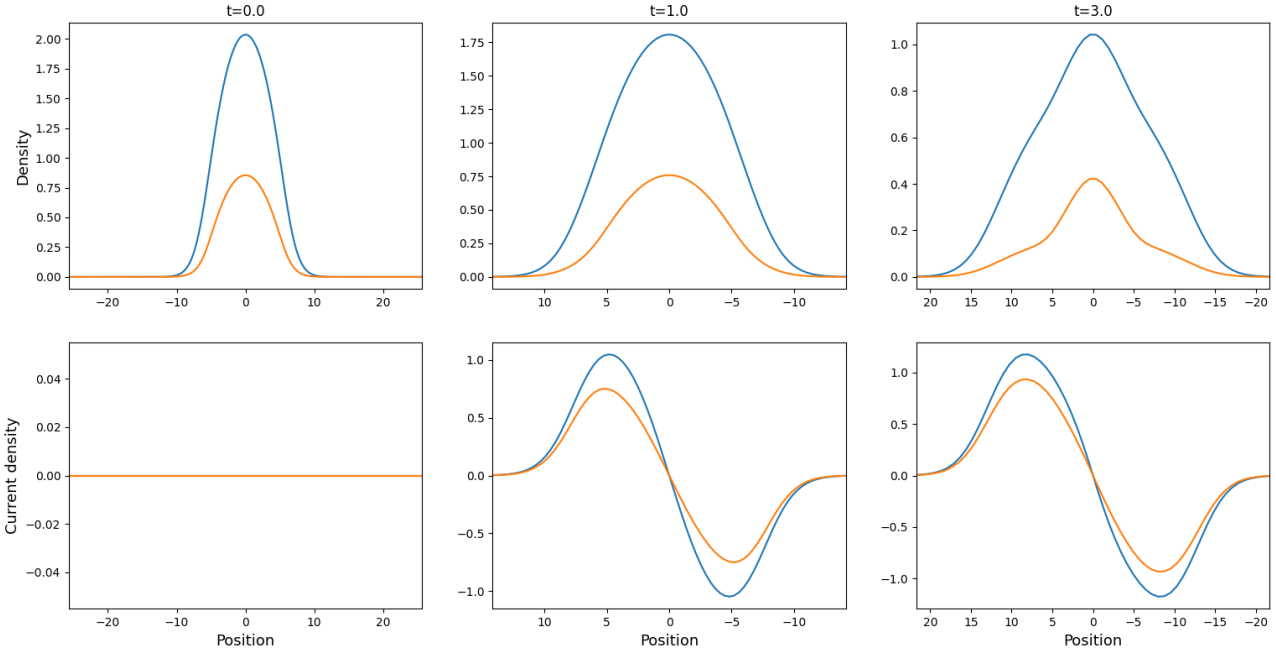

Figure 5.7: GHD evolution of the spinor Bose gas at T=1. The parameters are $c = 1$, $\mu = 2$ and $\Omega = 0.5$. The quench protocol is a release of a harmonic potential $\omega = 0.25 \overset{t=0}{\rightarrow} 0$.. In first row is shown the evolution for the particle density (blue line) and the magnetisation density (orange line). In the lower row is the same for the current densities.

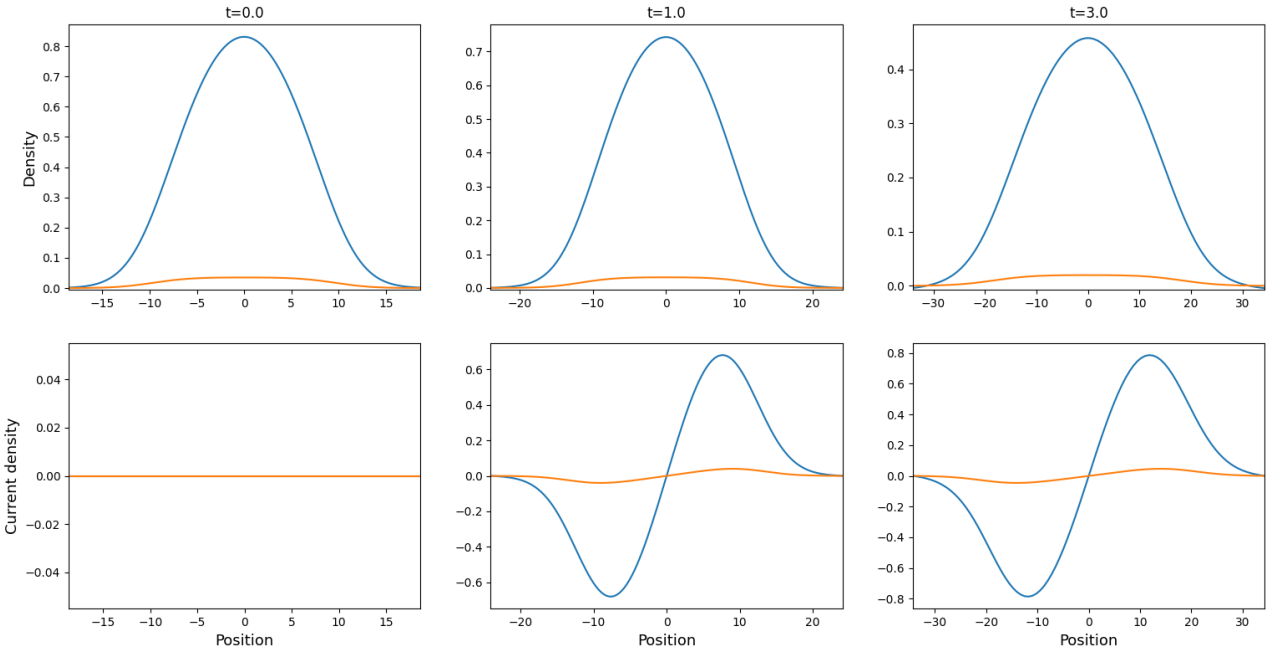

Figure 5.8: GHD evolution of the Yang-Gaudin gas at T=3. The parameters are $c = 1$, $\mu = 2$ and $h = 0.5$. The quench protocol is a release of a harmonic potential $\omega = 0.25 \overset{t=0}{\rightarrow} 0$. In first row is shown the evolution for the particle density (blue line) and the magnetisation density (orange line). In the lower row is the same for the current densities.

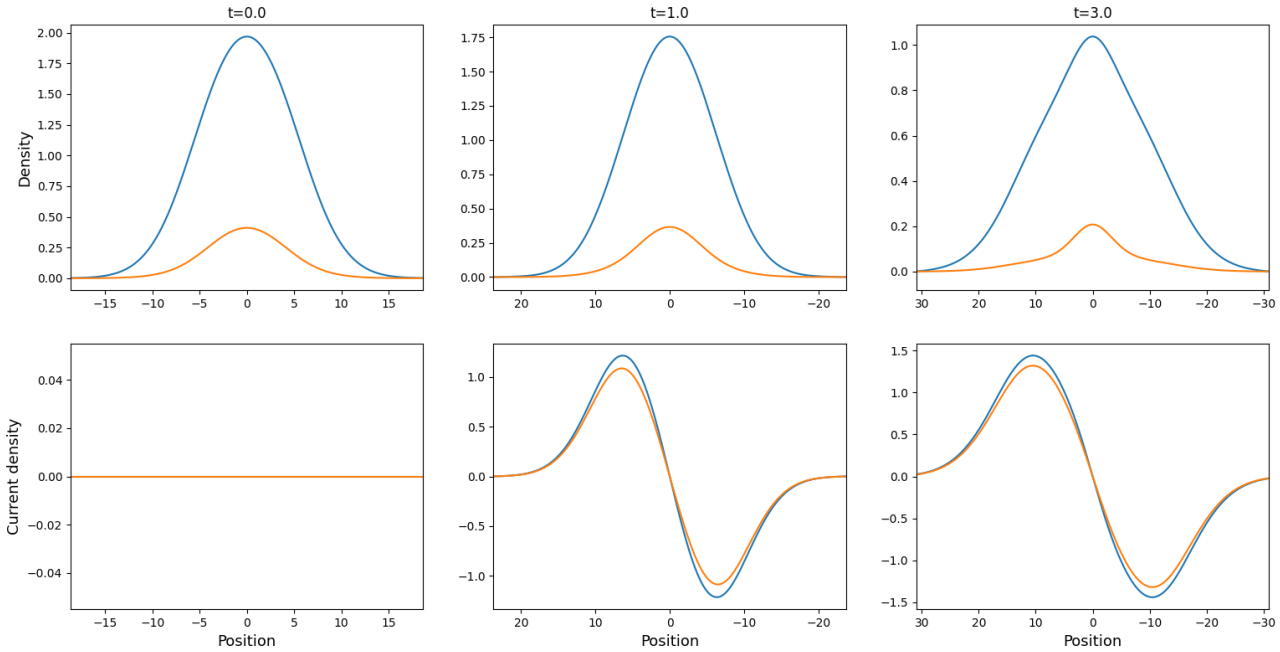

Figure 5.9: GHD evolution of the spinor Bose gas at T=3. The parameters are $c = 1$, $\mu = 2$ and $\Omega = 0.5$. The quench protocol is a release of a harmonic potential $\omega = 0.25 \overset{t=0}{\to} 0$.. In first row is shown the evolution for the particle density (blue line) and the magnetisation density (orange line). In the lower row is the same for the current densities.

differences due to the statistics, and in particular the Pauli repulsion, are compensated by the different number of particles. We define two quantifiers to take into account this, i.e. the ratio between the particles number N_B/N_F and the difference between the polarizations $P_B - P_F$. The plot of these quantities with respect to the temperature are reported in **Figure 5.10**. Despite a small increasing after the switching on of the temperature, probably due to the different way in which the strings are thermally activated, both the values start to decrease with the temperature. In particular, we expect a temperature T^* at which the two systems classicize, i.e. where $N_B/N_F = 1$ and $P_B - P_F = 0$ since at higher temperature we are not able to distinguish the different statistics.

In order to better understand these phenomenon, we have to carefully probe several values of the temperatures, and in particular at higher temperature more strings are activated and the numerical computations became challenging. In particular, we are interested in reconstruct the curve from temperature zero to the plateaux we expect in the classical regime to arise. From this analysis, it will be possible also to determine the crossover temperature T^* where the dependence on quantum statistics is expected to vanish. Indeed, due to the strongly interacting nature of the gases, an estimate of T^* based on physical arguments is not an easy task. Moreover, we have also to carefully study the low temperature region, since we observe a non-monotonic behaviour that highlights an enhancement of the quantum effects when the temperature is turned on. This non-monotonic behaviour was hard to guess a priori.

We are planning to do this in the following months and present these results in a paper.

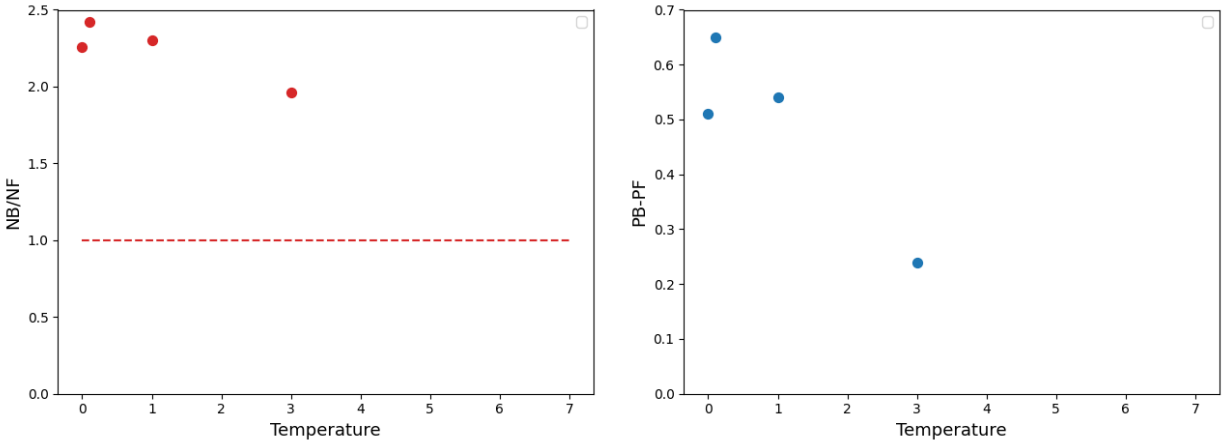

Figure 5.10: On the left the plot for the ratio between the total number of particles in the bosonic over the fermionic system N_B/N_F. The red dashed line represents the plateaux we expect to reach at higher temperatures. On the right the plot for the difference in the polarisation of the two gases $P_B - P_F$. For high temperatures we expect this to be zero.

Chapter 6

Conclusions and outlook

In this thesis, we have carried on the application of the theory of Generalised Hydrodynamics to multi-component systems, a bare-touch topic since its introduction in 2016. In particular, we started from the recently published work on the Generalised Hydrodynamics of the repulsive Yang-Gaudin model [28] to setting up a comparison with the corresponding bosonic model, i.e. a system with two bosonic species that interacts via contact interactions. The general idea that guided this analysis, was to understand what phenomenological qualitative difference brings the different statistics in the out-of-equilibrium behaviour of these two systems.

We decided to start with one of the simplest setups, i.e. the quantum quench in which a harmonic trap is instantaneously released and the system pursues a free expansion. From the theory of the two models, which are both exactly solvable via the nested Bethe ansatz procedure, we knew from the beginning that we would have several different regimes depending on the temperature. In fact, contrary to the fermionic system, the two-component spinor Bose gas is pseudospin ferromagnetic at zero temperature, and also with the increasing of the temperature it has a strong resistance, compared to Yang-Gaudin, to "activate" the spin excitations. Thus, we identify four different thermal regimes and we compare the expansion of the two gases in these different regimes. The results we found are quite remarkable. The difference in the two models is due to the Pauli exclusion principle for the fermions, so with the same strength of the repulsive parameter c, we would have expected to see a higher repulsive behaviour for the fermions, on the contrary, we found the two gases to expand at the same velocity. The effect of the Pauli principle has manifested itself in the densities of the two systems, which result to be significantly higher for the bosons. An interesting question to be explored in future studies could be to understand if the relationship between the densities is somehow related to the parameters of the model. We also introduced two numerical quantifiers for precisely taking a trace of this effect, and we plot them with respect to the temperature, and we see their tendency to move towards the *classical plateaux* at high temperature. We are planning to deepen this study in the following months and publish the results in a paper.

Another possible outlook for this work is to explore what happens in the setup opposite to the one we set in this work. We recall that in this work we decided to set the initial condition in order to have the two gases confined in the same volume. Currently, we are thinking to prepare the two gases with an initial condition that presents the same imbalance between the two species and checking how the expansion would proceed in this case.

Finally, another possible outlook we think is worth to be mention is the extension of this analysis to multi-component models involving a mixture of bosons and fermions [83–85] and check how these considerations would change in these models due to the interaction between bosons and fermions.

This work fits in the rising and promising field of the out-of-equilibrium dynamics of the multi-component integrable systems, and it is a piece in the comprehension of these models.

Appendix A

TBA decoupled

In **Section 4.3** we found the TBA equations for the Yang-Gaudin model

$$\varepsilon_1(k) = k^2 - \mu - h - T\sum_{n=1}^{\infty} \phi_n * \ln\Big(1 + e^{-\varepsilon_{2,n}/T}\Big)(k) \tag{A.1}$$

$$\varepsilon_{2,n}(k) = 2nh - T\phi_n * \ln\Big(1 + e^{-\varepsilon_1/T}\Big)(k) + T\sum_{m=1}^{\infty} \Phi_{n,m} * \ln\Big(1 + e^{-\varepsilon_{2,m}/T}\Big)(k) \qquad n = 1, 2, \dots \tag{A.2}$$

and we said that these admit a *partially decoupled* rewrite. Because of in the literature, as far as I concerned, the derivation is not present, here I will give it. First of all, let's simplify the notation

$$\zeta(k) \equiv e^{\varepsilon_1(k)/T}, \qquad \eta_n(k) \equiv e^{\varepsilon_{2,m}/T}. \tag{A.3}$$

Thus, the TBA equations become

$$\ln \zeta(k) = \frac{k^2 - \mu - h}{T} - \sum_{n=1}^{\infty} \phi_n * \ln\big(1 + \eta_n^{-1}\big)(k), \tag{A.4}$$

$$\ln \eta_n(k) = \frac{2nh}{T} - \phi_n * \ln\big(1 + \zeta^{-1}\big)(k) + \sum_{m=1}^{\infty} \Phi_{n,m} * \ln\big(1 + \eta_m^{-1}\big)(k), \qquad n = 1, 2, \dots. \tag{A.5}$$

As advised by Takahashi [14], we should use the following relations

$$\phi_n = s * (\phi_{n-1} + \phi_{n+1}), \qquad \Phi_{nm} = s * (\Phi_{n+1m} + \Phi_{n-1m}) + (\delta_{n-1m} + \delta_{n+1m})s. \tag{A.6}$$

Now we start from the back, so from the equation for $\ln \eta_n(k)$ for $n \geq 2$. Exploiting the second relation, we get

$$\begin{aligned} \ln \eta_n(k) = \frac{2nh}{T} - \phi_n * \ln\big(1 + \zeta^{-1}\big)(k) + s * \sum_{m=1}^{\infty} \Phi_{n-1,m} * \ln\big(1 + \eta_m^{-1}\big)(k) \\ + s * \sum_{m=1}^{\infty} \Phi_{n+1,m} * \ln\big(1 + \eta_m^{-1}\big)(k) + s * \ln\big(1 + \eta_{n-1}^{-1}\big) + +s * \ln\big(1 + \eta_{n+1}^{-1}\big). \end{aligned} \tag{A.7}$$

Now using (A.5), we can transform the two summations. For instance, the first can be rewritten as

$$\sum_{m=1}^{\infty} \Phi_{n-1,m} * \ln\big(1 + \eta_m^{-1}\big)(k) = \ln \eta_{n-1} - \frac{2(n-1)h}{T} + \phi_{n-1} * \ln\big(1 + \zeta^{-1}\big). \tag{A.8}$$

Thus, we get

$$\begin{aligned}\ln\eta_n(k) = &\frac{2nh}{T} - \phi_n * \ln\big(1+\zeta^{-1}\big)(k)\\ &+ s*\ln\eta_{n-1}(k) - s*\frac{2(n-1)h}{T} + s*\phi_{n-1}*\ln\big(1+\zeta^{-1}\big)(k)\\ &+ s*\ln\eta_{n+1}(k) - s*\frac{2(n+1)h}{T} + s*\phi_{n-1}*\ln\big(1+\zeta^{-1}\big)(k)\\ &+ s*\ln\big(1+\eta_{n-1}^{-1}\big)(k) + +s*\ln\big(1+\eta_{n+1}^{-1}\big)(k).\end{aligned} \tag{A.9}$$

Now look at the red terms. The convolutions of s are trivial because they are done with a constant. Thus, they turn into the integration of s over the real axis. It is simple to check that this function is normalized to $1/2$. Thus, the three red terms simplify. Moreover, also the blue pieces simplify due to the first relation in (A.6). So, finally we obtain

$$\ln\eta_n(k) = s*\ln\left((1+\eta_{n-1})(1+\eta_{n+1})\right), \tag{A.10}$$

which is exactly (4.37). Now, let's consider the case $n=1$

$$\ln\eta_1(k) = \frac{2h}{T} - \phi_1*\ln\big(1+\zeta^{-1}\big)(k) + \sum_{m=1}^{\infty}\Phi_{1,m}*\ln\big(1+\eta_m^{-1}\big)(k). \tag{A.11}$$

The difference compared to the case $n\geq 2$ is that the second relation in (A.6) "degenerates". It could be check that its correct expression in this case is

$$\Phi_{1m} = s*\Phi_{2m} + \delta_{2m}s. \tag{A.12}$$

Hence, equation (A.11) becomes

$$\ln\eta_1(k) = \frac{2h}{T} - \phi_1*\ln\big(1+\zeta^{-1}\big)(k) + s*\sum_{m=1}^{\infty}\Phi_{2,m}*\ln\big(1+\eta_m^{-1}\big)(k) + s*\ln\big(1+\eta_2^{-1}\big). \tag{A.13}$$

As before, we substitute the summation exploiting (A.5)

$$\sum_{m=1}^{\infty}\Phi_{2,m}*\ln\big(1+\eta_m^{-1}\big)(k) = \ln\eta_2 - \frac{4h}{T} + \phi_2*\ln\big(1+\zeta^{-1}\big). \tag{A.14}$$

After the substitution, the simplifications easily arise after adding and subtracting a term (in red)

$$\begin{aligned}\ln\eta_1(k) = &\cancel{\frac{2h}{T}} - \cancel{\phi_1*\ln\big(1+\zeta^{-1}\big)(k)} + s*\ln\eta_2 - s*\cancel{\frac{4h}{T}}\\ &+ \cancel{s*\phi_2*\ln\big(1+\zeta^{-1}\big)} + s*\ln\big(1+\eta_2^{-1}\big) + \cancel{s*\ln\big(1+\zeta^{-1}\big)} - +s*\ln\big(1+\zeta^{-1}\big).\end{aligned} \tag{A.15}$$

So, finally

$$\ln\eta_1(k) = s*\ln\left((1+\eta_2)/(1+\zeta^{-1})\right), \tag{A.16}$$

which is equation (4.36). Last but not least, the first equation

$$\ln\zeta(k) = \frac{k^2-\mu-h}{T} - \sum_{n=1}^{\infty}\phi_n*\ln\big(1+\eta_n^{-1}\big)(k). \tag{A.17}$$

The procedure is again the same, but this time we use the first relation of (A.6). In this way, we get

$$\ln\zeta(k) = \frac{k^2-\mu-h}{T} - s*\sum_{n=1}^{\infty}\phi_{n-1}*\ln\big(1+\eta_n^{-1}\big)(k) - s*\sum_{n=1}^{\infty}\phi_{n+1}*\ln\big(1+\eta_n^{-1}\big)(k). \tag{A.18}$$

This can be straightforwardly rewritten as

$$\begin{aligned}\ln\zeta(k) = \frac{k^2-\mu-h}{T} - s * \sum_{n=2}^{\infty} \phi_n * \ln\big(1+\eta_{n-1}^{-1}\big)(1+\eta_{n+1}^{-1})(k) \\ - s * \ln\big(1+\eta_1^{-1}\big)(k) - s * \phi_1 * \ln\big(1+\eta_2^{-1}\big)(k)\end{aligned} \tag{A.19}$$

Now let's focus on the summation

$$\sum_{n=2}^{\infty} \phi_n * s * \ln\big(1+\eta_{n-1}^{-1}\big)(1+\eta_{n+1}^{-1})(k). \tag{A.20}$$

Due to equation (A.10), this is equal to

$$\sum_{n=2}^{\infty} \phi_n * \ln\eta_n(k) - \sum_{n=2}^{\infty} s * \phi_n * \ln\eta_{n-1}(k) - \sum_{n=2}^{\infty} s * \phi_n * \ln\eta_{n+1}(k), \tag{A.21}$$

and again to

$$\sum_{n=2}^{\infty} \cancel{(\phi_n - s * (\phi_{n-1} + \phi_{n+1}))} * \ln\eta_n(k) - s * \phi_2 * \ln\eta_1(k) + s * \phi_1 * \ln\eta_2(k). \tag{A.22}$$

Thanks to this simplification, equation (A.19) becomes

$$\begin{aligned}\ln\zeta(k) = \frac{k^2-\mu-h}{T} + s * \phi_2 * \ln\eta_1(k) - \cancel{s * \phi_1 * \ln\eta_2(k)} \\ - s * \ln(1+\eta_1)(k) + s * \ln\eta_1(k) - s * \phi_1 * \ln(1+\eta_2)(k) + \cancel{s * \phi_1 * \ln\eta_2}(k).\end{aligned} \tag{A.23}$$

We can further rewrite the two red pieces

$$s * (\phi_2 + \phi_0) * \ln\eta_1(k) = \phi_1 * \ln\eta_1(k) = s * \phi_1 * \ln(1+\eta_2)(k) + s * \phi_1 * \ln\big(1+\zeta^{-1}\big)(k). \tag{A.24}$$

Substituting we obtain

$$\begin{aligned}\ln\zeta(k) = \frac{k^2-\mu-h}{T} + \cancel{s * \phi_1 * \ln(1+\eta_2)}(k) + s * \phi_1 * \ln\big(1+\zeta^{-1}\big)(k) \\ - s * \ln(1+\eta_1)(k) - \cancel{s * \phi_1 * \ln(1+\eta_2)}(k),\end{aligned} \tag{A.25}$$

which finally is the equation we were looking for

$$\ln\zeta = \frac{k^2-\mu-h}{T} - r * \ln\big(1+\zeta^{-1}\big)(k) - s * \ln(1+\eta_1)(k). \tag{A.26}$$

Acknowledgments

I want to acknowledge all the people who has been close to me during these five years of university. My family Mauro, Lorella and Pier Paolo, and all my friends, especially Nicola, Matteo, Elena, Alessio, Fabio and Davide.

I want to thank also the professors that helped me and inspired me during this years, especially prof. Pier Alberto Marchetti and prof. Luca Salasnich. Special thanks also to prof. Alessandro Sfondrini who introduced me to this topic and gave me the possibility to carry out this thesis.

Last but not least, I am very grateful to prof. Pasquale Calabrese and especially to dr. Stefano Scopa for guiding me during this thesis. In general, I am grateful to all the SISSA of Trieste for hosting me for three months in such a nice place.

Bibliography

[1] M. H. Anderson, J. R. Ensher, M. R. Matthews, C. E. Wieman, and E. A. Cornell, *Observation of bose-einstein condensation in a dilute atomic vapor*, *Science* **269** (1995), no. 5221 198–201.

[2] C. C. Bradley, C. A. Sackett, J. J. Tollett, and R. G. Hulet, *Evidence of bose-einstein condensation in an atomic gas with attractive interactions*, *Phys. Rev. Lett.* **75** (Aug, 1995) 1687–1690.

[3] K. B. Davis, M. O. Mewes, M. R. Andrews, N. J. van Druten, D. S. Durfee, D. M. Kurn, and W. Ketterle, *Bose-einstein condensation in a gas of sodium atoms*, *Phys. Rev. Lett.* **75** (Nov, 1995) 3969–3973.

[4] T. Giamarchi, *One-dimensional physics in the 21st century*, *Comptes Rendus Physique* **17** (2016) 322–331.

[5] S. Coleman, *There are no Goldstone bosons in two dimensions*, *Communications in Mathematical Physics* **31** (Dec., 1973) 259–264.

[6] H. Bethe, *Zur Theorie der Metalle*, *Zeitschrift fur Physik* **71** (Mar., 1931) 205–226.

[7] E. H. Lieb and W. Liniger, *Exact analysis of an interacting bose gas. i. the general solution and the ground state*, *Phys. Rev.* **130** (May, 1963) 1605–1616.

[8] C. N. Yang, *Some exact results for the many-body problem in one dimension with repulsive delta-function interaction*, *Phys. Rev. Lett.* **19** (Dec, 1967) 1312–1315.

[9] M. Gaudin, *Un systeme a une dimension de fermions en interaction*, *Physics Letters A* **24** (1967), no. 1 55–56.

[10] B. Sutherland, *Further results for the many-body problem in one dimension*, *Phys. Rev. Lett.* **20** (Jan, 1968) 98–100.

[11] M. T. Batchelor, A. Foerster, X.-W. Guan, and C. C. N. Kuhn, *Exactly solvable models and ultracold fermi gases*, *Journal of Statistical Mechanics: Theory and Experiment* **2010** (dec, 2010) P12014.

[12] C. N. Yang and C. P. Yang, *Thermodynamics of a One-Dimensional System of Bosons with Repulsive Delta-Function Interaction*, *Journal of Mathematical Physics* **10** (July, 1969) 1115–1122.

[13] M. Takahashi, *One-Dimensional Electron Gas with Delta-Function Interaction at Finite Temperature*, *Progress of Theoretical Physics* **46** (11, 1971) 1388–1406.

[14] M. Takahashi, *Thermodynamics of One-Dimensional Solvable Models*. Cambridge University Press, 1999.

[15] G. Arutyunov, S. Frolov, and M. Staudacher, *Bethe ansatz for quantum strings*, *Journal of High Energy Physics* **2004** (oct, 2004) 016–016.

[16] N. Beisert and M. Staudacher, *Long-range psu(2,2—4) bethe ansätze for gauge theory and strings*, *Nuclear Physics B* **727** (2005), no. 1 1–62.

[17] A. Sfondrini, *Towards integrability for* $\mathrm{AdS}_3/\mathrm{CFT}_2$, *J. Phys. A* **48** (2015), no. 2 023001, [arXiv:1406.2971].

[18] N. Beisert, *The dilatation operator of n=4 super yang-mills theory and integrability*, *Physics Reports* **405** (2003) 1–202.

[19] T. Kinoshita, T. Wenger, and D. S. Weiss, *Observation of a one-dimensional tonks-girardeau gas*, *Science* **305** (2004), no. 5687 1125–1128, [https://www.science.org/doi/pdf/10.1126/science.1100700].

[20] B. Paredes, A. Widera, V. Murg, O. Mandel, S. Fölling, I. I. Cirac, G. V. Shlyapnikov, T. W. Hänsch, and I. Bloch, *Tonks–girardeau gas of ultracold atoms in an optical lattice*, *Nature* **429** (2004) 277–281.

[21] B. L. Tolra, K. M. O'Hara, J. H. Huckans, W. D. Phillips, S. L. Rolston, and J. V. Porto, *Observation of reduced three-body recombination in a correlated 1d degenerate bose gas*, *Phys. Rev. Lett.* **92** (May, 2004) 190401.

[22] L. Pollet, S. M. A. Rombouts, and P. J. H. Denteneer, *Ultracold atoms in one-dimensional optical lattices approaching the tonks-girardeau regime*, *Phys. Rev. Lett.* **93** (Nov, 2004) 210401.

[23] A. H. van Amerongen, J. J. P. van Es, P. Wicke, K. V. Kheruntsyan, and N. J. van Druten, *Yang-yang thermodynamics on an atom chip*, *Phys. Rev. Lett.* **100** (Mar, 2008) 090402.

[24] X.-W. Guan, M. T. Batchelor, and C. Lee, *Fermi gases in one dimension: From bethe ansatz to experiments*, *Rev. Mod. Phys.* **85** (Nov, 2013) 1633–1691.

[25] P. Calabrese, F. H. L. Essler, and G. Mussardo, *Introduction to 'quantum integrability in out of equilibrium systems'*, *Journal of Statistical Mechanics: Theory and Experiment* **2016** (2016).

[26] J.-S. Caux and J. Mossel, *Remarks on the notion of quantum integrability*, *Journal of Statistical Mechanics: Theory and Experiment* **2011** (feb, 2011) P02023.

[27] S. Scopa, P. Calabrese, and L. Piroli, *Real-time spin-charge separation in one-dimensional fermi gases from generalized hydrodynamics*, *Phys. Rev. B* **104** (Sep, 2021) 115423.

[28] S. Scopa, P. Calabrese, and L. Piroli, *Generalized hydrodynamics of the repulsive spin-*$\frac{1}{2}$ *fermi gas*, *Phys. Rev. B* **106** (Oct, 2022) 134314.

[29] T. Kinoshita, T. Wenger, and D. S. Weiss, *A quantum newton's cradle*, *Nature* **440** (2006) 900–903.

[30] J.-S. Caux, B. Doyon, J. Dubail, R. Konik, and T. Yoshimura, *Hydrodynamics of the interacting bose gas in the quantum newton cradle setup*, *SciPost Physics* **6** (jun, 2019).

[31] F. Franchini, *An Introduction to Integrable Techniques for One-Dimensional Quantum Systems*. Springer International Publishing, 2017.

[32] O. A. Castro-Alvaredo, B. Doyon, and T. Yoshimura, *Emergent hydrodynamics in integrable quantum systems out of equilibrium*, *Phys. Rev. X* **6** (Dec, 2016) 041065.

[33] B. Bertini, M. Collura, J. De Nardis, and M. Fagotti, *Transport in out-of-equilibrium xxz chains: Exact profiles of charges and currents*, *Phys. Rev. Lett.* **117** (Nov, 2016) 207201.

[34] J. De Nardis, D. Bernard, and B. Doyon, *Hydrodynamic diffusion in integrable systems*, *Phys. Rev. Lett.* **121** (Oct, 2018) 160603.

[35] J. Durnin, A. D. Luca, J. D. Nardis, and B. Doyon, *Diffusive hydrodynamics of inhomogenous hamiltonians*, *Journal of Physics A: Mathematical and Theoretical* **54** (nov, 2021) 494001.

[36] A. Bastianello, V. Alba, and J.-S. Caux, *Generalized hydrodynamics with space-time inhomogeneous interactions*, *Phys. Rev. Lett.* **123** (Sep, 2019) 130602.

[37] P. Ruggiero, P. Calabrese, B. Doyon, and J. Dubail, *Quantum generalized hydrodynamics*, *Phys. Rev. Lett.* **124** (Apr, 2020) 140603.

[38] M. Collura, A. De Luca, P. Calabrese, and J. Dubail, *Domain wall melting in the spin-$\frac{1}{2}$ xxz spin chain: Emergent luttinger liquid with a fractal quasiparticle charge*, *Phys. Rev. B* **102** (Nov, 2020) 180409.

[39] S. Scopa, P. Calabrese, and J. Dubail, *Exact hydrodynamic solution of a double domain wall melting in the spin-1/2 XXZ model*, *SciPost Phys.* **12** (2022) 207.

[40] S. Scopa, A. Krajenbrink, P. Calabrese, and J. Dubail, *Exact entanglement growth of a one-dimensional hard-core quantum gas during a free expansion*, *Journal of Physics A: Mathematical and Theoretical* **54** (sep, 2021) 404002.

[41] F. Ares, S. Scopa, and S. Wald, *Entanglement dynamics of a hard-core quantum gas during a joule expansion*, *Journal of Physics A: Mathematical and Theoretical* **55** (aug, 2022) 375301.

[42] M. Fagotti, *Locally quasi-stationary states in noninteracting spin chains*, *SciPost Phys.* **8** (2020) 048.

[43] P. Ruggiero, P. Calabrese, B. Doyon, and J. Dubail, *Quantum generalized hydrodynamics of the tonks–girardeau gas: density fluctuations and entanglement entropy*, *Journal of Physics A: Mathematical and Theoretical* **55** (dec, 2021) 024003.

[44] S. Scopa and D. X. Horváth, *Exact hydrodynamic description of symmetry-resolved rényi entropies after a quantum quench*, *Journal of Statistical Mechanics: Theory and Experiment* **2022** (aug, 2022) 083104.

[45] M. Schemmer, I. Bouchoule, B. Doyon, and J. Dubail, *Generalized hydrodynamics on an atom chip*, *Phys. Rev. Lett.* **122** (Mar, 2019) 090601.

[46] N. Malvania, Y. Zhang, Y. Le, J. Dubail, M. Rigol, and D. S. Weiss, *Generalized hydrodynamics in strongly interacting 1d bose gases*, *Science* **373** (sep, 2021) 1129–1133.

[47] Y. Nozawa and H. Tsunetsugu, *Generalized hydrodynamic approach to charge and energy currents in the one-dimensional hubbard model*, *Phys. Rev. B* **101** (Jan, 2020) 035121.

[48] Y. Nozawa and H. Tsunetsugu, *Generalized hydrodynamics study of the one-dimensional hubbard model: Stationary clogging and proportionality of spin, charge, and energy currents*, *Phys. Rev. B* **103** (Jan, 2021) 035130.

[49] M. Mestyán, B. Bertini, L. Piroli, and P. Calabrese, *Spin-charge separation effects in the low-temperature transport of one-dimensional fermi gases*, *Phys. Rev. B* **99** (Jan, 2019) 014305.

[50] F. Møller, C. Li, I. Mazets, H.-P. Stimming, T. Zhou, Z. Zhu, X. Chen, and J. Schmiedmayer, *Extension of the generalized hydrodynamics to the dimensional crossover regime*, *Phys. Rev. Lett.* **126** (Mar, 2021) 090602.

[51] J. Cardy, *Scaling and Renormalization in Statistical Physics*. Cambridge Lecture Notes in Physics. Cambridge University Press, 1996.

[52] U. Rössler, *Spin Waves: Magnons*, pp. 157–187. Springer Berlin Heidelberg, Berlin, Heidelberg, 2004.

[53] L. Tonks, *The complete equation of state of one, two and three-dimensional gases of hard elastic spheres*, *Phys. Rev.* **50** (Nov, 1936) 955–963.

[54] Y. Castin, *Simple theoretical tools for low dimension bose gases*, .

[55] L. Pitaevskii and S. Stringari, *Bose-Einstein Condensation and Superfluidity*. Oxford University Press, 01, 2016.

[56] P. Dorey, *Exact s-matrices*, 1998.

[57] F. Levkovich-Maslyuk, *The bethe ansatz*, *Journal of Physics A: Mathematical and Theoretical* **49** (jul, 2016) 323004.

[58] B. Doyon, *Lecture notes on Generalised Hydrodynamics*, *SciPost Phys. Lect. Notes* (2020) 18.

[59] M. Rigol, V. Dunjko, V. Yurovsky, and M. Olshanii, *Relaxation in a completely integrable many-body quantum system: An ab initio study of the dynamics of the highly excited states of 1d lattice hard-core bosons*, *Phys. Rev. Lett.* **98** (Feb, 2007) 050405.

[60] T. Bonnemain, B. Doyon, and G. El, *Generalized hydrodynamics of the kdv soliton gas*, *Journal of Physics A: Mathematical and Theoretical* **55** (aug, 2022) 374004.

[61] B. Davies and V. E. Korepin, *Higher conservation laws for the quantum non-linear schroedinger equation*, 2011.

[62] B. Davies, *Higher conservation laws for the quantum non-linear schrödinger equation*, *Physica A: Statistical Mechanics and its Applications* **167** (1990), no. 2 433–456.

[63] J. Eisert, M. Friesdorf, and C. Gogolin, *Quantum many-body systems out of equilibrium*, *Nature Physics* **11** (feb, 2015) 124–130.

[64] F. H. L. Essler and M. Fagotti, *Quench dynamics and relaxation in isolated integrable quantum spin chains*, *Journal of Statistical Mechanics: Theory and Experiment* **2016** (jun, 2016) 064002.

[65] E. Ilievski, J. De Nardis, B. Wouters, J.-S. Caux, F. H. L. Essler, and T. Prosen, *Complete generalized gibbs ensembles in an interacting theory*, *Phys. Rev. Lett.* **115** (Oct, 2015) 157201.

[66] T. Langen, S. Erne, R. Geiger, B. Rauer, T. Schweigler, M. Kuhnert, W. Rohringer, I. E. Mazets, T. Gasenzer, and J. Schmiedmayer, *Experimental observation of a generalized gibbs ensemble*, *Science* **348** (2015), no. 6231 207–211, [https://www.science.org/doi/pdf/10.1126/science.1257026].

[67] M. Borsi, B. Pozsgay, and L. Pristy'ak, *Current operators in integrable models: a review*, *Journal of Statistical Mechanics: Theory and Experiment* **2021** (2021).

[68] B. Doyon, J. Dubail, R. Konik, and T. Yoshimura, *Large-scale description of interacting one-dimensional bose gases: Generalized hydrodynamics supersedes conventional hydrodynamics*, *Physical Review Letters* **119** (nov, 2017).

[69] B. Doyon and T. Yoshimura, *A note on generalized hydrodynamics: inhomogeneous fields and other concepts*, *SciPost Physics* **2** (apr, 2017).

[70] F. S. Møller and J. Schmiedmayer, *Introducing iFluid: a numerical framework for solving hydrodynamical equations in integrable models*, *SciPost Physics* **8** (mar, 2020).

[71] B. Doyon, J. Dubail, R. Konik, and T. Yoshimura, *Large-scale description of interacting one-dimensional bose gases: Generalized hydrodynamics supersedes conventional hydrodynamics*, *Phys. Rev. Lett.* **119** (Nov, 2017) 195301.

[72] J. B. McGuire, *Interacting fermions in one dimension. i. repulsive potential*, *Journal of Mathematical Physics* **6** (1965), no. 3 432–439.

[73] J. B. McGuire, *Interacting fermions in one dimension. ii. attractive potential*, *Journal of Mathematical Physics* **7** (1966), no. 1 123–132.

[74] M. Flicker and E. H. Lieb, *Delta-function fermi gas with two-spin deviates*, *Phys. Rev.* **161** (Sep, 1967) 179–188.

[75] C. K. Lai, *Thermodynamics of fermions in one dimension with a δ-function interaction*, *Phys. Rev. Lett.* **26** (Jun, 1971) 1472–1475.

[76] R. P. Anderson, C. Ticknor, A. I. Sidorov, and B. V. Hall, *Spatially inhomogeneous phase evolution of a two-component bose-einstein condensate*, *Phys. Rev. A* **80** (Aug, 2009) 023603.

[77] J.-S. Caux, A. Klauser, and J. van den Brink, *Polarization suppression and nonmonotonic local two-body correlations in the two-component bose gas in one dimension*, *Phys. Rev. A* **80** (Dec, 2009) 061605.

[78] A. Klauser and J.-S. Caux, *Equilibrium thermodynamic properties of interacting two-component bosons in one dimension*, *Phys. Rev. A* **84** (Sep, 2011) 033604.

[79] O. I. Pâţu and A. Klümper, *Thermodynamics, density profiles, and correlation functions of the inhomogeneous one-dimensional spinor bose gas*, *Phys. Rev. A* **92** (Oct, 2015) 043631.

[80] X.-W. Guan, M. T. Batchelor, and M. Takahashi, *Ferromagnetic behavior in the strongly interacting two-component bose gas*, *Phys. Rev. A* **76** (Oct, 2007) 043617.

[81] Y. Li, S. Gu, Z.-J. Ying, and U. Eckern, *Exact results of the ground state and excitation properties of a two-component interacting bose system*, *EPL (Europhysics Letters)* **61** (11, 2002).

[82] S.-J. Gu, Y.-Q. Li, Z.-J. Ying, and X.-A. Zhao, *Thermodynamics of two component bosons in one dimension*, *International Journal of Modern Physics B* (11, 2002).

[83] O. I. Pâţu and A. Klümper, *Momentum reconstruction and contact of the one-dimensional bose-fermi mixture*, *Phys. Rev. A* **99** (Jan, 2019) 013628.

[84] S. Wang, X. Yin, Y.-Y. Chen, Y. Zhang, and X.-W. Guan, *Emergent ballistic transport of bose–fermi mixtures in one dimension*, *Journal of Physics A: Mathematical and Theoretical* **53** (oct, 2020) 464002.

[85] O. I. Pâţu, *Dynamical fermionization in a one-dimensional bose-fermi mixture*, *Phys. Rev. A* **105** (Jun, 2022) 063309.